CELLULAR METAL ION SENSING USING DNAZYMES

BY

KEVIN HWANG

DISSERTATION

Submitted in partial fulfillment of the requirements
for the degree of Doctor of Philosophy in Chemistry
in the Graduate College of the
University of Illinois at Urbana-Champaign, 2016

Urbana, Illinois

Doctoral Committee:

Professor Yi Lu, Chair
Professor Jefferson Chan
Professor Catherine J. Murphy
Professor Kenneth S. Suslick

ABSTRACT

Metal ions are important elements in biology and are involved in numerous reactions essential for maintaining life on earth. Most commonly, metal ions confer their role as structural elements or catalytic cofactors within metalloproteins. Metalloproteins comprise more than half of all known proteins and are at the heart of several important biological processes including photosynthesis, respiration, and nitrogen fixation. Another equally important role of metal ions is as signaling molecules. It has been shown that changes in concentrations of calcium, zinc, or copper can trigger downstream signaling effect in neurons. Despite these important functions, high levels of many metal ions, especially transition metal ions, are known to be toxic to cells. Thus, cells have adapted strategies to finely regulate the uptake, storage, and distribution of metal ions within different compartments. The importance of these mechanisms for maintaining metal ion homeostasis within cells and the key role of metal ions in life have been of major interest for years. However, the understanding of these mechanisms and how metal ions play their role is largely unknown in many cases. An important step towards advancing our understanding of metal ions is developing the ability to measure their concentrations in different cellular compartments with accuracy and sensitivity.

To achieve this goal, several techniques are available that have greatly advanced our understanding of metal ions. However, current methods suffer from a number of limitations that have slowed progress. Analytical tools such as ICP-MS and AAS, while effective at measuring the cocnentrations of metal ions very sensitively, usually work in bulk and thus are not easily amenable to single cell studies let alone the distribution in different cellular compartments. Moreover, these techniques are often unable to distinguish between different oxidation states of a metal ion or between bound and mobile forms. Techniques based on X-ray absorption, such as X-ray fluorescence microscopy (XFM) can simultaneously detect multiple metal ions and can distinguish between different oxidation states. However, these techniques require the use of highly focused X-ray beams limiting more widespread availability of such techniques. Furthermore, biological samples cannot be examined in a real time manner, and the obtained distribution of metal ions represents only total metal content, without regard to whether the metals are easily exchangeable or are tightly bound, a major factor determining biological activity.

To overcome these issues several metal ion sensors have been designed based on either small molecules or proteins with great sensitivities of detection. The use of such sensors has provided great insight into the functions of metal ions. However, as these sensors are usually rationally designed through a trial and error process, it is challenging to generalize the successful designs to sense other metal ions or to meet new desired criteria. DNAzymes, DNA sequences with catalytic activity, have recently emerged as an alternative class of sensors for metal ions. As selection of DNAzymes for different metal ions is carried out through a combinatorial process, new sequences with desired activity and selectivity can be easily obtained by changing the selection conditions. Many DNAzymes have been selected with high sensitivity for different metal ions including zinc, copper, lead, and uranyl. Surprisingly, despite the promise of using DNAzymes as sensors for cellular metal ions, almost all applications of DNAzyme-based sensors until now have been in environmental metal ion detection and DNAzyme-based sensors for cellular metal detection have only very recently been explored as an option.

The goal of my PhD research was to establish novel strategies to make DNAzymes viable sensors for cellular metal ion detection. Chapter 1 briefly describes the background and overall aims of my research. In chapter 2, I describe my efforts in designing “caged” DNAzyme-based sensors that can be activitated by light when they reach the desired cellular compartments. This method reduces the off-target signals and as demonstrated in this chapter is highly generalizable to other DNAzyme-based sensors. In chapter 3, I explain my efforts in designing a ratiometric DNAzyme-based sensor to enable quantitative measurement within the cells. Finally, chapter 4 summarizes my efforts in enhancing the caging strategy to enable better stability, faster decaging, or the use of long-wavelength light for decaging by using lanthanide-doped metal nanoparticles.

To my family

ACKNOWLEDGMENTS

There are many people who have helped me through the long journey that has been graduate school. First of all I would like to thank my advisor, Dr. Yi Lu, for his support and guidance over the years. I am deeply appreciative for all of his continued patience and advice, on so many topics both research-related and otherwise. I thank him for making me a better scientist.

I would like to thank my committee members, Professors Jefferson Chan, Catherine J. Murphy, and Kenneth S. Suslick, for contributing your time and energy, for providing ideas and advice, and for your continued support throughout the years. I would also like to thank collaborators past and present, including Professor Yingxiao Wang and his group members Dr. Taejin Kim and Dr. Lei Lei, and Professor James Imlay, all of whom have been incredible sources of knowledge and wonderful people to work with. I would also like to express my deep gratitude to Professor Bill Brieher for a lot of great discussion and for his infectious enthusiasm, and to Professor Claudio Grosman for his advice and unwavering support and for placing his trust in me. I would like to acknowledge Dr. Sandra McMasters from the UIUC Cell Media Facility and Dr. Mayandi Sivaguru from IGB for technical support. I also gratefully acknowledge research support from the Department of Chemistry in the form of the Lester E. and Kathleen A. Coleman and Ullyot fellowships, as well as support from the Molecular Biophysics Training Grant.

There are so many people in the Lu group, past and present, who have made this journey an amazing one. To single a few of them out by name, I want to start with those who came before me, who I look up to (you're all doctors now!): Thanks to Dr. Peiwen Wu, Dr. Seyed-Fakhreddin Torabi, Dr. Shiliang Tian, Dr. Lele Li, Dr. Parisa Hosseinzadeh, Dr. Li Huey Tan, Dr. Hang Xing, Dr. Jingjing Zhang, and Dr. Ngo Yin Wong for everything – for midnight microscopy, for the puzzling field trips, for late-night discussions, for liposome summer camp, for the utterly incomparable Beckman experience, and for the many adventures both inside and out of the lab. I am deeply grateful for the years of continuing support and friendship. To the newer generation of Lu group members, Nitya Sai Reddy, Ryan Lake, Claire McGhee, I know I can trust that the lab is in good hands. I was also lucky enough to have two exceptional undergraduates work with me in the Lu group, Kang Yong Loh and Brandalynn Holland. They were great to work with and I have every confidence they will continue to excel in the future.

I need to give my deepest thanks to my parents Yu-Wen Hwang and Mo-Chou Chen Hwang for their unconditional love and support, as well as occasional much-needed perspective, and to my brother Hubert for somehow continuing to put up with his sibling despite everything.

TABLE OF CONTENTS

Chapter 1:

Introduction

1.1 Metals in biology

Metal ions are essential elements in biology, playing critical roles in many important functions within cells. Most commonly, metal ions play their role as structural or catalytic cofactors within metalloproteins, where they assist in protein folding or enable catalytic reactivity not possible by amino acids alone.[1] Metalloproteins comprise more than half of all known proteins[2,3] and even more microbial metalloproteomes have yet to be explored.[4] Many of these metalloproteins are involved in biochemical reactions essential to life, such as photosynthesis and respiration, that are only possible due to the added chemical functionality offered by these metal ions.[1] As a result, cells must have methods for taking up sufficient concentrations of metal ions to ensure their availability for incorporation into metalloproteins.[2] At the same time, many metal ions, especially transition metals, are toxic when in excess. To balance the requirement for sufficient metal ion uptake with the need to avoid toxicity, cells have developed sophisticated mechanisms for regulation and storage of metal ions to control intracellular levels within a narrow range, even when extracellular levels of the metal may fluctuate widely.[5,6] The importance of these mechanisms for maintaining the homeostasis of metal ions in cells has made them a subject of major interest.[7-10] As a result, a great deal of effort has been employed to better elucidate them.

On par with their catalytic activity, metal ions play another essential function in life as intra- or inter-cellular signaling agents. It has been identified that alterations in the levels of metals including calcium,[11] zinc,[12] and copper[13] can trigger downstream effects, which can be critical in the proper functioning of cells. The best-known example of such effects is the use of calcium (Ca^{2+}) by excitable cells such as neurons, where the calcium ion is normally constitutively exported from the cell but is rapidly transported into the cell at the end of the action potential.[11] The calcium ion then is recognized by intracellular calcium sensing proteins such as calmodulin and calpain, which control myriad pathways within the cell, before being re-exported to prime the cell for further activation.[11,14,15] Another example is that of zinc

(Zn^{2+}), which is found in extremely high levels in presynaptic vesicles of "gluzinergic" neurons in the hippocampus.[16-19] Zinc from these neurons is released along with other neurotransmitters such as glutamine after activation of the neuron, whereupon the zinc is believed to function as a neuromodulator due to its ability to bind to and inhibit AMPA and NMDA receptors.[17,20] Finally, copper (Cu^{2+}) is also present in high levels in central nervous system where it plays a role in synaptic transmission through modulating the function of type A GABA receptor, NMDA, and voltage-gated calcium channels.[13,21]

It is important to note that a metal ion within a cell can perform several functions simultaneously without one function precluding others. Furthermore, beyond calcium, zinc, and copper, other metal ions are known to be necessary for life including iron, manganese, magnesium, and many others.[22-26]

Despite the important roles played by metal ions, our understanding of their functions varies significantly and is in some cases very limited. An important step in understanding the function of metal ions is measuring the levels of those ions, particularly within a cell. Thus, the development of appropriate tools for detection of intracellular metal ions has thus been a subject of major interest.

1.2 Methods for metal ion detection in biological systems

There are many methods for the sensitive detection of metal ions. One method is to use analytical techniques including atomic absorption spectroscopy (AAS), flame absorption spectroscopy, inductively coupled plasma mass spectrometry (ICP-MS), and others.[27] While these analytical techniques are extremely sensitive and very good at differentiating between different elements, they are not always capable of differentiating between ionic forms of the same element. This can be problematic as multiple oxidation states can play significantly different functions within a particular biological environment. Furthermore, these methods are typically bulk methods, which limits study of individual cells, and are difficult to use to distinguish between metals located in different cellular compartments or organelles. It is possible to use ultracentrifugation or other separation methods in order to physically separate and study a particular organelle prior to sample analysis,[28] but such separation methods are extremely laborious and add extra steps that may confound accurate data collection.

Another major class of techniques is based on the use of X-rays, most often through X-ray fluorescence (XRF) microscopy methods. The physical basis underlying these techniques is the absorbance of X-rays by metal ions, which varies depending on element and oxidation state.[29] As a result, these techniques are element- and even ion-specific. Using XRF, it is possible to obtain maps indicating

the distribution of oxidation states within a fixed cell.[30,31] In these methods it is possible to measure multiple elements simultaneously, which is extremely helpful for correlative studies. This level of information is extremely valuable, but comes with some significant limitations. The first limitation is the need to use high-energy X-rays, which typically requires the use of a synchrotron. Another limitation is that biological samples used for these techniques must be frozen before use (and often fixed using organic solvent or polyaldehydes), meaning that the final image corresponds only to a single snapshot. Finally, with XRF, it is difficult to assess the ligand environment of the metal. Images obtained from XRF will indicate the total amount of a metal ion within the cell regardless of its ligand environment.[29] This means that XRF alone may not be capable of distinguishing between a metal ion that is tightly bound (for instance, one within the active site of a metalloprotein) and a metal ion of the same oxidation state that is loosely bound by organic or inorganic ligands within the cell (such as nucleotides or polyphosphates);[29-31] from a biological standpoint, however, the difference between these two types of metal ions (strongly- or loosely-bound) is significant.[12,13,30,32] This fact has led to the investigation of other methods capable of measuring not only the distribution of metal ions within the cell, but also able to distinguish between metal ions on the basis of biological *accessibility* (also termed *lability*).[7-9,33]

1.3 Fluorescent metal ion sensors

In order to help understand the distribution of metal ions within cells, a number of cellular sensors have been developed, most commonly those based on small organic molecules or proteins.[7-10] Of the available methods for real-time sensing in cells, fluorescent sensors have been the predominant choice due to their high signal intensity, fast response times, and ability to directly probe labile pools of metal ions.[7-10] A number of examples and the corresponding metal ions probed are shown in Figure 1.1.[10] While these sensors have greatly expanded our understanding of the biological role of metal ions, much still remains to be understood. One problem that has slowed the progress in understanding the role of metals in biology is the significant heterogeneity of conditions under which metal ions can be found, necessitating the development of a wide variety of sensors for different applications.[10,34]

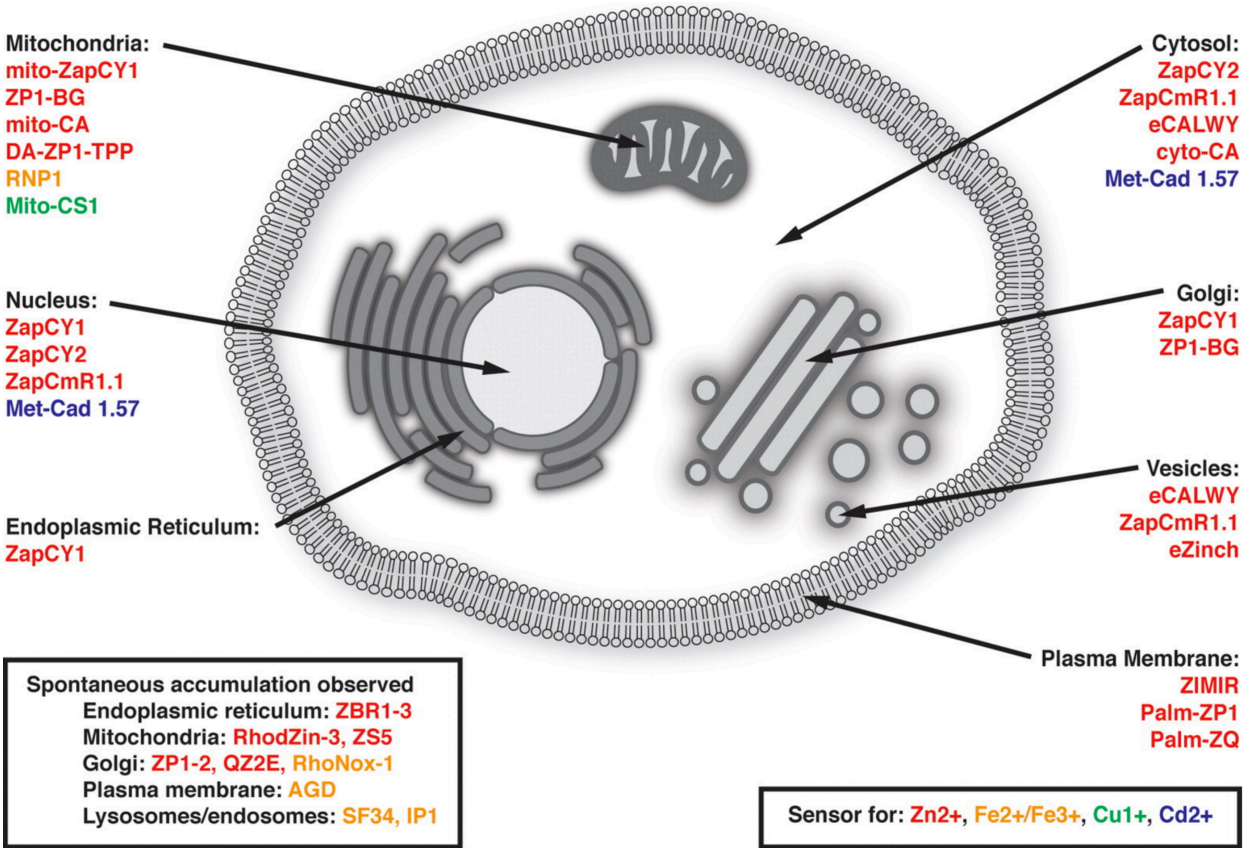

Figure 1.1. Sensors used for studying cellular metal ions, and the corresponding metal ions detected. Originally from Ref. 10.[10]

1.4 Rational design versus combinatorial selection

A major roadblock in the process of sensor design is that current paradigm of sensor design relies heavily on *rational design* for both small molecules and proteins. This process is essentially one of trial and error, in which success in creating one sensor for one metal ion may not generalize towards the creation of other sensors for the same or different metal ions. An alternative approach is *combinatorial selection*, for which the requirements to generate a sensor are different. In combinatorial selection the selection conditions are tuned to fit the desired final properties of the sensor and large quantities of chemical space are screened. As a result, it is not necessary to use the accumulated knowledge of potentially subtle differences in coordination preference and geometry for different metal ions in order to obtain appropriate sensors with desired selectivity and sensitivity.[35,36]

An excellent example of the power of combinatorial selection is in the production of antibodies, which is one of the most commonly utilized combinatorial selection techniques. Antibody selection takes

advantage of the natural variation performed by alternative splicing of antibody sequences in developing lymphocytes, in what is known as "VDJ recombination".[37,38] This process generates a wide variety of possible antibody sequences, which enables recognition of a huge range of possible targets by the immune system. The importance of this approach is evidenced by the ubiquity of antibody use in the biological sciences, and the huge and constantly growing catalog of commercially available antibodies for both research and therapeutic use.[39,40] The method for producing specific antibodies for a particular antigen is simply to introduce the desired antigen into an animal at various times with a particular dosage schedule. If the animal is immunocompetent and the target appropriate for antibody recognition, the immune system produces memory cells that recognize the antigen and produce appropriate antibodies to bind it. After a series of injections of the antigen, it is then possible to inject the antigen at a later time-point, which induces production of antigen-specific antibodies. These can either be harvested directly from the blood,[41] or antibody-producing immune cells can be collected from the blood, screened, and used to create hybridomas for continuous production of monoclonal antibodies (Figure 1.2).[42,43]

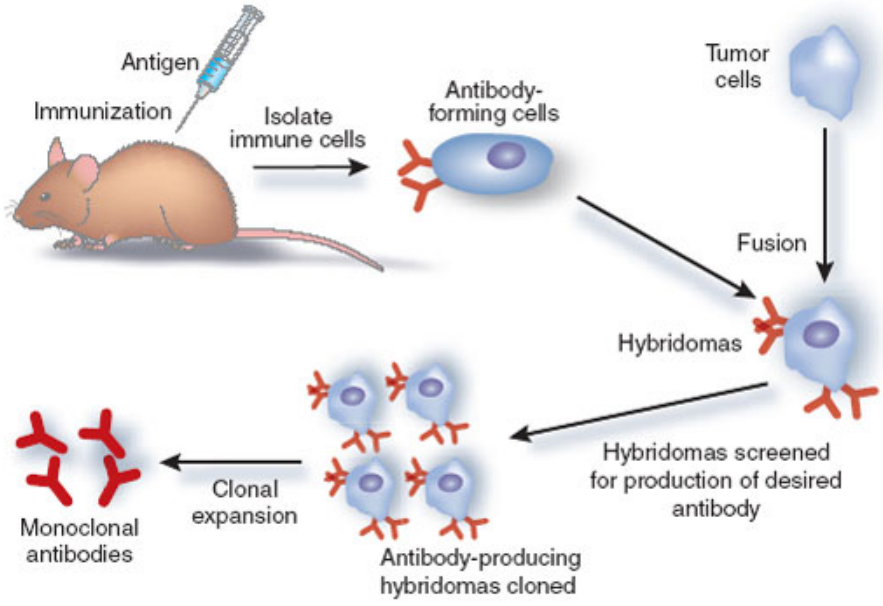

Figure 1.2. Diagram for hybridoma production of monoclonal antibodies. Originally from Ref. 44.[44]

A similar strategy to antibody selection is phage display, which is used to obtain recognition peptides (also called *peptide aptamers*).[40,45,46] In the most common implementation of this method a library of peptides is affixed to the surface of the M13 bacteriophage by ligation of corresponding DNA sequences to one of the coat proteins of the bacteriophage.[46] The phage particles produced are then introduced to a lawn of bacteria with the intended target attached to their surface, and only phages capable

of binding to and infecting bacteria are collected.[45,46] Alternatively, the phages can be exposed to a surface coated with the target. Unbound phages are separated by simple washing, and bound phages can be eluted by the addition of excess ligands and amplified for the next round (Figure 1.3).[45,46] This amplification method allows the production of small peptides capable of recognizing targets including proteins, peptides, nucleotides, and small molecules.

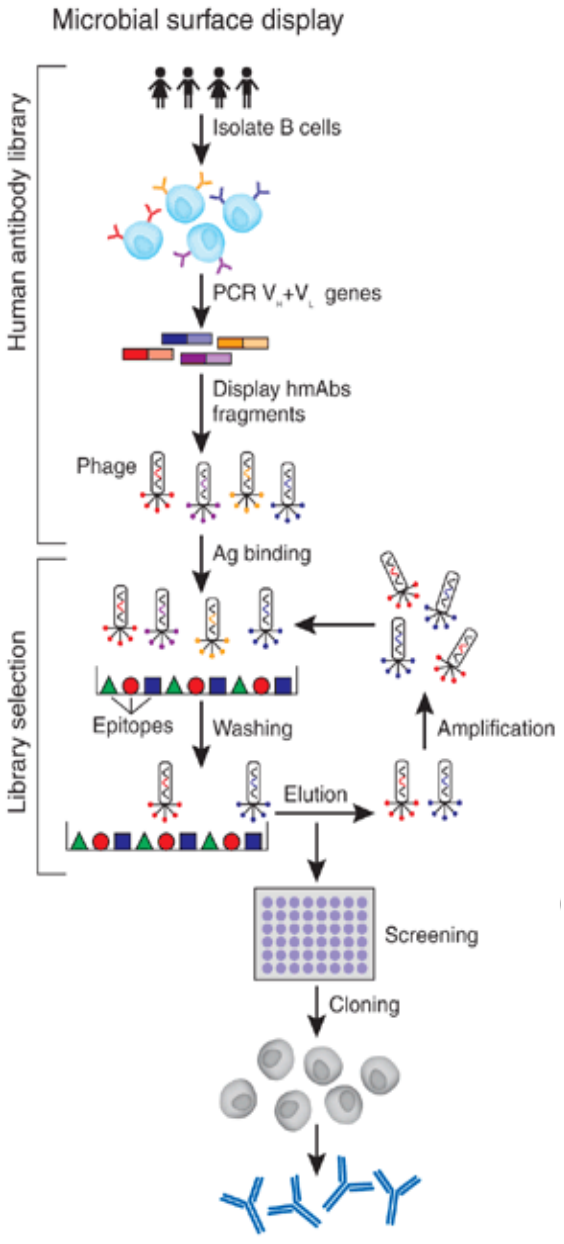

Figure 1.3. Schematic representation of phage display technique for production of antibodies. Originally from Ref. 47.[47]

While these methods are powerful and capable of producing recognition elements for a wide variety of targets, there are certain technical limitations shared by both these and similar methods that limit the scope of possible targets. For antibody selection, the method for selection requires injecting an animal and having the immune system recognize the target.[41] There are several requirements for an appropriate antigen for this process. First, it must not be a component of the animal host. Targets that are highly conserved between species can be very difficult to address using such techniques.[48] Many other targets such as oligonucleotides or common biological small molecules (e.g. ATP) that are used by all forms of life also cannot be targeted by antibodies as the immune system is designed to recognize those as self-antigens. Finally, in order for an antigen to be presented to immune cells, it should not be smaller than a certain threshold. In particular, metal ions are far too small to be recognized by antibodies.[49] To a limited extent, it is possible to carry out phage display methods to avoid some of these issues and produce peptide aptamers towards some targets not addressed by antibodies.[45] However, phage display, while perhaps applicable to a wider range of targets, has additional technical issues. The first is that the peptide sequence itself must be attached to the phage without compromising phage capsid formation, which can be challenging for proteins and very large peptides. The second major issue is the need to immobilize the target onto a surface. Metal ions in particular are difficult to immobilize in such a fashion that they are still recognizable by peptides, as their extremely small size hinders immobilization methods. Chelation of metal ions is the only effective method to immobilize a metal ion, but necessarily hinders the selective binding of any alternative ligand, such as the peptide aptamer.[50] This means that the ability to effectively immobilize the metal ion is in direct competition with the ability of the combinatorially selected ligand to recognize the metal ion itself.

1.5 DNAzymes, a potential scaffold

An alternative type of sensor that has shown some promise of addressing the challenges of sensor production is based on a catalytic DNA scaffold.[51,52] DNAzymes are sequences of DNA whose sequence defines a three-dimensional structure that can carry out catalytic activity. First discovered in 1994, DNAzymes have been shown to carry out a wide range of reactivity from RNA hydrolysis to porphyrin metallation to Diels-Alder catalysis.[53] In the majority of the cases, these DNAzymes use specific metal ion cofactors in order to carry out reactivity, but the metal ions necessary can vary depending on the sequence.

Previously, methods have been developed for obtaining DNAzymes with altered cofactor specificity for the same catalytic reaction - RNA cleavage (transesterification).[36] Using a combinatorial process called systematic evolution of ligands by exponential enrichment (SELEX) or simply *in vitro* selection,[35,36] massive random pools of DNA (up to 10^{15} different sequences) can be screened in a straightforward fashion (Figure 1.4). This process does not require immobilization of the metal ion, instead relying on observation of the RNA cleavage process to measure metal binding and activity. By carefully defining conditions for activity and control conditions for negative selection, DNAzymes with specific binding affinity, selectivity, and sensitivity have been obtained, for a variety of metal ions including Zn^{2+}, Pb^{2+}, Cu^{2+}, UO_2^{2+}, Mg^{2+} and Hg^{2+}.[51,52]

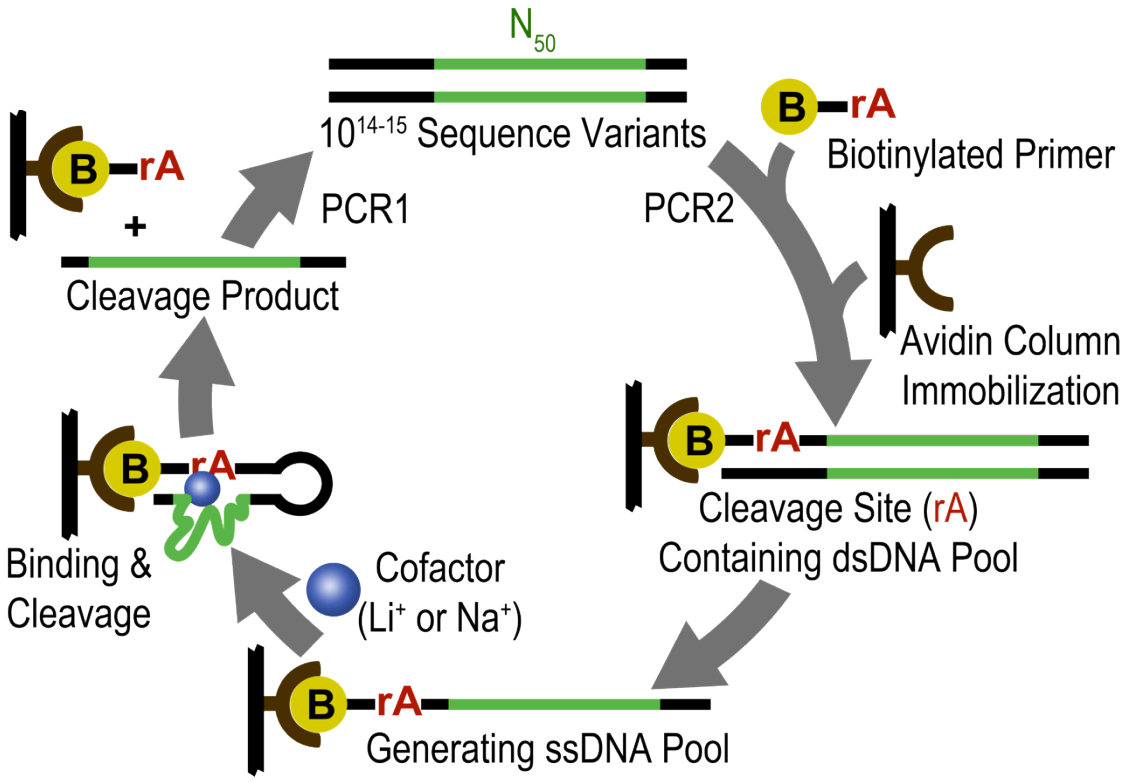

Figure 1.4. General strategy for *in vitro* selection of metal ion-specific DNAzymes. Each cycle results in a random pool more enriched in sequences active for the target of interest.

A further development was the recognition that the similarity in catalytic function between these DNAzyme sequences would allow a single reporter strategy to convert all DNAzymes with the same type of reactivity into sensors (Figure 1.5.a).[51,52,54] This so-called "catalytic beacon" approach allowed the generation of DNAzyme-based metal ion sensors from the corresponding DNAzymes. In this construct the cleaved substrate will dissociate from the enzyme-substrate complex due to its lower melting

temperature of Watson-Crick base pairing compared to an uncleaved intact strand. By incorporation of a fluorophore and quencher adjacent to each other but on opposite strands, the catalytic beacon transforms metal ion-dependent catalysis into a metal ion-dependent turn-on fluorescent signal (Figure 1.5.b). The major advantage of this system is that the generality of the *in vitro* selection protocol is then carried over to sensor design, or in other words, that sensors for metal ions can be effectively obtained through a combinatorial selection process.[51,52,54]

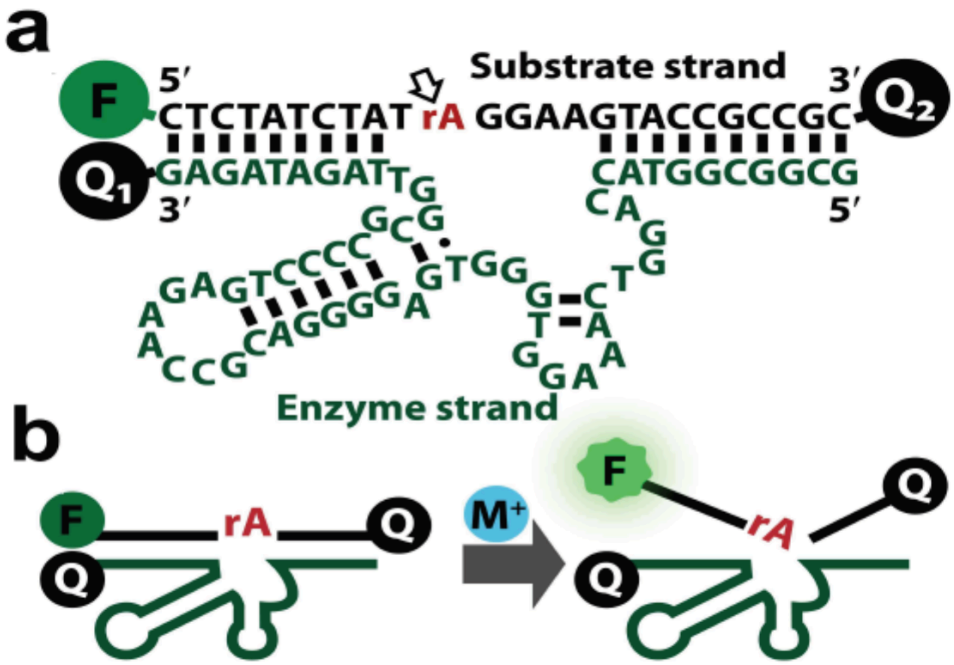

Figure 1.5. (a) General form of catalytic beacon design, with terminology labeled. F, Q_1, and Q_2 represent fluorophore and quenchers 1 and 2. (b) Mechanism of fluorescence response. After cleavage of RNA base (rA, in red) substrate arms dehybridize, isolating fluorophore from quenchers and resulting in fluorescence turn-on signal.

1.6 Thesis goals and outlook

DNAzyme sensors are interesting and useful sensing scaffolds that have been applied in many environmental applications with great success.[51] However, although DNAzymes would have significant advantages in cellular sensing applications, most of this potential has thus far been unreached. This thesis looks to explore the application of DNAzymes for cellular sensing of metal ions.

One barrier in the use of DNAyzmes within the cells is its instability under cellular conditions and the possibility of substrate cleavage before being targeted to the cellular components of interest. In chapter two, I describe my efforts in overcoming this barrier, and a method for enabling cell sensing using photoactivation. I describe the design and implementation of a photocaging strategy for enabling the general usage of DNAzymes as cellular sensors.

Another difficulty on the way of using DNAzymes as cellular metal ion sensors is that the process of introducing the DNAzyme into cells is not consistent. Hence, different cells can have different numbers of the sensor which in turn will effect the intensity of the output signal. To address this issue, in chapter three I describe work on a modified ratiometric sensor allowing quantitative sensing. I demonstrated a modification of the classic catalytic beacon design that allows for ratiometric sensing, which can enable quantitative detection within cells.

In chapter four, I describe a refinement of the photocaging strategy involving upconversion nanoparticles to enable uncaging of a DNAzyme by long-wavelength irradiation. This chapter demonstrates a proof of concept method that potentially enables the future use of DNAzyme sensor technology in more complex biological models.

1.7 References

1. Lippard SJ, Berg JM. Principles of Bioinorganic Chemistry. Mill Valley, CA: University Science Books; 1994. 411 p.

2. Waldron KJ, Rutherford JC, Ford D, Robinson NJ. Metalloproteins and metal sensing. Nature. 2009;460(7257):823-30. Epub 2009/08/14. doi: 10.1038/nature08300. PubMed PMID: 19675642.

3. Thomson AJ, Gray HB. Bio-inorganic chemistry. Current opinion in chemical biology. 1998;2(2):155-8. Epub 1998/07/17. PubMed PMID: 9667942.

4. Cvetkovic A, Menon AL, Thorgersen MP, Scott JW, Poole FL, 2nd, Jenney FE, Jr., Lancaster WA, Praissman JL, Shanmukh S, Vaccaro BJ, Trauger SA, Kalisiak E, Apon JV, Siuzdak G, Yannone SM, Tainer JA, Adams MW. Microbial metalloproteomes are largely uncharacterized. Nature. 2010;466(7307):779-82. Epub 2010/07/20. doi: 10.1038/nature09265. PubMed PMID: 20639861.

5. Hantke K. Iron and metal regulation in bacteria. Current opinion in microbiology. 2001;4(2):172-7. Epub 2001/04/03. PubMed PMID: 11282473.

6. Eide DJ. Zinc transporters and the cellular trafficking of zinc. Biochimica et biophysica acta. 2006;1763(7):711-22. Epub 2006/05/06. doi: 10.1016/j.bbamcr.2006.03.005. PubMed PMID: 16675045.

7. Domaille DW, Que EL, Chang CJ. Synthetic fluorescent sensors for studying the cell biology of metals. Nature Chemical Biology. 2008;4(3):168-75. Epub 2008/02/19. doi: 10.1038/nchembio.69. PubMed PMID: 18277978.

8. Que EL, Domaille DW, Chang CJ. Metals in neurobiology: probing their chemistry and biology with molecular imaging. Chemical Reviews. 2008;108(5):1517-49. Epub 2008/04/23. doi: 10.1021/cr078203u. PubMed PMID: 18426241.

9. McRae R, Bagchi P, Sumalekshmy S, Fahrni CJ. In situ imaging of metals in cells and tissues. Chemical reviews. 2009;109(10):4780-827. Epub 2009/09/24. doi: 10.1021/cr900223a. PubMed PMID: 19772288; PubMed Central PMCID: PMC3812694.

10. Carter KP, Young AM, Palmer AE. Fluorescent sensors for measuring metal ions in living systems. Chemical reviews. 2014;114(8):4564-601. Epub 2014/03/05. doi: 10.1021/cr400546e. PubMed PMID: 24588137; PubMed Central PMCID: PMC4096685.

11. Clapham DE. Calcium signaling. Cell. 2007;131(6):1047-58. Epub 2007/12/18. doi: 10.1016/j.cell.2007.11.028. PubMed PMID: 18083096.

12. Hirano T, Murakami M, Fukada T, Nishida K, Yamasaki S, Suzuki T. Roles of Zinc and Zinc Signaling in Immunity: Zinc as an Intracellular Signaling Molecule. In: Frederick WA, editor. Advances in Immunology: Academic Press; 2008. p. 149-76.

13. Gaier ED, Eipper BA, Mains RE. Copper signaling in the mammalian nervous system: synaptic effects. Journal of neuroscience research. 2013;91(1):2-19. Epub 2012/11/02. doi: 10.1002/jnr.23143. PubMed PMID: 23115049; PubMed Central PMCID: PMC3926505.

14. Rudolf R, Mongillo M, Rizzuto R, Pozzan T. Looking forward to seeing calcium. Nature reviews Molecular cell biology. 2003;4(7):579-86. Epub 2003/07/03. doi: 10.1038/nrm1153. PubMed PMID: 12838340.

15. Grienberger C, Konnerth A. Imaging calcium in neurons. Neuron. 2012;73(5):862-85. Epub 2012/03/13. doi: 10.1016/j.neuron.2012.02.011. PubMed PMID: 22405199.

16. Khan M, Goldsmith CR, Huang Z, Georgiou J, Luyben TT, Roder JC, Lippard SJ, Okamoto K. Two-photon imaging of Zn2+ dynamics in mossy fiber boutons of adult hippocampal slices. Proceedings of the National Academy of Sciences of the United States of America. 2014;111(18):6786-91. Epub 2014/04/24. doi: 10.1073/pnas.1405154111. PubMed PMID: 24757053; PubMed Central PMCID: PMC4020060.

17. Anderson CT, Radford RJ, Zastrow ML, Zhang DY, Apfel UP, Lippard SJ, Tzounopoulos T. Modulation of extrasynaptic NMDA receptors by synaptic and tonic zinc. Proceedings of the National Academy of Sciences of the United States of America. 2015;112(20):E2705-14. Epub 2015/05/08. doi: 10.1073/pnas.1503348112. PubMed PMID: 25947151; PubMed Central PMCID: PMC4443361.

18. Kay AR, Toth K. Is zinc a neuromodulator? Science signaling. 2008;1(19):re3. Epub 2008/05/16. doi: 10.1126/stke.119re3. PubMed PMID: 18480018; PubMed Central PMCID: PMC2730821.

19. Paoletti P, Vergnano AM, Barbour B, Casado M. Zinc at glutamatergic synapses. Neuroscience. 2009;158(1):126-36. Epub 2008/03/21. doi: 10.1016/j.neuroscience.2008.01.061. PubMed PMID: 18353558.

20. Perez-Rosello T, Anderson CT, Ling C, Lippard SJ, Tzounopoulos T. Tonic zinc inhibits spontaneous firing in dorsal cochlear nucleus principal neurons by enhancing glycinergic neurotransmission. Neurobiology of disease. 2015;81:14-9. Epub 2015/03/23. doi: 10.1016/j.nbd.2015.03.012. PubMed PMID: 25796568; PubMed Central PMCID: PMC4575225.

21. Opazo CM, Greenough MA, Bush AI. Copper: from neurotransmission to neuroproteostasis. Frontiers in aging neuroscience. 2014;6:143. Epub 2014/07/30. doi: 10.3389/fnagi.2014.00143. PubMed PMID: 25071552; PubMed Central PMCID: PMC4080678.

22. Kakhlon O, Cabantchik ZI. The labile iron pool: characterization, measurement, and participation in cellular processes(1). Free radical biology & medicine. 2002;33(8):1037-46. Epub 2002/10/11. PubMed PMID: 12374615.

23. Romani AM. Cellular magnesium homeostasis. Archives of biochemistry and biophysics. 2011;512(1):1-23. Epub 2011/06/07. doi: 10.1016/j.abb.2011.05.010. PubMed PMID: 21640700; PubMed Central PMCID: PMC3133480.

24. Afzal MS, Pitteloud JP, Buccella D. Enhanced ratiometric fluorescent indicators for magnesium based on azoles of the heavier chalcogens. Chemical communications. 2014;50(77):11358-61. Epub 2014/08/29. doi: 10.1039/c4cc04460f. PubMed PMID: 25164869.

25. Aschner M. Manganese homeostasis in the CNS. Environmental research. 1999;80(2 Pt 1):105-9. Epub 1999/03/27. doi: 10.1006/enrs.1998.3918. PubMed PMID: 10092401.

26. Culotta VC, Yang M, Hall MD. Manganese transport and trafficking: lessons learned from Saccharomyces cerevisiae. Eukaryotic cell. 2005;4(7):1159-65. Epub 2005/07/09. doi: 10.1128/EC.4.7.1159-1165.2005. PubMed PMID: 16002642; PubMed Central PMCID: PMC1168969.

27. Ott I, Biot C, Hartinger C. AAS, XRF, and MS Methods in Chemical Biology of Metal Complexes. Inorganic Chemical Biology: John Wiley & Sons, Ltd; 2014. p. 63-97.

28. Reynolds ES, Thiers RE, Vallee BL. Mitochondrial function and metal content in carbon tetrachloride poisoning. The Journal of biological chemistry. 1962;237:3546-51. Epub 1962/11/01. PubMed PMID: 13986421.

29. Fahrni CJ. Biological applications of X-ray fluorescence microscopy: exploring the subcellular topography and speciation of transition metals. Current opinion in chemical biology. 2007;11(2):121-7. Epub 2007/03/14. doi: 10.1016/j.cbpa.2007.02.039. PubMed PMID: 17353139.

30. Dodani SC, Domaille DW, Nam CI, Miller EW, Finney LA, Vogt S, Chang CJ. Calcium-dependent copper redistributions in neuronal cells revealed by a fluorescent copper sensor and X-ray fluorescence microscopy. Proceedings of the National Academy of Sciences of the United States of America. 2011;108(15):5980-5. Epub 2011/03/30. doi: 10.1073/pnas.1009932108. PubMed PMID: 21444780; PubMed Central PMCID: PMC3076884.

31. Bourassa D, Gleber SC, Vogt S, Yi H, Will F, Richter H, Shin CH, Fahrni CJ. 3D imaging of transition metals in the zebrafish embryo by X-ray fluorescence microtomography. Metallomics : integrated biometal science. 2014;6(9):1648-55. Epub 2014/07/06. doi: 10.1039/c4mt00121d. PubMed PMID: 24992831; PubMed Central PMCID: PMC4160025.

32. Gupta A, Bhattacharjee A, Dmitriev OY, Nokhrin S, Braiterman L, Hubbard AL, Lutsenko S. Cellular copper levels determine the phenotype of the Arg875 variant of ATP7B/Wilson disease protein. Proceedings of the National Academy of Sciences of the United States of America. 2011;108(13):5390-5. Epub 2011/03/17. doi: 10.1073/pnas.1014959108. PubMed PMID: 21406592; PubMed Central PMCID: PMC3069211.

33. Tomat E, Lippard SJ. Imaging mobile zinc in biology. Current opinion in chemical biology. 2010;14(2):225-30. Epub 2010/01/26. doi: 10.1016/j.cbpa.2009.12.010. PubMed PMID: 20097117; PubMed Central PMCID: PMC2847655.

34. Nolan EM, Lippard SJ. Small-molecule fluorescent sensors for investigating zinc metalloneurochemistry. Accounts of chemical research. 2009;42(1):193-203. Epub 2008/11/08. doi: 10.1021/ar8001409. PubMed PMID: 18989940; PubMed Central PMCID: PMC2646817.

35. Bruesehoff PJ, Li J, Augustine AJ, 3rd, Lu Y. Improving metal ion specificity during in vitro selection of catalytic DNA. Combinatorial chemistry & high throughput screening. 2002;5(4):327-35. Epub 2002/06/08. PubMed PMID: 12052183.

36. Ihms HE, Lu Y. In vitro selection of metal ion-selective DNAzymes. Methods in molecular biology. 2012;848:297-316. Epub 2012/02/09. doi: 10.1007/978-1-61779-545-9_18. PubMed PMID: 22315076; PubMed Central PMCID: PMC4162312.

37. Bassing CH, Swat W, Alt FW. The mechanism and regulation of chromosomal V(D)J recombination. Cell. 2002;109 Suppl:S45-55. Epub 2002/05/02. PubMed PMID: 11983152.

38. Schatz DG, Swanson PC. V(D)J recombination: mechanisms of initiation. Annual review of genetics. 2011;45:167-202. Epub 2011/08/23. doi: 10.1146/annurev-genet-110410-132552. PubMed PMID: 21854230.

39. Zider A, Drakeman DL. The future of monoclonal antibody technology. mAbs. 2010;2(4):361-4. Epub 2010/08/03. PubMed PMID: 20676053; PubMed Central PMCID: PMC3180083.

40. Nelson AL, Dhimolea E, Reichert JM. Development trends for human monoclonal antibody therapeutics. Nature reviews Drug discovery. 2010;9(10):767-74. Epub 2010/09/03. doi: 10.1038/nrd3229. PubMed PMID: 20811384.

41. Overkamp D, Mohammed-Ali S, Cartledge C, Landon J. Production of polyclonal antibodies in ascitic fluid of mice: technique and applications. Journal of immunoassay. 1988;9(1):51-68. Epub 1988/01/01. doi: 10.1080/01971528808053210. PubMed PMID: 3283169.

42. Kohler G, Milstein C. Continuous cultures of fused cells secreting antibody of predefined specificity. Nature. 1975;256(5517):495-7. Epub 1975/08/07. PubMed PMID: 1172191.

43. Liu JK. The history of monoclonal antibody development - Progress, remaining challenges and future innovations. Annals of medicine and surgery. 2014;3(4):113-6. Epub 2015/01/09. doi: 10.1016/j.amsu.2014.09.001. PubMed PMID: 25568796; PubMed Central PMCID: PMC4284445.

44. Michnick SW, Sidhu SS. Submitting antibodies to binding arbitration. Nature chemical biology. 2008;4(6):326-9. Epub 2008/05/20. doi: 10.1038/nchembio0608-326. PubMed PMID: 18488004.

45. Geyer CR, McCafferty J, Dubel S, Bradbury AR, Sidhu SS. Recombinant antibodies and in vitro selection technologies. Methods in molecular biology. 2012;901:11-32. Epub 2012/06/23. doi: 10.1007/978-1-61779-931-0_2. PubMed PMID: 22723092.

46. Winter G, Griffiths AD, Hawkins RE, Hoogenboom HR. Making antibodies by phage display technology. Annual review of immunology. 1994;12:433-55. Epub 1994/01/01. doi: 10.1146/annurev.iy.12.040194.002245. PubMed PMID: 8011287.

47. Marasco WA, Sui J. The growth and potential of human antiviral monoclonal antibody therapeutics. Nature biotechnology. 2007;25(12):1421-34. Epub 2007/12/11. doi: 10.1038/nbt1363. PubMed PMID: 18066039.

48. Zhou H, Wang Y, Wang W, Jia J, Li Y, Wang Q, Wu Y, Tang J. Generation of monoclonal antibodies against highly conserved antigens. PloS one. 2009;4(6):e6087. Epub 2009/07/01. doi: 10.1371/journal.pone.0006087. PubMed PMID: 19564921; PubMed Central PMCID: PMC2699554.

49. Janeway CAJ, Travers P, Walport M, Shlomchik MJ. Immunobiology. New York: Garland Science; 2001.

50. Day JW, Kim CH, Smider VV, Schultz PG. Identification of metal ion binding peptides containing unnatural amino acids by phage display. Bioorganic & medicinal chemistry letters.

2013;23(9):2598-600. Epub 2013/04/02. doi: 10.1016/j.bmcl.2013.02.106. PubMed PMID: 23541674.

51. Liu J, Cao Z, Lu Y. Functional nucleic acid sensors. Chemical reviews. 2009;109(5):1948-98. Epub 2009/03/24. doi: 10.1021/cr030183i. PubMed PMID: 19301873; PubMed Central PMCID: PMC2681788.

52. Zhang XB, Kong RM, Lu Y. Metal ion sensors based on DNAzymes and related DNA molecules. Annual review of analytical chemistry. 2011;4:105-28. Epub 2011/03/05. doi: 10.1146/annurev.anchem.111808.073617. PubMed PMID: 21370984; PubMed Central PMCID: PMC3119750.

53. Baum DA, Silverman SK. Deoxyribozymes: useful DNA catalysts in vitro and in vivo. Cellular and molecular life sciences : CMLS. 2008;65(14):2156-74. Epub 2008/04/01. doi: 10.1007/s00018-008-8029-y. PubMed PMID: 18373062.

54. Xiang Y, Lu Y. DNA as sensors and imaging agents for metal ions. Inorganic chemistry. 2014;53(4):1925-42. Epub 2013/12/24. doi: 10.1021/ic4019103. PubMed PMID: 24359450; PubMed Central PMCID: PMC3955431.

Chapter 2:

Development of a caged DNAzyme for cellular metal ion sensing

* Portions of this chapter have been previously published in *Angew. Chem.* as "Photocaged DNAzymes as a General Method for Sensing Metal Ions in Living Cells" (Hwang K., Wu P., Kim T., Lei L., Tian S., Wang Y., Lu Y.). Wu P. assisted with cell culture, Tian S. assisted in caged nucleotide synthesis and characterization, and Kim T. and Lei L. provided assistance in confocal microscopy.

2.1 Introduction

The widespread applicability of DNAzymes as metal ion sensors for environmental applications led to interest in potentially applying them as cellular sensors. However, for many years the majority of work using DNAzymes was limited purely to detection of environmental samples such as water or soil samples, with very few demonstrating detection in any biological context, whether tissue, cells, or even growth media.[1,2] The potential impact of being able to convert as-selected DNAzymes into cellular sensors is that it might enable researchers to sidestep the current difficult process of rationally designing the cellular sensor to fit all necessary properties for cellular application.[3]

Previously our group demonstrated a method for conjugating DNAzymes to a gold nanoparticle carrier (DNAzyme-AuNP), which enabled moderate serum stability and the ability to deliver the DNAzyme-AuNP conjugates to the lysosomes of HeLa cells.[4] While this approach demonstrated efficient cell uptake and retention of the UO_2^{2+}-specific activity of the 39E DNAzyme, certain limitations remained. The first was the adventitious localization of DNAzyme-AuNP conjugates to the lysosome due to the endocytic mechanism of uptake. While the 39E DNAzyme is most active under acidic conditions such as those within late endosomes or the lysosome, the majority of DNAzymes obtained so far are not optimized for activity at low pH. Moreover, being able to sense the metal ions in other compartments is of interest for many applications. The second limitation is that the DNAzyme is always active. Since many of the other metal ions of interest may be present within the extracellular environment, the DNAzyme sensor might react with those metal ions and report on the presence of metals in the extracellular

environment and not intracellular metal ions as originally intended. Finally, although the AuNP conjugation strategy afforded moderate serum stability, another major concern would be the presence of intra- or extracellular nucleases that might be able to degrade the RNA base incorporated in the DNA-RNA chimeric substrate strand.

The above-mentioned issues are not restricted to DNAzymes only and have been observed for many types of small-molecule or protein-based signals or sensors as well.[5-9] One common strategy to address undesired off-target activity of the molecule in question is to inactivate it until it reaches the desired location in the cell. There are several types of "caging" strategies to achieve this goal. Most frequently caging is achieved through attachment of a protecting group to part of the sensor that is known to be critical for the sensor's activity.[9,10] Ideally, this attachment is labile and can later be removed, or "decaged." This decaging process can be induced by a change in pH, irradiation of light, or the action of an enzyme within the cell, among many other choices.[10-15]

Light-activated caging groups are of particular interest as they can provide spatiotemporal control over the sensor.[9] Since activation by light is independent of the cellular location of the sensor, it can be generalized to all types of sensor regardless of the compartment it is ultimately transported to. Several reports are available of the design of light-activated caged compounds with significant success in providing insight or control over multiple cellular processes.[10,16,17] Although there have been reports of caging strategies to control the activity of DNAzymes,[18-22] the applicability of such techniques towards DNAzymes is limited as they often do not address both the issue of substrate RNA stability and the issue of controlling DNAzyme activity at the same time, which may explain why no other caged DNAzyme strategy had previously successfully demonstrated control over DNAzyme activity within a biological context.

In this chapter I present a strategy for caging DNAzymes with a photolabile group enabling the protection and light-controlled activation of a DNAzyme sensor. I also demonstrate that this method can be generalized well to other DNAzymes, and places no restriction on choice of DNA delivery method.

2.2 Materials and methods

2.2.1 Synthesis of 5'-O-(4,4'-dimethoxytrityl)-2'-O-(2-nitrobenzyl)-N^6-benzoyladenosine 3'-O-(2-cyanoethyl-N,N-diisopropylamino) phosphoramidite

The synthesis of the caged adenosine phosphoramidite was carried out following an established protocol[23] and characterized by ESI-MS and ^{1}H-NMR. Mass spectra of the compounds were acquired using a Waters Quattro II spectrometer operating in positive-ion mode. Samples were injected into a 50 μL/min flow of 100% CH_3CN as mobile phase and integrated over the first minute of detection.

The mass spectra were collected from 200-2000 m/z. ^{1}H-NMR spectra were carried out on a U400 FT-NMR instrument. All reactions carried out under inert atmosphere unless otherwise noted. 4,4'-dimethoxytrityl chloride was obtained from Acros Organics (Geel, Belgium) and used as received. DMF, THF, and hexanes were distilled before use; pyridine was dried over molecular sieves. All other compounds used during synthesis were obtained from Sigma-Aldrich (St. Louis, MO) and used as received.

2.2.2 Oligonucleotide synthesis

Oligonucleotides (see Table 2.1 for sequences used) were synthesized by Integrated DNA Technologies (Coralville, IA). Sequences were synthesized on 1 μmol scale and were obtained with HPLC purification, then used without further purification. To standardize stock solution concentration, UV-Vis measurements at 260 nm were obtained using a Hewlett-Packard 8453 spectrophotometer. Absorption spectra were obtained on the same instrument.

Table 2.1 DNA sequences used

Name	**Sequence (5' to 3')**
Caged substrate	/56-FAM/ACT CAC TAT /iNiBenz-rA/GG AAG AGA TGG ACG TG/3-BHQ1/
Unmodified substrate	/56-FAM/ACT CAC TAT rAGG AAG AGA TGG ACG TG/3-BHQ1/
Active 8-17E	/5ThioMC6-D/CAC GTC CAT CTC TTC TCC GAG CCG GTC GAA ATA GTG AGT/3Dab/
Inactive 8-17E	/5ThioMC6-D/CAC GTC CAT CTC TTC TCC GGC CCG GTC GAA ATA GTG AGT/3Dab/
GR-5E	/5ThioMC6-D/CAC GTC CAT CTC TGA AGT AGC GCC GCC GTA TAG TGA GT/3Dab/

All sequences were obtained from IDT (Coralville, IA) and use the following notation:

/iNiBenz-rA/ = internal 2'-nitrobenzyl-caged adenosine (described above)

/56-FAM/ = Fluorescein

/3-BHQ1/ = Black Hole Quencher-1

/5ThioMC6-D/ = thiol linker (used to cap 5' end of enzyme strand)

/3Dab/ = Dabcyl

2.2.3 Fluorescence response and measurement

Equal concentrations of enzyme and substrate strands were added to a buffer solution (50 mM Tris, 100 mM NaCl, pH 7.4) and heated to 80 °C for 5 minutes, then removed from heat and allowed to cool to room temperature to anneal.

Fluorescence measurements were obtained on a HORIBA Jobin Yvon FluoroMAX-P using 488 nm excitation and 518 nm emission. Fluorescence spectra were collected on the same instrument, from 500-650 nm using 488 nm excitation; DNAzyme concentration used was 25 nM. To start the reaction $Zn(NO_3)_2$ was added to a final concentration of 50 μM while vortexing. Irradiation of the DNAzymes was carried out using a Spectroline hand lamp on the long-wavelength (365 nm) setting.

Decaging efficiency of both 8-17 and GR-5 DNAzymes were assessed using polyacrylamide gel electrophoresis (PAGE). DNAzyme reactions were initiated with addition of Zn^{2+} or Pb^{2+}, and quenched at specific time points using a stop solution containing 8 M urea and 50 mM EDTA. Samples were loaded onto 20% polyacrylamide gels and run for 1.5-2 hours at 35 W to separate cleaved from uncleaved fragments. Fluorescence of the 5'-FAM tag was measured using a STORM 840 optical scanner using 450 nm excitation.

2.2.4 Measurement of decaging efficiency

Caged DNAzymes were annealed as before, except in PBS buffer solution. DNAzymes were diluted to a concentration of 2 μM in a well of a 24-well plate (surface area ~200 mm^2) and irradiated with 365 nm light from either a Spectroline hand lamp on the long-wavelength (365 nm) setting or Blak-Ray B100 365 nm lamp. Aliquots were removed at various timepoints up to 30 minutes. Decaging efficiency was measured using HPLC instrumentation at the Roy J. Carver Biotechnology Center (UIUC, Urbana, IL) equipped with a 3.5 μm SunFire C_{18} column (Waters) following the following program: 0-3 min, 14%B; 3-15 min, 14-32%B; 15-20 min, 32-60%B, 20-22 min, 60-14%B; 22-33 min, 14%B using the following buffers:

Buffer A = 1 L Millipore water + 10 mL 1 M triethylamonium acetate (TEAA) (final 10 mM TEAA)

Buffer B = 800 mL acetonitrile + 200 mL Millipore water + 2 mL 1 M TEAA

Flow rate 0.2 mL/min throughout.

Decaged substrate eluted at 19.6 min, caged substrate at 20.2 min. Peaks were integrated to determine decaging efficiency.

2.2.5 Cell culture

HeLa cells were cultured in Dulbecco's Modified Eagle's Medium (DMEM) media supplemented with 10% fetal bovine serum (FBS), 100 U/mL penicillin, and 100 µg/mL streptomycin solution (Cell Media Facility, UIUC), and were incubated at 37 °C in a humidified 5% CO_2 environment. Cells were subcultured every 3 days, and cultures were restarted from frozen stocks after 30 passages. For microscopy, cells were passed into 35 mm glass-bottom petri dishes (MatTek) in growth media lacking penicillin/streptomycin and grown to 70-90% confluence before imaging.

2.2.6 Long-term stability

Caged and unmodified DNAzymes were annealed in buffer by heating to 80 °C for 5 minutes and cooling to room temperature. Reactions were initiated by adding annealed 8-17 DNAzyme into a solution containing 50 µM Zn^{2+} or containing 80% human serum, and terminated at specific time points by adding aliquots into equal volumes of a stop solution containing 8 M urea and 50 mM EDTA. Extent of degradation was measured using PAGE, as before.

2.2.7 Imaging

Cells grown in glass-bottom plates were transfected using Lipofectamine 2000 reagent (Invitrogen) using a modification of manufacturer's protocols. Caged active or inactive DNAzymes were annealed by heating to 80 °C for 5 minutes and cooling to room temperature. Lipofectamine 2000 (5 µL) and annealed DNAzymes (1 nmol) were incubated separately in Opti-MEM media (Invitrogen) for 5 minutes, then combined and allowed to incubate for an additional 25 minutes. The prepared DNAzyme-Lipofectamine mixture was added to HeLa cells and allowed to incubate for 11 hours. Cells were also stained with

Hoechst 33258 (Sigma) at a final concentration of 2.5 ng/mL for 30 minutes. After incubation, cells were washed several times with PBS and covered with DMEM without FBS or antibiotics.

Images were obtained using a Zeiss LSM 710 NLO confocal microscope at 40x magnification equipped with a Mai-Tai Ti-Sapphire laser, using the ZEN software suite (Zeiss). Fluorescence emission was measured over a 500-550 nm range, with excitation at 488 nm, respectively. The pinhole and gain settings were kept constant throughout the whole imaging process.

Cells were irradiated at 365 nm with a Spectroline hand lamp while on the microscope stage. 50 μM zinc was added afterwards, also on the microscope stage, as the citrate salt. Individual cells showing response were chosen for further analysis. Quantification was carried out with the ImageJ software (NIH, Bethesda, MD, USA) and is represented as fold-change relative to starting fluorescence level.

To analyze subcellular localization, another set of images was obtained on a Nikon eclipse microscope using MetaFluor 6.2 and MetaMorph software (Universal Imaging) with a 420DF20 excitation filter, a 450DRLP dichroic mirror, and two emission filters controlled by a filter changer (475DF40 for ECFP and 535DF25 for YPet). The microscope was equipped with an environmental chamber that is temperature controlled at 37 °C and contains humidified 5% CO_2 air. Cells transfected with caged active or caged inactive DNAzymes as before were imaged every 30 seconds using YFP filter settings (495 nm excitation/535 nm emission). Delivered DNAzymes were decaged using 340 nm irradiation (using a Fura2 excitation filter) at maximum light intensity for 5 seconds, then regularly imaged for 5 minutes. Zinc was added on the microscope stage to a final concentration of 50 μM as the pyrithione salt and fluorescence monitored for an additional 10 minutes. Cellular regions of interest were defined in MetaMorph within the nucleus (as determined by colocalization with Hoechst 33258 staining) and within the cytoplasm. Quantification was carried out with MetaMorph and is represented as fold-change relative to starting fluorescence level.

2.3 Results and discussion

2.3.1 Catalytic beacon and design of the photoactivation system

Based on previous work using RNA-cleaving DNAzymes, the basic design of the catalytic beacon sensor is shown in Figure 2.1. In this scheme, the enzyme strand (containing the DNAzyme catalytic core) and substrate strand (containing a single RNA base) are represented as black lines. In the absence of the specific metal ion cofactor, the two strands remain hybridized at both binding regions (binding arms)

by normal Watson-Crick base pairing; the melting temperature for enzyme and substrate hybridization is above the appropriate working temperature for the application of interest (for environmental detection applications, typically ~ 25 °C). While hybridized, the fluorophore on the substrate strand and a quencher moiety on the enzyme strand are in close proximity and the sensor fluorescence is thus suppressed. However, in the presence of the metal ion cofactor, the RNA base in the substrate strand is cleaved. After cleavage, the substrate strand's binding arms are unable to remain hybridized due to the lowered melting temperature of each individual arm. As a result, the fragments dehybridize, spatially separating the fluorophore and quencher and producing a turn-on fluorescent signal.

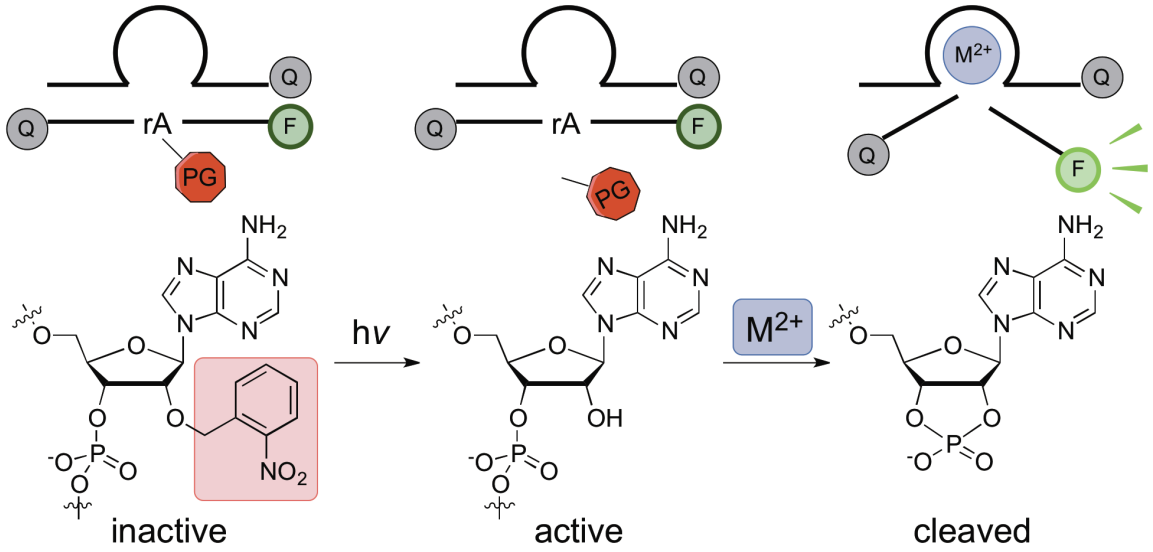

Figure 2.1. Schematic showing catalytic beacon photocaging strategy. The 2' hydroxyl is modified with a protecting group which can be removed with light to restore the native 2'-OH functionality critical for metal-dependent activity.

The strategy for photoactivation of the DNAzyme sensor was focused on the 2'-hydroxyl moiety at the RNA cleavage site. This functional group is known to be critical for DNAzyme activity, and removal of this group (by substitution with a 2'-H moiety, as in the RNA-to-DNA substitution) is known to abolish DNAzyme activity. It is also known that modifications of the 2'-hydroxyl group such as the 2'-methoxy or 2'-fluoro groups are commonly used to stabilize RNA for biological delivery (for RNAi or gene therapy applications). Consequently I rationalized that controllable modification at this location might enable control over DNAzyme activity.

The other major component necessary for this strategy was the choice of an appropriate controllable functionality. Light-removable protecting groups have been previously used for the activation of proteins, organic compounds, and oligonucleotides.[9,12,14,16] They have also been used for controlling the activity of DNAzymes.[18-22] However, previously published methods for DNAzyme photoactivation are unable to

simultaneously control both activity of the DNAzyme and stability of the substrate strand, which is critical for cellular application of DNAzymes as metal ion sensors.

2.3.2 Synthetic characterization

The synthesis of the caged adenosine phosphoramidite was carried out following an established protocol[23] and characterized by ESI-MS and ^{1}H-NMR. The synthetic route is shown in Figure 2.2.

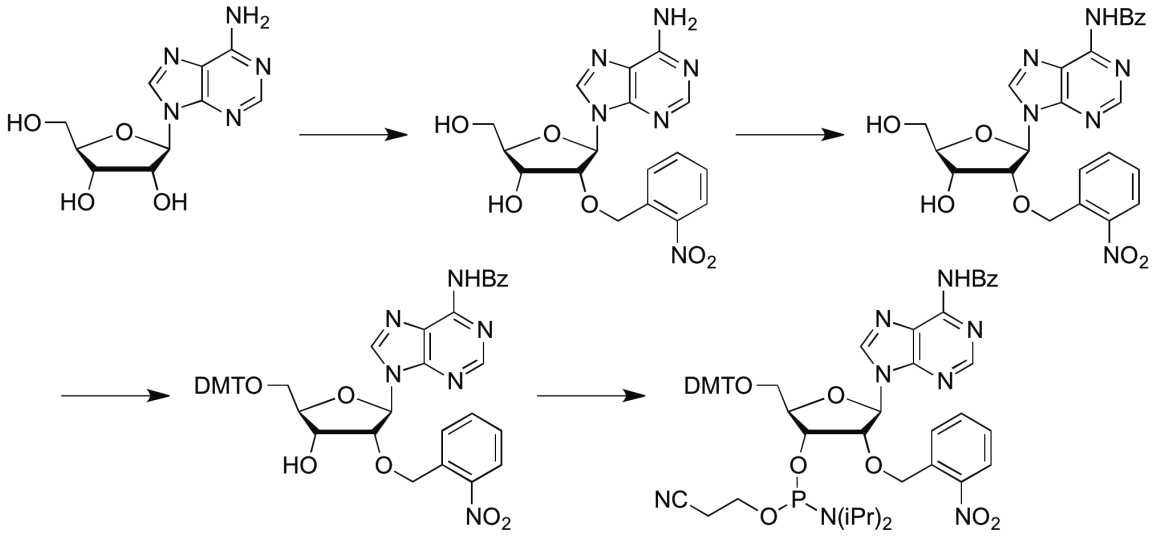

Figure 2.2. Synthetic strategy for oNB-caged adenosine phosphoramidite**.** Synthetic scheme adapted from Ref. 23.[23]

Synthesis of each intermediate product was confirmed by ESI-MS (Figure 2.3) and ^{1}H NMR spectra were in agreement with previously published values. Mass spectral analysis indicated the presence of fragmentation products at $[M-135]^{+}$ corresponding to loss of nitrobenzyl group, and in the case of the final product peaks at $[M-83]^{+}$ and $[M-406]^{+}$ corresponding to hydrolysis of the $N(iPr)_2$ acid and simultaneous loss of $N(iPr)_2$ and dimethoxytrityl groups, respectively.

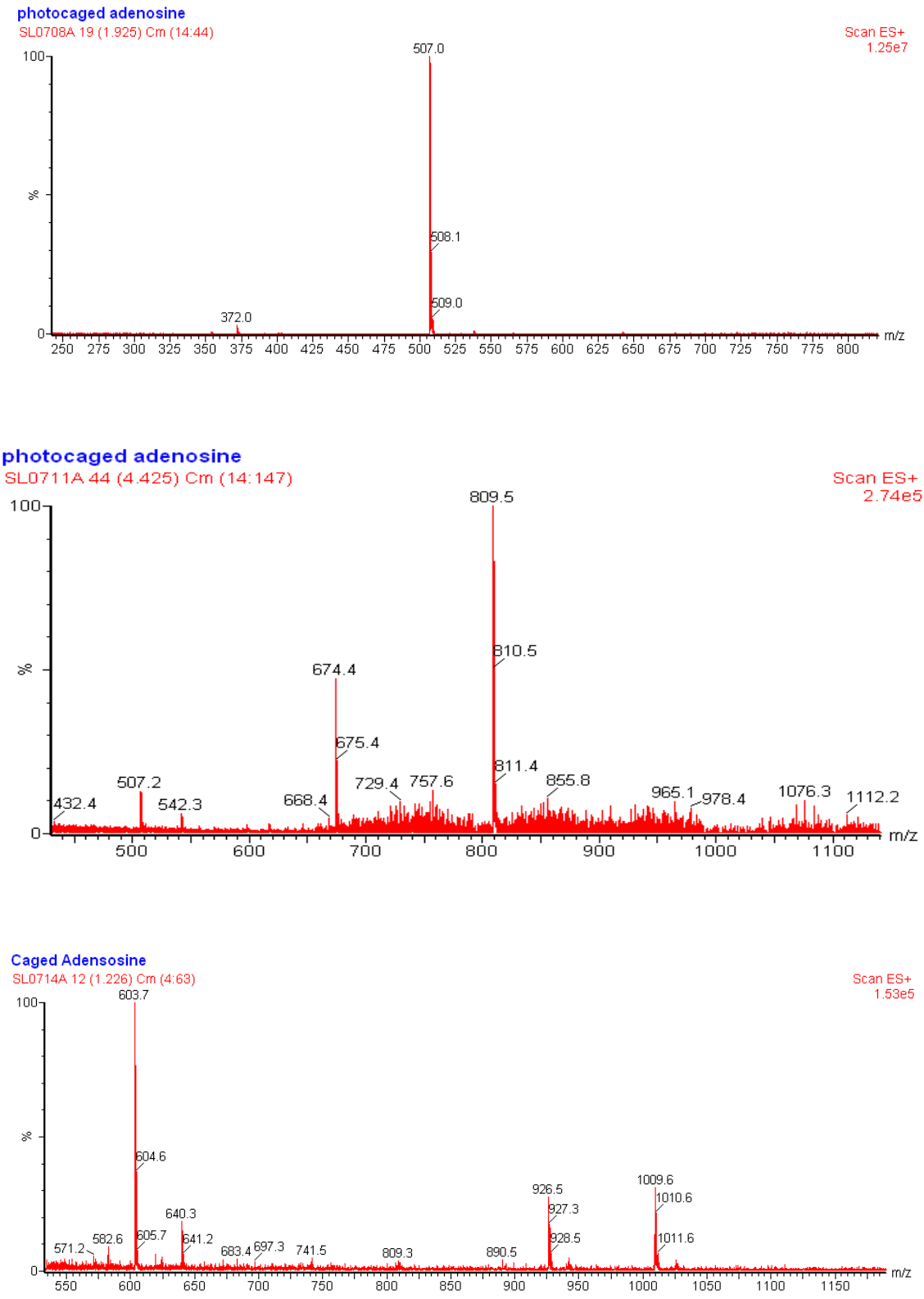

Figure 2.3. Characterization of (a) 2'-O-(2-nitrobenzyl)-N^6-benzoyladenosine, expected mass: 507.1628; (b) 5'-O-(4,4'-dimethoxytrityl)-2'-O-(2-nitrobenzyl)-N^6-benzoyladenosine, expected mass: 809.29347; (c) 5'-O-(4,4'-dimethoxytrityl)-2'-O-(2-nitrobenzyl)-N^6-benzoyladenosine 3'-O-(2-cyanoethyl-N,N-diisopropylamino) phosphoramidite, expected mass: 1009.4013

2.3.3 Characterization of sensor properties

After synthesis of the phosphoramidite, the 2'-nitrobenzyl-functionalized adenosine base was incorporated in place of the riboadenosine base of a standard DNAzyme substrate strand by standard solid-phase oligonucleotide synthesis (Integrated DNA Technologies, Coralville, IA). DNA sequences used are found in Table 2.1. Both caged and decaged substrate strands were assessed by UV-Vis and fluorescence (in the case of the FAM-labeled strands) spectroscopy. (Figure 2.4) Although it is not possible to resolve the photoremovable nitrobenzyl group by UV-Vis due to the large UV absorbance peak of DNA (nitrobenzyl $\varepsilon = 3700\ mol^{-1}cm^{-1}$, versus ~300000 for substrate strand alone[23]), an increase in mass is observed by MALDI-MS, indicating successful incorporation of the nitrobenzyl moiety. The fluorescence spectrum of a FAM-labeled caged substrate shows no change in the expected fluorescence properties of the attached dye.

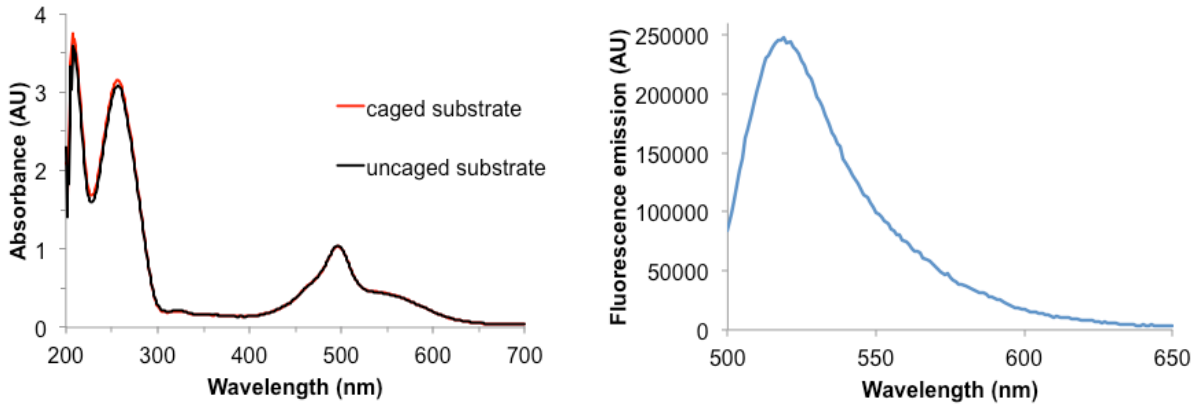

Figure 2.4. (left) UV-Vis absorbance and (right) fluorescence spectra of caged substrate

The performance of the photocaged DNAzyme was first assessed in a buffer under physiological conditions. The substrate strand containing either caged adenosine or native adenosine was annealed to the enzyme strand. The DNAzyme reaction was initiated with the addition of 50 μM Zn^{2+}. In the absence of 365 nm light, the fluorescent signal increased rapidly only in the case of the unmodified substrate containing the native adenosine (Figure 2.5), similar to those observed previously. In contrast, when the substrate strand containing the caged adenosine was used, no increase in fluorescent signal was observed, indicating complete inhibition of DNAzyme activity.

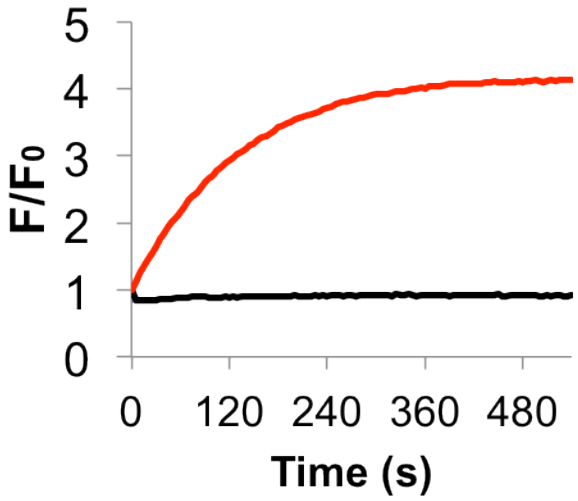

Figure 2.5. Zinc response of caged (black) and decaged (red) sequences to 50 μM Zn^{2+}

To confirm that activity was due to the Zn^{2+}-specific catalysis of the DNAzyme, an inactive sequence in which an AG dinucleotide sequence within the predicted loop region of the 8-17 DNAzyme is mutated to GC was also tested under the same conditions. Compared to the active enzyme sequence, no fluorescent response is observed after Zn^{2+} addition, indicating a lack of nonspecific Zn^{2+}-induced activity (Figure 2.6).

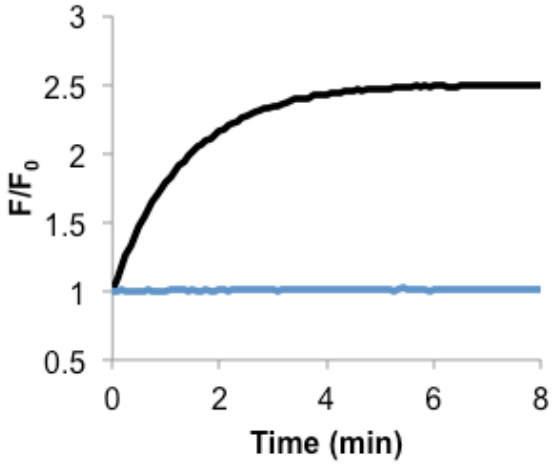

Figure 2.6. Zinc response of active (black) and inactive (blue) 8-17 DNAzyme sequences to 50 μM Zn^{2+}

To test whether the protective effect of the 2'-O-nitrobenzyl PG could be reversed with light activation, we used both a portable hand lamp (Spectroline, 365 nm) and a Blak-Ray B100 365 nm lamp to irradiate samples of the caged 8-17 DNAzyme for different amount of time. While no fluorescent signal increase was observed in the absence of light, the fluorescent signal showed an increase with time after addition of metal ions (Figure 2.7). Longer exposure to 365 nm light led to greater increase in fluorescent signal. (Figure 2.7). These results strongly suggest that the DNAzyme activity can be restored after light activation: the longer the exposure to light, the more active DNAzyme was uncovered and thus more fluorescent signal increase could be observed.

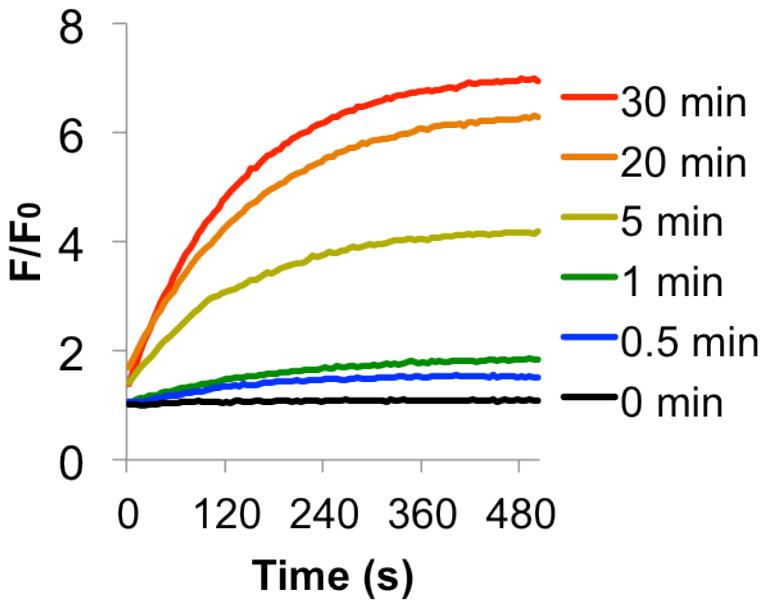

Figure 2.7. Zinc response of caged DNAzyme after 365 nm irradiation for indicated times (Spectroline hand lamp)

The same conclusion can be drawn from the results of polyacrylamide gel electrophoresis (PAGE, Figure 2.8).

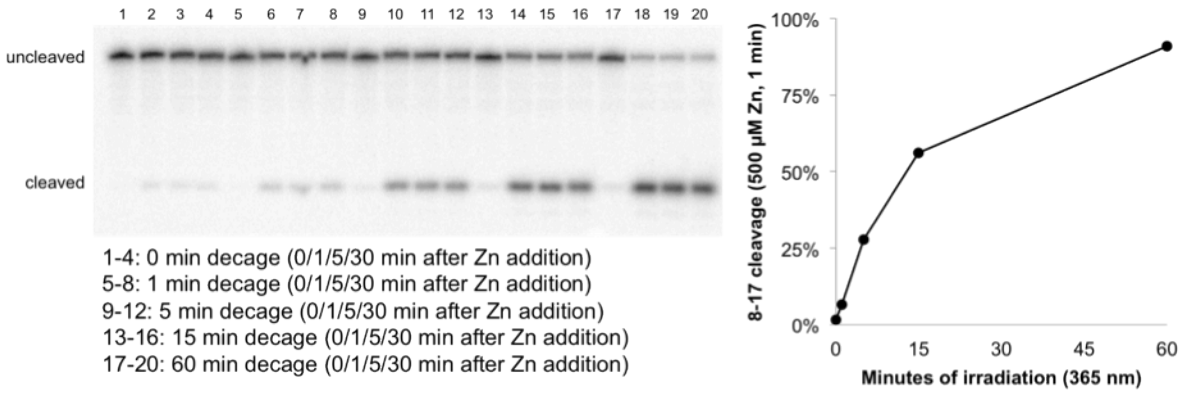

Figure 2.8. 365 nm-induced decaging of caged DNAzyme assessed by polyacrylamide gel electrophoresis.

The activity assays above are an indirect measure of DNAzyme decaging. HPLC separation of caged DNAzyme substrate photoproducts was carried out in order to directly assess the rate of decaging using different light sources (Figure 2.9). A Blak-Ray B100 and Spectroline hand lamp were tested and results were in agreement with the results of previous indirect methods.

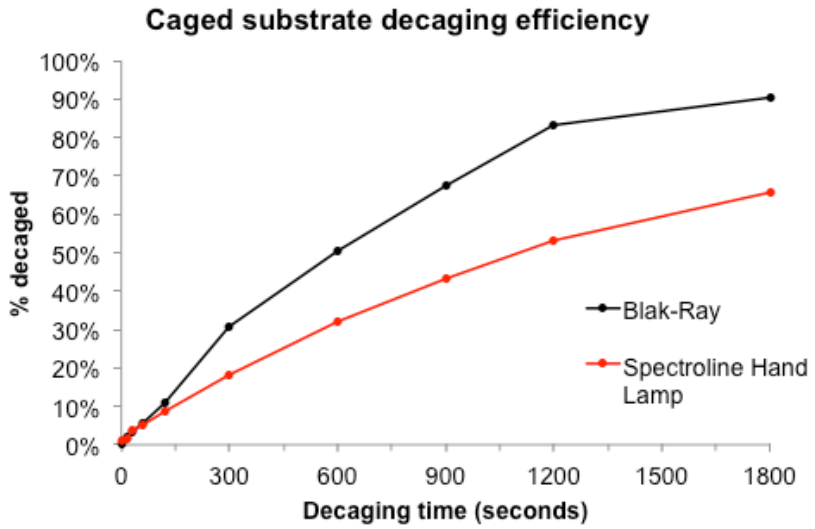

Figure 2.9. UV decaging efficiency profile using different light sources.

For biological applications, the stability of the 2'-protecting group is paramount. To test the stability of caged DNAzymes, substrates containing either caged or native adenosine were annealed to the DNAzyme strand and incubated in either buffer containing 50 µM Zn^{2+} or 80% human serum for extended periods of time. PAGE analysis revealed that the substrate containing the native adenosine was cleaved in <1 hour

under both conditions, but little cleavage was observed even at times up to 7 days in the presence of 50 μM Zn^{2+}, or 2 days in the presence of human serum (Figure 2.10).

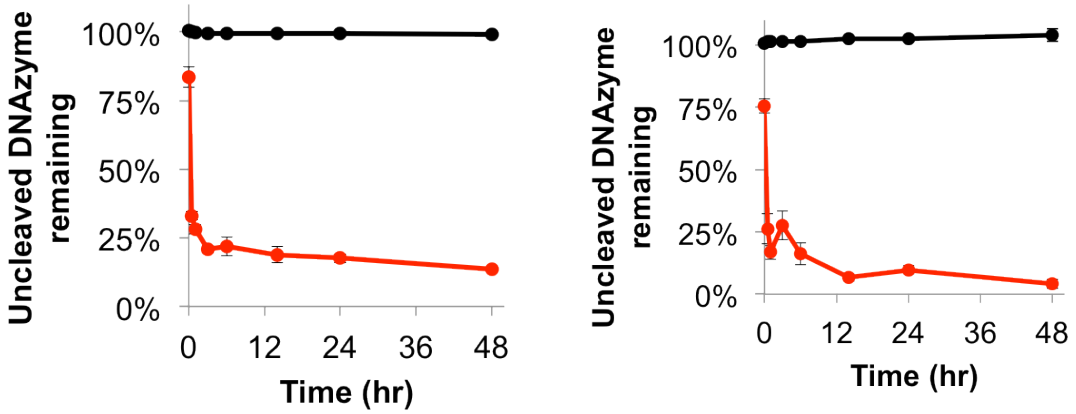

Figure 2.10. (a) Long-term stability of caged (black) and unmodified (red) 8-17 DNAzymes in presence of 50 μM Zn^{2+} (b) Long-term stability of caged (black) and unmodified (red) 8-17 DNAzymes in 80% human serum.

2.3.4 Cell delivery and activation

Having demonstrated that the caged DNAzymes are stable, we then proceeded to use the caged DNAzymes for sensing metal ions within cultured HeLa cells, using the Zn^{2+}-responsive 8-17 DNAzyme as our model system. Zinc is present in both cells and growth media, thus the cell-delivery process itself poses a major challenge because the presence of endogenous Zn^{2+} can promote DNAzyme-based cleavage of the substrate strand before the DNAzyme can be delivered to the interior of the cells, in the absence of a protection strategy. The 8-17 DNAzyme containing the caged adenosine was delivered to HeLa cells *via* Lipofectamine 2000 following a modification of manufacturer's protocols. Briefly, enzyme and caged substrate strands were heated to 80 °C and allowed to anneal. Lipofectamine 2000 (5 μL) and annealed DNAzymes (1 nmol) were incubated separately in Opti-MEM media (Invitrogen) for 5 minutes, then combined and allowed to incubate for an additional 25 minutes. The prepared DNAzyme-Lipofectamine mixture was added to HeLa cells and allowed to incubate for several hours. Confocal microscopy images of the cells transfected with DNAzyme (Figure 2.11) showed that the fluorescent DNAzyme was delivered inside the cells, in a diffuse staining pattern mainly localized in the nucleus (determined by colocalization with Hoechst stain). This distribution pattern is in agreement with previous reports demonstrating nuclear accumulation of DNA delivered via cationic liposomes (Lipofectamine PLUS).[24] To localize the DNAzyme probe into other organelles, alternative delivery methods can be used, such as the use of gold nanoparticles for lysosomal distribution.[4]

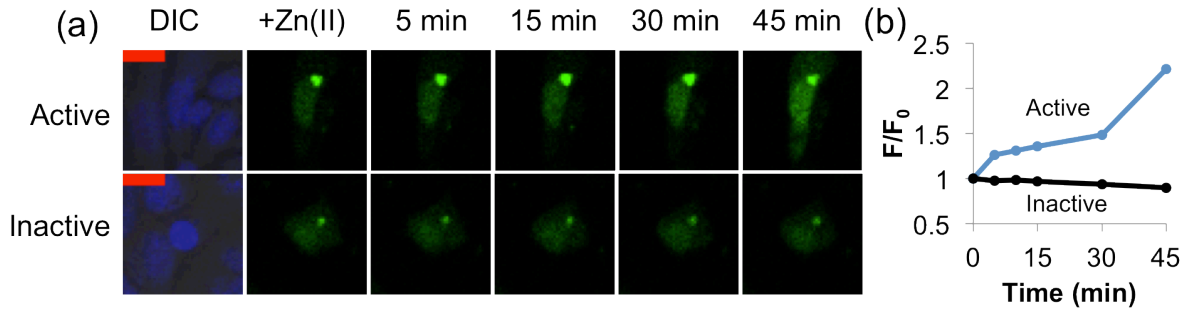

Figure 2.11. (a) HeLa cells transfected with caged active or caged inactive 8-17 DNAzyme (0.5 µM) for 11 hr, then irradiated for 30 m at 365 nm (Spectroline hand lamp), followed by addition of 50 µM Zn citrate. DIC shows cell morphology, with Hoechst 33258 stain overlay. Scale bar = 20 µm. (b) Normalized fluorescence intensity of cells shown in part (a).

Upon irradiation with a 365 nm lamp, followed by Zn^{2+}-citrate addition, an increase in fluorescence intensity was observed with time (Figure 2.11b). To confirm that the observed increase in fluorescence was caused by DNAzyme activity and not nonspecific cleavage by other cellular components, we again used the inactive DNAzyme sequence previously demonstrated to lack Zn^{2+}-specific activity.[25] Within cells, the inactive DNAzyme showed no significant increase in fluorescence over 45 minutes (Figure 2.11), confirming that the observed signal is related to DNAzyme-specific Zn^{2+} activity. Together, these results strongly indicate that the caged DNAzyme can be used to detect and image metal ions in living cells.

2.3.5. Subcellular localization

I investigated whether the DNAzyme delivery method used here (Lipofectamine) would lead to adventitious subcellular localization and whether functionality was retained throughout the cell. Using another confocal microscope setup, HeLa cells transfected with DNAzymes for 24h were tracked regularly for 15 minutes, including brief decaging at 340 nm and for 10 minutes after Zn^{2+} addition as the pyrithione salt. A diffuse localization of fluorescence was observed within the cell, with higher intensity in nuclear regions (as determined by colocalization with Hoechst 33258 staining) (Figure 2.12.a). This is in agreement with other studies on the subcellular fate of intracellularly introduced DNAzymes. A fluorescence turn-on ratio of approximately 1.2 was consistently observed in both nuclear and cytoplasmic regions, and was not observed in cells transfected with inactive caged DNAzymes (Figure 2.12.b).

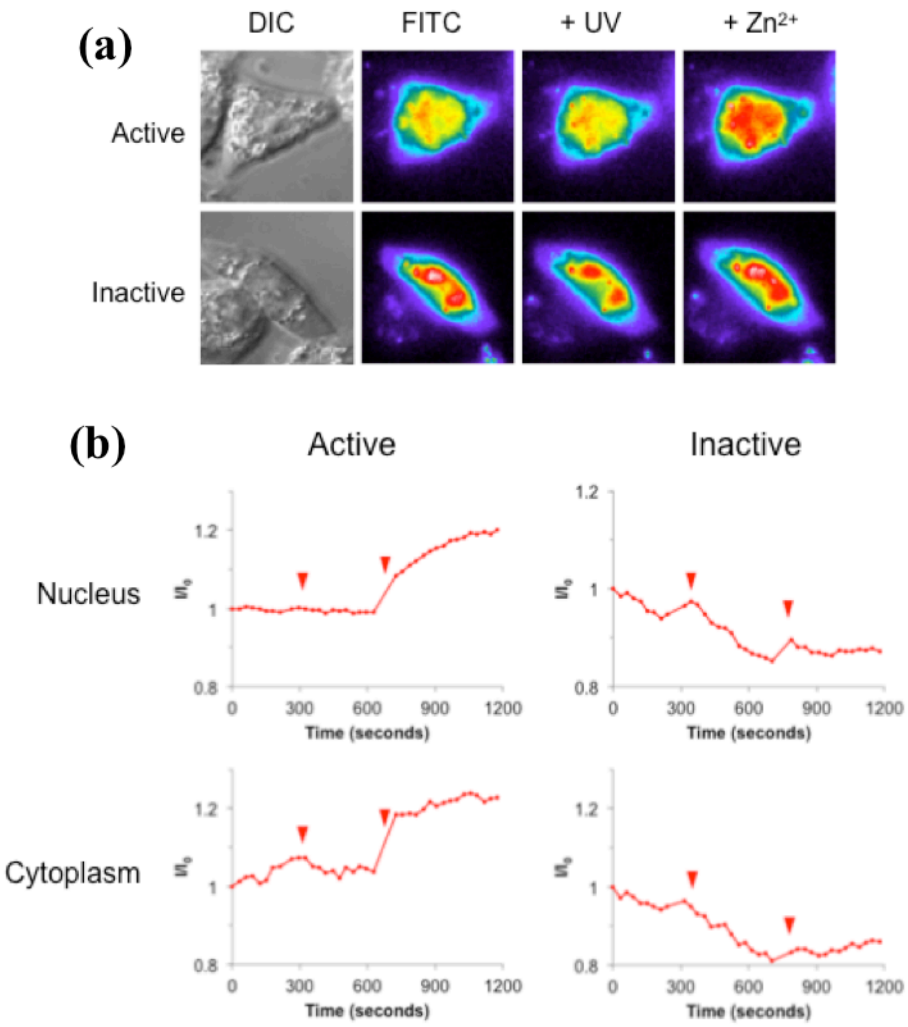

Figure 2.12. Organelle-specific timecourses. (a) Images of HeLa cells transfected for 18 hr. with 0.125 nmol caged active or caged inactive DNAzymes. DIC shows cellular structure, FITC shows initial fluorescence, "+UV" fluorescence 5 minutes after decaging at 340 nm, and "+Zn" 10 minutes after subsequent addition of 50 µM zinc as pyrithione salt. (b) Nuclear and cytoplasmic ROIs of cells transfected with caged active or caged inactive DNAzymes were defined and normalized fluorescence within the ROI plotted. Red wedges indicate UV irradiation and Zn^{2+} addition, in order.

2.3.6 Generalizability

After demonstrating the use of 8-17 DNAzyme for cellular sensing and imaging of Zn^{2+}, I investigated whether such a method could be applied generally to other DNAzymes for detection of their respective target metal ions as well. Since the first discovery of DNAzymes in 1994 using *in vitro* selection, many DNAzymes have been obtained using similar selection methods. As a result, the majority of currently identified DNAzymes share a similar secondary structure consisting of two double stranded

DNA binding arms flanking the cleavage site. More interestingly, the sequence identity of the two binding arms are not conserved, as long as they can form Watson-Crick base pairs with the chosen substrate. The metal ion selectivity of DNAzymes comes from the sequence identity of the loop in the enzyme strand. As a result, the exact substrate sequence that can be recognized by a DNAzyme can be arbitrarily chosen. This feature also allows multiple DNAzymes to recognize the same substrate sequence (Figure 2.13.a-b). An attractive advantage of our photocaging strategy is that we can use the same caged substrate strand to achieve sensing of different metal ions by using different enzyme strands. To demonstrate this advantage, we synthesized a DNAzyme sequence that can hybridize to the same caged substrate strand as the 8-17 DNAzyme, but contains the catalytic loop of the GR-5 DNAzyme, (the first DNAzyme, obtained in 1994), which has significant activity in the presence of Pb^{2+} but not with any other metal ions.[26] As shown in Figure 2.13.c-d, the caged GR-5 DNAzyme showed little cleavage activity in the absence of light activation, but increasing dose-dependent increase of DNAzyme activity upon light activation.

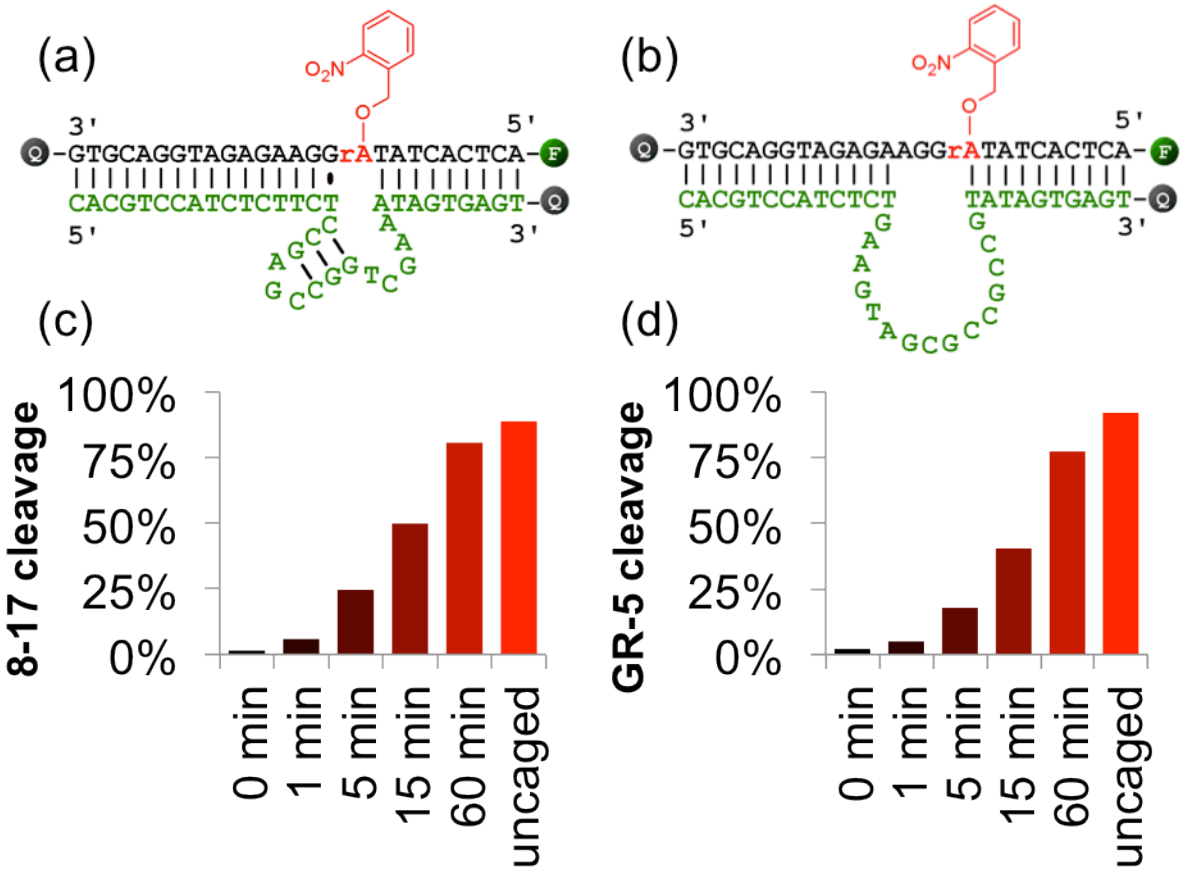

Figure 2.13. Generalizability of caging strategy. (a) Schematic showing hybridization of different DNAzymes (a: 8-17 and b: GR-5) to the same caged substrate strand. Caged and decaged (c) 8-17 and (d) GR-5 activity in presence of Zn^{2+} (8-17, 500 μM) or Pb^{2+} (GR-5, 2 μM).

2.4 Summary and conclusions

In conclusion, I have demonstrated a general and effective strategy for protecting the substrate of a DNAzyme sensor, enabling its delivery into cells without being cleaved during the process, and allowing it to be used as a cellular metal ion sensor upon photoactivation. This strategy provides enhanced stability (up to multiple days in serum) and allows temporal control over DNAzyme activity. As the only modification to the original DNAzyme is on the substrate strand, one can replace the enzyme strand without needing to re-optimize for each new substrate sequence, greatly improving the generalizability of this protection strategy. Furthermore, the enhanced stability of the caged DNAzyme does not require the use of a specific nanomaterial vehicle as a delivery agent, further demonstrating the wider accessibility of this protection approach. This work will greatly expand the applicability of DNAzymes as versatile biosensors and will improve the field of metal ion sensing.

2.5 References

1. Liu J, Cao Z, Lu Y. Functional nucleic acid sensors. Chemical reviews. 2009;109(5):1948-98. Epub 2009/03/24. doi: 10.1021/cr030183i. PubMed PMID: 19301873; PubMed Central PMCID: PMC2681788.

2. Zhang XB, Kong RM, Lu Y. Metal ion sensors based on DNAzymes and related DNA molecules. Annual review of analytical chemistry. 2011;4:105-28. Epub 2011/03/05. doi: 10.1146/annurev.anchem.111808.073617. PubMed PMID: 21370984; PubMed Central PMCID: PMC3119750.

3. Torabi SF, Lu Y. Functional DNA nanomaterials for sensing and imaging in living cells. Current opinion in biotechnology. 2014;28:88-95. Epub 2014/01/29. doi: 10.1016/j.copbio.2013.12.011. PubMed PMID: 24468446; PubMed Central PMCID: PMC4110194.

4. Wu P, Hwang K, Lan T, Lu Y. A DNAzyme-gold nanoparticle probe for uranyl ion in living cells. Journal of the American Chemical Society. 2013;135(14):5254-7. Epub 2013/03/28. doi: 10.1021/ja400150v. PubMed PMID: 23531046; PubMed Central PMCID: PMC3644223.

5. Walker JW, Somlyo AV, Goldman YE, Somlyo AP, Trentham DR. Kinetics of smooth and skeletal muscle activation by laser pulse photolysis of caged inositol 1,4,5-trisphosphate. Nature. 1987;327(6119):249-52. Epub 1987/05/21. doi: 10.1038/327249a0. PubMed PMID: 3494954.

6. Matsuzaki M, Ellis-Davies GC, Nemoto T, Miyashita Y, Iino M, Kasai H. Dendritic spine geometry is critical for AMPA receptor expression in hippocampal CA1 pyramidal neurons. Nature neuroscience. 2001;4(11):1086-92. Epub 2001/11/01. doi: 10.1038/nn736. PubMed PMID: 11687814; PubMed Central PMCID: PMC4229049.

7. Nguyen A, Rothman DM, Stehn J, Imperiali B, Yaffe MB. Caged phosphopeptides reveal a temporal role for 14-3-3 in G1 arrest and S-phase checkpoint function. Nature biotechnology. 2004;22(8):993-1000. Epub 2004/07/27. doi: 10.1038/nbt997. PubMed PMID: 15273693.

8. Gwizdala C, Burdette SC. Following the Ca(2)(+) roadmap to photocaged complexes for Zn(2)(+) and beyond. Current opinion in chemical biology. 2013;17(2):137-42. Epub 2012/12/29. doi: 10.1016/j.cbpa.2012.11.015. PubMed PMID: 23270780.

9. Ellis-Davies GC. Caged compounds: photorelease technology for control of cellular chemistry and physiology. Nature methods. 2007;4(8):619-28. Epub 2007/08/01. doi: 10.1038/nmeth1072. PubMed PMID: 17664946; PubMed Central PMCID: PMC4207253.

10. Lee S, Xie J, Chen X. Activatable molecular probes for cancer imaging. Current topics in medicinal chemistry. 2010;10(11):1135-44. Epub 2010/04/15. PubMed PMID: 20388112; PubMed Central PMCID: PMC3629980.

11. Pelliccioli AP, Wirz J. Photoremovable protecting groups: reaction mechanisms and applications. Photochemical & photobiological sciences : Official journal of the European Photochemistry Association and the European Society for Photobiology. 2002;1(7):441-58. Epub 2003/03/28. PubMed PMID: 12659154.

12. Klan P, Solomek T, Bochet CG, Blanc A, Givens R, Rubina M, Popik V, Kostikov A, Wirz J. Photoremovable protecting groups in chemistry and biology: reaction mechanisms and efficacy. Chemical reviews. 2013;113(1):119-91. Epub 2012/12/22. doi: 10.1021/cr300177k. PubMed PMID: 23256727; PubMed Central PMCID: PMC3557858.

13. Chan J, Dodani SC, Chang CJ. Reaction-based small-molecule fluorescent probes for chemoselective bioimaging. Nature chemistry. 2012;4(12):973-84. Epub 2012/11/24. doi: 10.1038/nchem.1500. PubMed PMID: 23174976; PubMed Central PMCID: PMC4096518.

14. Deiters A. Principles and Applications of the Photochemical Control of Cellular Processes. ChemBioChem. 2010;11(1):47-53. doi: 10.1002/cbic.200900529.

15. Urano Y, Asanuma D, Hama Y, Koyama Y, Barrett T, Kamiya M, Nagano T, Watanabe T, Hasegawa A, Choyke PL, Kobayashi H. Selective molecular imaging of viable cancer cells with pH-activatable fluorescence probes. Nature medicine. 2009;15(1):104-9. Epub 2008/11/26. doi: 10.1038/nm.1854. PubMed PMID: 19029979; PubMed Central PMCID: PMC2790281.

16. Elias DR, Thorek DL, Chen AK, Czupryna J, Tsourkas A. In vivo imaging of cancer biomarkers using activatable molecular probes. Cancer biomarkers : section A of Disease markers. 2008;4(6):287-305. Epub 2009/01/08. PubMed PMID: 19126958.

17. Wirz J. Photoremovable protecting groups: development and applications. Photochemical & photobiological sciences : Official journal of the European Photochemistry Association and the European Society for Photobiology. 2012;11(3):445. Epub 2012/02/22. doi: 10.1039/c2pp90005j. PubMed PMID: 22344622.

18. Ting R, Lermer L, Perrin DM. Triggering DNAzymes with light: a photoactive C8 thioether-linked adenosine. Journal of the American Chemical Society. 2004;126(40):12720-1. Epub 2004/10/08. doi: 10.1021/ja046964y. PubMed PMID: 15469235.

19. Keiper S, Vyle JS. Reversible photocontrol of deoxyribozyme-catalyzed RNA cleavage under multiple-turnover conditions. Angewandte Chemie. 2006;45(20):3306-9. Epub 2006/04/19. doi: 10.1002/anie.200600164. PubMed PMID: 16619331.

20. Lusic H, Young DD, Lively MO, Deiters A. Photochemical DNA activation. Organic letters. 2007;9(10):1903-6. Epub 2007/04/24. doi: 10.1021/ol070455u. PubMed PMID: 17447773; PubMed Central PMCID: PMC2532984.

21. Richards JL, Seward GK, Wang YH, Dmochowski IJ. Turning the 10-23 DNAzyme on and off with light. Chembiochem : a European journal of chemical biology. 2010;11(3):320-4. Epub 2010/01/16. doi: 10.1002/cbic.200900702. PubMed PMID: 20077457; PubMed Central PMCID: PMC2908382.

22. Young DD, Lively MO, Deiters A. Activation and deactivation of DNAzyme and antisense function with light for the photochemical regulation of gene expression in mammalian cells. Journal of the American Chemical Society. 2010;132(17):6183-93. Epub 2010/04/16. doi: 10.1021/ja100710j. PubMed PMID: 20392038; PubMed Central PMCID: PMC2862549.

23. Chaulk SG, MacMillan AM. Synthesis of oligo-RNAs with photocaged adenosine 2'-hydroxyls. Nature protocols. 2007;2(5):1052-8. Epub 2007/06/05. doi: 10.1038/nprot.2007.154. PubMed PMID: 17546010.

24. Akita H, Ito R, Khalil IA, Futaki S, Harashima H. Quantitative Three-Dimensional Analysis of the Intracellular Trafficking of Plasmid DNA Transfected by a Nonviral Gene Delivery System Using Confocal Laser Scanning Microscopy. Mol Ther. 2004;9(3):443-51.

25. Schlosser K, Li Y. A Versatile Endoribonuclease Mimic Made of DNA: Characteristics and Applications of the 8–17 RNA-Cleaving DNAzyme. Chembiochem. 2010;11(7):866-79. doi: 10.1002/cbic.200900786.

26. Lan T, Furuya K, Lu Y. A highly selective lead sensor based on a classic lead DNAzyme. Chemical communications. 2010;46(22):3896-8. Epub 2010/04/22. doi: 10.1039/b926910j. PubMed PMID: 20407665; PubMed Central PMCID: PMC3071848.

Chapter 3:

Ratiometric sensing for quantitative detection of cellular metal ions

3.1 Introduction

Although many cellular sensors have been developed for the detection of labile metal ions, the majority of those reported are intensity-based sensors.[1-4] While these sensors can have excellent dynamic range (especially turn-on fluorescent sensors) and have been widely used for the study of cellular metal ions, the use of a one-dimensional intensity-based readout can provide only qualitative data.[2] A major complicating factor is that cell uptake of sensors cannot be expected to be consistent from one cell to another, or potentially even in different locations within the same cell. As a result, any observed increase in fluorescence from one cell to another may result from either an increased concentration of the target metal or from uneven loading of the sensor. This limitation is even more pronounced when cell uptake involves active processes, as is the case with DNAzyme delivery.[5-7]

In order to obtain quantifiable results with sensors, a common method has been the development of *ratiometric* sensors.[2] The fundamental concept behind a ratiometric sensor is the use of a parameter that remains invariant with sensor concentration to correct for the actual concentration of the sensor. This can be obtained through multiple methods. The first is the direct incorporation of an additional invariant signal (an internal standard). One such example is demonstrated below (Figure 3.1). This example consists of two components – one is a target-responsive fluorophore (responding to Zn^{2+}), and the other a spectrally distinct fluorophore that is designed not to interact with the metal ion. As a result, the fluorescent signal from the second fluorophore does not vary with variation in the analyte concentration, which provides a signal that is directly proportional to the total sensor concentration.

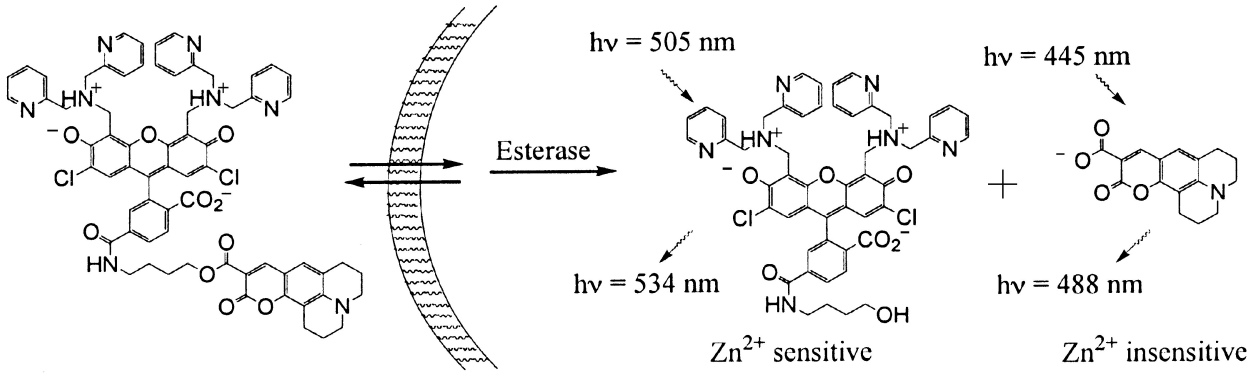

Figure 3.1. An example of a ratiometric sensor (Coumazin-1) based on incorporation of an internal standard. The top portion of the molecule (fluorescein derivative) is a zinc-responsive fluorophore. The bottom portion of the molecule is a coumarin moiety that is zinc-unresponsive. Figure originally from Ref. 8.[8]

The other common strategy that is applied to sensors is the use of Fluorescence Resonance Energy Transfer (FRET).[9] FRET is the most common method used for ratiometric cellular sensing with protein-based sensors due to the availability of a spectrum of fluorescent proteins.[10-12] FRET is the observed property that energy transfer from one dye (termed the *FRET donor*) to another (termed the *FRET acceptor*) can occur in a distance-dependent manner (Figure 3.2).[9] This provides information about the distance between the donor and acceptor molecule. In FRET-based sensing, the sensor is designed such that a conformational change occurs after target recognition, changing the distance between FRET donor and acceptor and leading to a change in FRET efficiency.[13] As a result, either the FRET efficiency or a simpler FRET ratio (ratio of acceptor fluorescence to donor fluorescence with consistent excitation of the donor only) can be calculated and used to correct for variations in sensor concentration.[9,14]

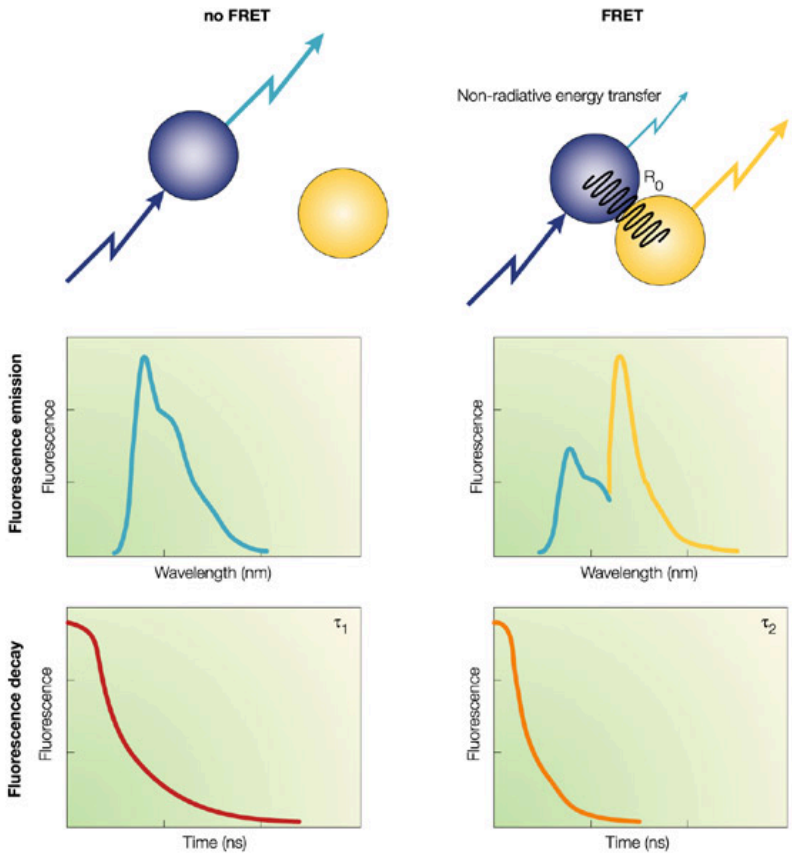

Figure 3.2. Schematic showing basic principle behind FRET-based sensing. Proximity of a donor and acceptor fluorophore enables energy transfer between the two, reporting on the relative distance of the two molecules. Figure adapted from Ref. 15.[15]

The catalytic beacon sensor that has been demonstrated for cellular detection is an intensity-based sensor, and thus all reported cellular applications are qualitative.[16-18] One of the major advantages of the use of the DNAyzme scaffold is the ease of incorporating modifications during the process of DNA synthesis.[19] As a result, it is relatively simple to envision methods for incorporation of an internal standard fluorophore, or for use of a FRET donor/acceptor pair in place of the classic fluorophore/quencher design. In this chapter, I present designs for the production of a ratiometric FRET sensor and early tests demonstrating their function within cells. I further demonstrate a detailed analysis of the sensor properties of such a FRET-enabled 8-17 DNAzyme and show that the FRET response remains consistent over a wide range of DNAzyme and Zn^{2+} concentrations. Finally, I further demonstrate work for optimization of the standard Lipofectamine protocol in an attempt to facilitate the use of DNAzymes within cell culture.

3.2 Materials and methods

3.2.1 Oligonucleotide synthesis

Oligonucleotides (see Table 3.1 for sequences used) were synthesized by Integrated DNA Technologies (Coralville, IA). Sequences were synthesized on 250 nmol or 1 μmol scale and used without further purification. To standardize stock solution concentration, UV-Vis measurements at 260 nm were obtained using a Hewlett-Packard 8453 spectrophotometer using extinction coefficients calculated from IDT OligoAnalyzer. Absorption spectra were obtained on the same instrument.

Table 3.1 DNA sequences used

Name	**Sequence (5' to 3')**
Design 1 substrate	/56-FAM/ACT CAC TAT rAGG AAG AGA TGG ACG TG/3InvdT/
Design 2 substrate	/56-FAM/ACT CAC TAT rAGG AAG TGA TGG ACG TG/36-TAMSp/
Design 3 substrate	/56-FAM/ACT CAC TAT rAGG AAG /i6-TAMN/GA TGG ACG TGT/3InvdT/
Design 1 enzyme	/5ThioMC6-D/ CAC GTC CAT CTC TTC TCC GAG CCG GTC GAA ATA GTG AGT/36-TAMSp/
Design 2, 3 enzyme	CAC GTC CAT CAC TTC TCC GAG CCG GTC GAA ATA GTG AGT
Design 4 enzyme	/5Cy5/ ATA GTT TCT CCG AGC CGG TCG AAA CTT CTC TAC CTG CAA
Design 4 substrate	TTG CAG GTA GAG AAG TrAG GAA ACT AT /3Cy3Sp/

All sequences were obtained from IDT (Coralville, IA) and use the following notation:

/56-FAM/ = 5' fluorescein

/5-TAMN/ = 5' TAMRA

/36-TAMSp/ = 3' TAMRA

/i6-TAMN/ = internal (thymine-linked) TAMRA base

/3Cy3Sp/ = 3'- Cy3

/5Cy5/ = 5'- Cy5

/3InvdT/ = 3’ inverted dT (to block 3’ end)

/5ThioMC6-D/ = 5’ thiol linker (to block 5’ end)

3.2.2 Fluorescence measurements (FAM/TAMRA, Designs 1-3)

Equal concentrations of enzyme and substrate strands were added to a buffer solution (50 mM Tris, 100 mM NaCl, pH 7.4) and heated to 80 °C for 5 minutes, then removed from heat and allowed to cool to room temperature to anneal.

Fluorescence measurements were obtained on a HORIBA Jobin Yvon FluoroMAX-P using 488 nm excitation for FAM and 518 nm excitation for direct TAMRA excitation. Fluorescence spectra were collected on the same instrument, from 500-650 nm using 488 nm excitation; DNAzyme concentration used was 25 nM. To start the reaction $Zn(NO_3)_2$ was added to a final concentration of 50 μM while vortexing.

After annealing, cleavable and uncleavable DNAzymes were mixed with 20% glycerol and loaded onto a 16% native polyacrylamide gel (50 mM Tris/acetic acid, pH 8.0, 100 mM $NaNO_3$), then run at a power of 4W at 4 °C for 10 hours. Fluorescence of the 5'-FAM tag was measured using a STORM 840 optical scanner using 450 nm excitation. Specific bands were cut from the gel, crushed, and soaked by shaking for 3 h in a soaking buffer containing 100 mM total Na^+ (50 mM Na-MES, pH 5.5, 50 mM $NaNO_3$) and previously treated with Chelex 100 to remove divalent metal ions. DNA samples were recovered from the supernatant after centrifugation.

3.2.3 Fluorescence measurements (Cy3/Cy5, Design 4)

Equal concentrations of enzyme and substrate strands were added to a buffer solution (50 mM Tris, 100 mM NaCl, pH 7.4) and heated to 80°C for 5 minutes, then removed from heat and allowed to cool to room temperature to anneal. Fluorescence measurements were obtained on a HORIBA Jobin Yvon FluoroMAX-P using 500 nm excitation (to excite Cy3) or 590 nm excitation (to excite Cy5 directly). In all cases fluorescence spectra were obtained over the range 510-800 nm. For timecourse measurements three scans were made at 30 second intervals: 500 nm ex/564 nm em, 500 nm ex/666 nm em, and 590 nm ex/666 nm em, corresponding to (excitation/emission) Cy3/Cy3, Cy3/Cy5, and Cy5/Cy5. DNAzyme concentrations used ranged from 2 to 2000 nM. To initiate the DNAzyme reaction $Zn(NO_3)_2$ was added to a final concentration of 0, 6.25, 12.5, 25, 50, or 100 μM while vortexing.

3.2.4 Data processing and calculations ($Ratio_A$, E_{FRET}, and curve fitting)

Data was processed in OriginPro9.0 (OriginLab, Massachusetts), licensed to UIUC. Individual contributions to the overall fluorescent spectrum from Cy3 and Cy5 were deconvoluted by scaling spectra taken of each dye independently, then integrated to obtain total fluorescence from each dye. E_{FRET} was calculated based on the $Ratio_A$ method,[20,21] using reference values for absorbance of each dye. E_{FRET} was calculated at each timepoint and the initial rate of change (k) of E_{FRET} was determined by fitting to a one-phase exponential decay function (ExpDec1). Calculated values for k and standard deviation σ were plotted versus added Zn^{2+} concentration and limit of detection was calculated based on the formula LOD = $3\sigma_{blank}$.

3.2.5 Cell culture

HeLa cells were cultured in Dulbecco's Modified Eagle's Medium (DMEM) media supplemented with 10% fetal bovine serum (FBS), 100 U/mL penicillin, and 100 µg/mL streptomycin solution (Cell Media Facility, UIUC), and were incubated at 37°C in a humidified 5% CO_2 environment. Cells were subcultured every 3 days, and cultures were restarted from frozen stocks after 30 passages. For microscopy, cells were passed into 35 mm glass-bottom petri dishes (MatTek) in growth media lacking penicillin/streptomycin and grown to 70-90% confluence before imaging.

3.2.6 Flow cytometry

HeLa cells grown in 24-well plates were transfected using Lipofectamine 2000 reagent (Invitrogen) using a modification of manufacturer's protocols. Caged active or inactive DNAzymes were annealed in PBS by heating to 80°C for 5 minutes and cooling to room temperature. Lipofectamine 2000 (5 µL) and annealed DNAzymes (1 nmol) were incubated separately in one of five types of media for 5 minutes, then combined and allowed to incubate together for an additional 25 minutes. The incubation media used were Opti-MEM (Invitrogen), PBS (Gibco), DMEM supplemented with 10% FBS, DMEM media, HEPES buffer (50 mM, pH 7.2, 100 mM NaCl), and Tris-Acetate buffer (50 mM, pH 7.2, 100 mM Na-acetate). The prepared DNAzyme-Lipofectamine mixture was added to HeLa cells and allowed to incubate for 6 hours. Cells were washed several times with PBS, then lifted with 0.25% trypsin-EDTA, pelleted by centrifugation, resuspended in PBS, and analyzed on a BD LSR II flow cytometer equipped with 488 nm,

640 nm, and 403 nm lasers. Fluorescence of FAM was assessed using a 505 longpass dichroic mirror and 530/30 bandpass filter set.

3.2.7 Confocal microscopy

Cells grown in glass-bottom plates were transfected using Lipofectamine 2000 reagent (Invitrogen) using a modification of manufacturer's protocols. Caged active or inactive DNAzymes were annealed by heating to 80°C for 5 minutes and cooling to room temperature. Lipofectamine 2000 (5 µL) and annealed DNAzymes (1 nmol) were incubated separately in PBS for 5 minutes, then combined and allowed to incubate for an additional 25 minutes. The prepared DNAzyme-Lipofectamine mixture was added to HeLa cells and allowed to incubate for 11 hours. Cells were also stained with Hoechst 33258 (Sigma) at a final concentration of 2.5 ng/mL for 30 minutes. After incubation, cells were washed several times with PBS and covered with DMEM without FBS or antibiotics.

Images were obtained using a Zeiss LSM 710 NLO confocal microscope at 63x magnification equipped with a Mai-Tai Ti-Sapphire laser, using the ZEN software suite (Zeiss). Fluorescence emission of Cy3 and Cy5 were gated separately using an installed twin gate beam splitter and recorded independently using both Cy3 excitation (514 nm laser) and Cy5 excitation (564 nm laser) conditions. Pinhole and gain settings were kept constant throughout the whole imaging process. Activity of transfected DNAzymes was measured after addition of 50 µM zinc on the microscope stage, as the pyrithione salt.

Images were processed using ImageJ (NIH, Bethesda). Cellular regions of interest were selected and RGB values integrated using batch calculations. The FRET ratio R was calculated as the ratio of integrated fluorescence (at constant Cy3 excitation), R = F(Cy5)/F(Cy3).

3.3 Results and discussion

3.3.1 Initial design of the ratiometric sensor

The initial designs of the ratiometric sensor utilized the dyes FAM and TAMRA, which have been previously utilized as a FRET donor/acceptor pair.[22] Predicted secondary structures for the DNAzyme and the placement of the fluorophores for three designs are shown in Figure 3.3. In design 1, FAM and TAMRA were placed on the 5' of the substrate strand and 3' of the enzyme strand, respectively. In design

2 FAM and TAMRA were placed on opposite termini of the substrate strand. In design 3, FAM was attached to the 5' terminus of the substrate strand and TAMRA was incorporated into the other binding arm by incorporation of a TAMRA-linked dT base.

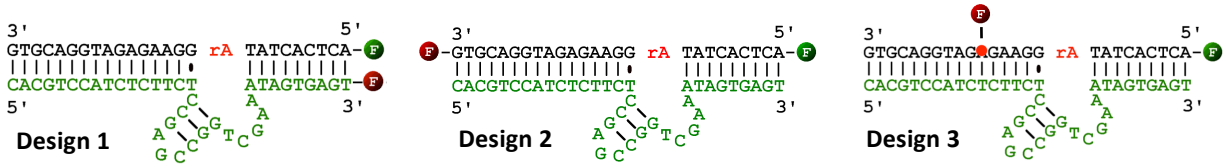

Figure 3.3. Designs 1, 2, and 3 for FRET-labeled constructs. Green and red circles indicate locations of FAM and TAMRA, respectively.

3.3.2 Fluorescence properties

A native PAGE gel run using uncaged FAM- and TAMRA-labeled DNAzymes (Design 1) demonstrated FRET qualitatively by reduction of FAM fluorescence (caused by energy transfer to proximal TAMRA dyes), as shown in Figure 3.4. However, despite using divalent metal-free conditions, significant degradation of the cleavable DNAzyme constructs was observed, and purification of the band corresponding to intact DNAzyme using standard protocols resulted in recovery only of fully cleaved substrate.

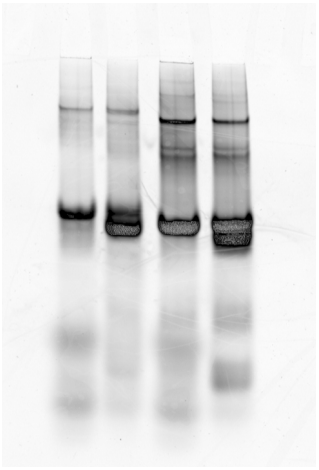

FAM	+	+	+	+
TAMRA	+	+	–	–
Inactive DNAzyme	+	–	+	–
Cleavable DNAzyme	–	+	–	+

Figure 3.4. Native gel of initial DNAzyme FRET construct (Design 1). All lanes have equal FAM loading, differences in observed fluorescence are attributed to FRET to adjacent TAMRA dye.

Fluorescence properties of the annealed FAM-TAMRA labeled DNAzymes were measured to assess whether FRET occurs between the attached dyes. As shown in figure 3.5, Design 1 shows energy transfer from the FRET donor FAM to the FRET acceptor TAMRA, evidenced by FAM quenching. However, the corresponding increase in TAMRA fluorescence was very slight.

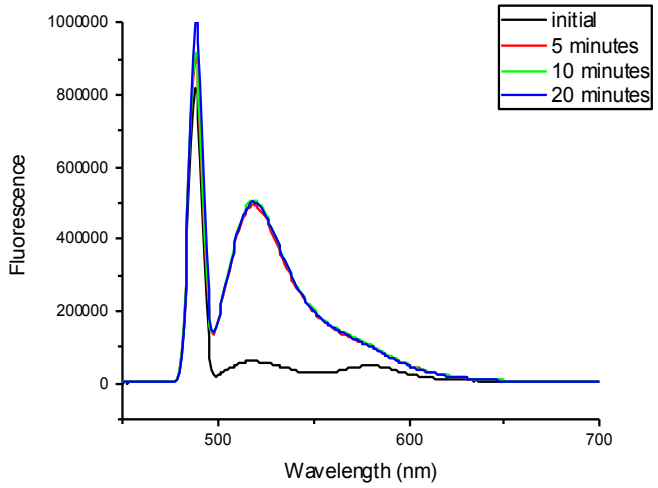

Figure 3.5. (black line) Initial fluorescence of Design 1 (adjacent FAM, TAMRA), and (red, green, blue lines) after subsequent addition of 100 μM Zn^{2+}. Times indicated in legend.

To ensure that the TAMRA and FAM fluorophores were intact and functional, I measured the fluorescence of each dye independently (Figure 3.6). As demonstrated in the figure, a much higher TAMRA increase is expected in the concentration used for the fluorescent studies. Spectra were taken at timepoints of 5, 10, and 20 minutes after addition of 100 μM Zn^{2+} to ensure complete cleavage. This provided spectra showing the minimum FRET possible for each construct.

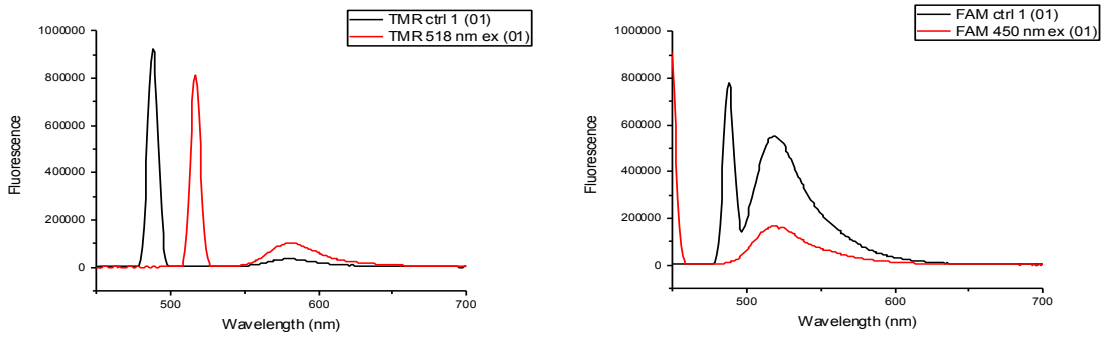

Figure 3.6. Individual fluorescence scans of DNA singly modified with one dye: (a) TAMRA, (b) FAM. Concentrations of dye are the same as in Figure 3.5.

Design 3 (Figure 3.7) showed very similar properties to design 1; while FRET was observed due to FAM quenching, the increase in TAMRA fluorescence was much lower than expected.

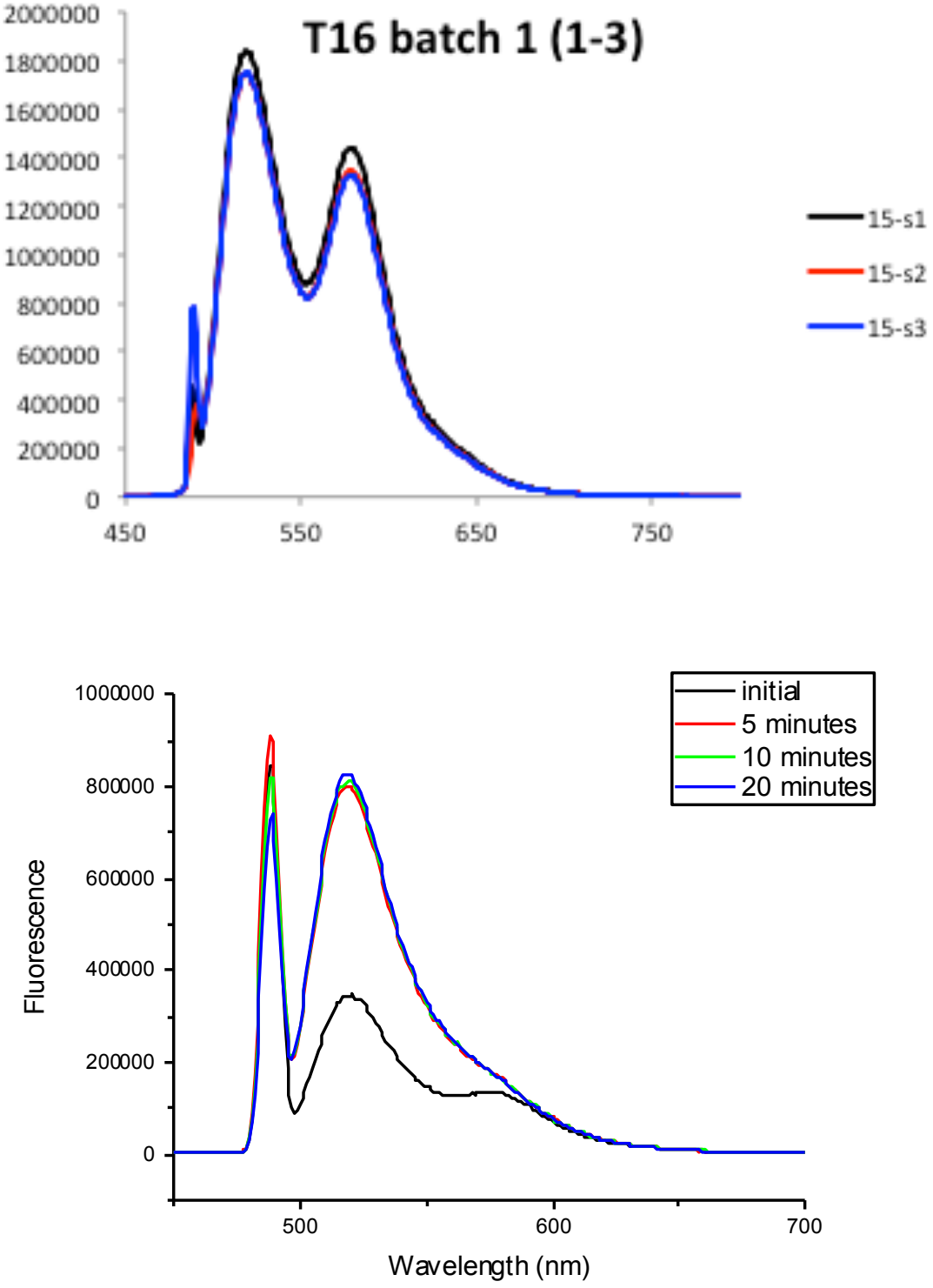

Figure 3.7. Fluorescent measurements of Design 3 (internal TAMRA): (a) initial fluorescence of Design 3, in triplicate, (b) fluorescence after addition of 100 µM Zn^{2+}.

Design 2 showed no observable FRET or fluorescent changes upon addition of Zn^{2+} (Figure 3.8).

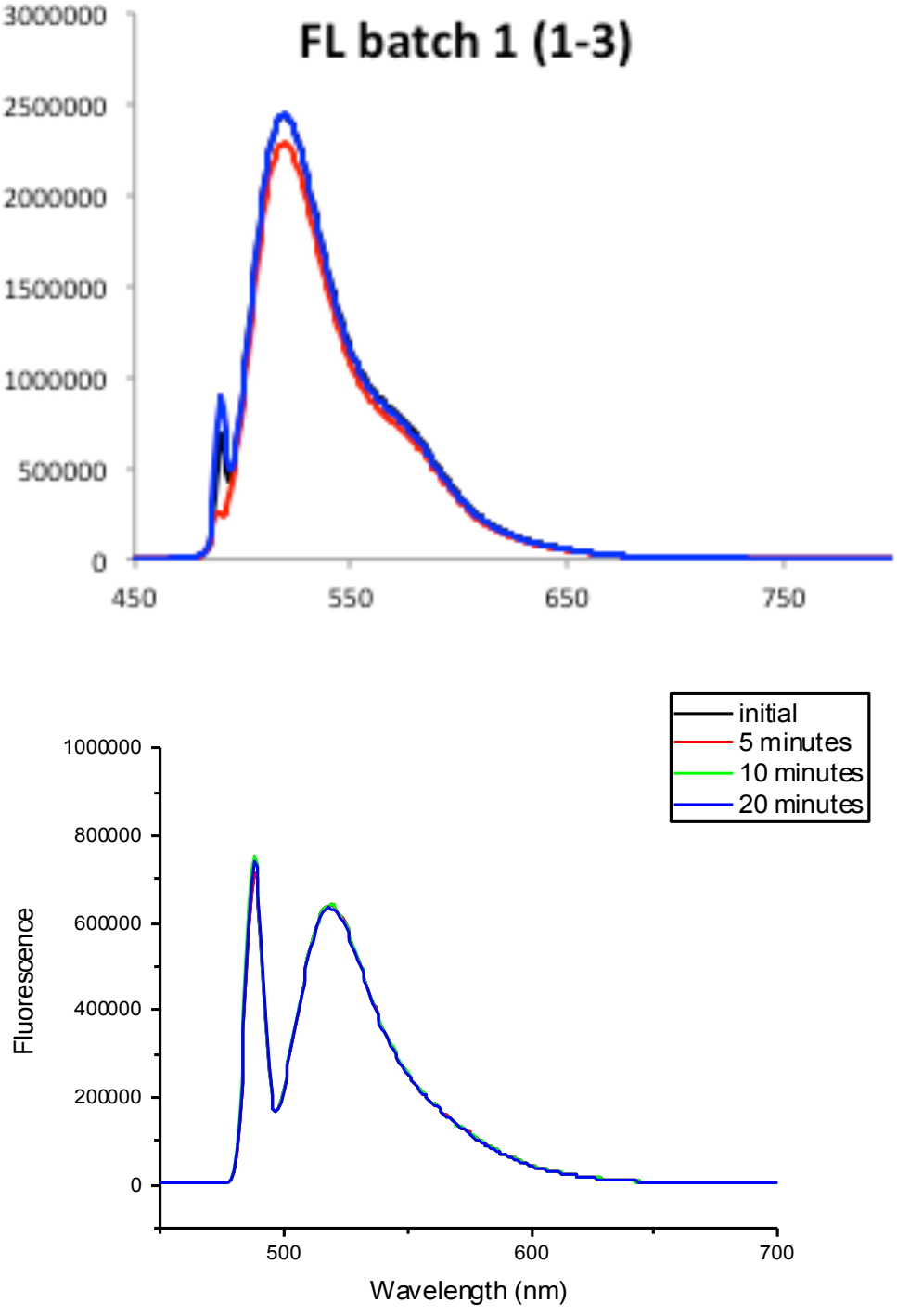

Figure 3.8. Fluorescent measurements of Design 2 (full-length FAM-TAMRA): (a) initial fluorescence of Design 2, in triplicate, (b) Activity after addition of 100 µM Zn^{2+}.

The qualitative results shown above indicate significant changes in the fluorescence output of Design 1 and 3 after DNAzyme cleavage. Fluorescence timecourses using Design 3 were carried out to determine the kinetics of this change (Figure 3.9).

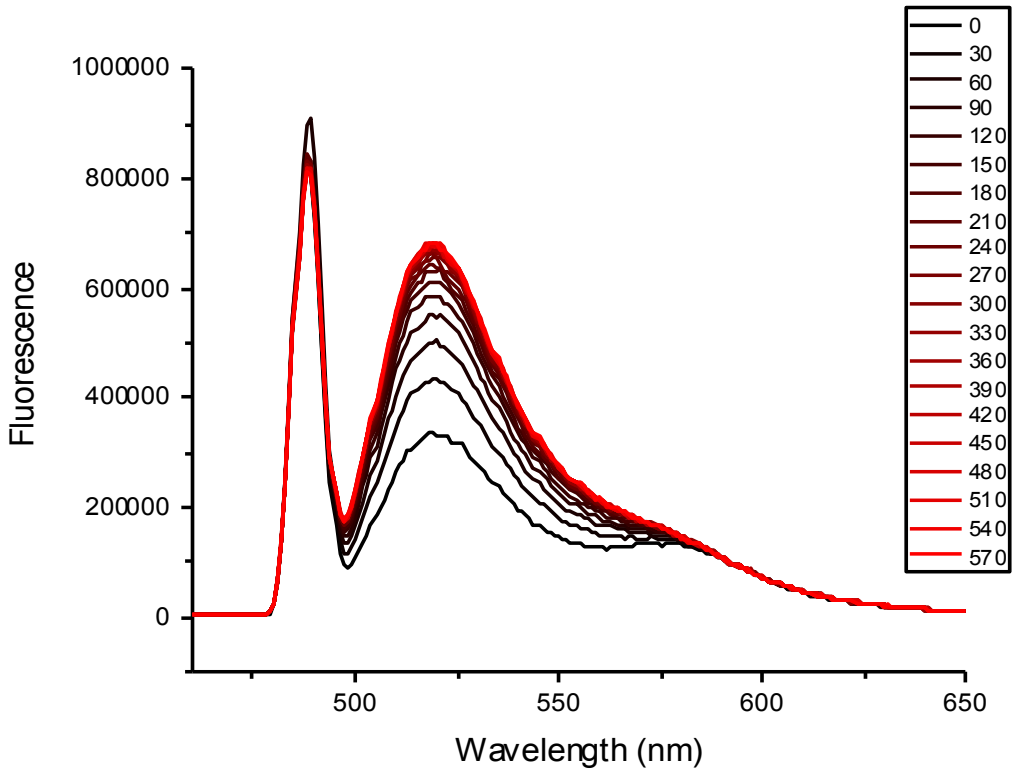

Figure 3.9. Example fluorescence trace of Design 3 DNAzyme taken over 10 minutes after addition of 100 μM Zn^{2+}. Times shown are in seconds.

$Ratio_A$ is a method for measuring the FRET efficiency E_{FRET} quantitatively based on measurement of two fluorescent spectra: the fluorescence of the FRET acceptor when exciting only the FRET donor, and the fluorescence of the FRET acceptor when directly exciting the FRET acceptor.[21] However, calculating FRET efficiency using $Ratio_A$ is only valid when the FRET donor and acceptor are not in direct contact.[20] If too close, the formation of exciton states by collisional contact of the donor and accept alters fluorescence properties in a way that is difficult to predict.[20] Based on the spectra shown in Figure 3.5, $Ratio_A$ calculations would be inaccurate for Design 1 due to quenching of both dyes observed.[20] While Design 2 and 3 did not show collisional quenching due to the much longer distance between dyes, E_{FRET} was lowered due to the increased distance between donor and acceptor in these designs. The distance between the FAM and TAMRA dyes in Design 2 was predicted to be approximately 9 nm (25 bp) based

on a typical estimate of 3.5 nm per 10 base pairs for B-form DNA, or ~ 5.25 nm for Design 3 (16 bp). For the FAM/TAMRA FRET pair, the Förster radius R_0 is reported to be 4.9-5.4 nm, leading to a calculated theoretical E_{FRET} of 0.03 for Design 2 and 0.5 in Design 3.

However, although E_{FRET} could not be accurately calculated in Design 1 and was predicted (and observed) to be extremely low in Design 2, it could be calculated for Design 3. Using reference values of 0.8 and 0.2 for FAM and TAMRA absorbance, respectively, E_{FRET} for the FAM/TAMRA pair was calculated for a series of DNAzymes at different Zn^{2+} concentrations over the range 6.25-100 μM. (Figure 3.10a) The initial rate of change of E_{FRET} was plotted against Zn^{2+} concentration, and a linear response was observed. (Figure 3.10b) Based on the standard definition of limit of detection (LOD) as three times the standard deviation of a blank sample ($LOD = 3\sigma_{blank}$), the limit of detection was calculated to be 0.427 μM Zn^{2+}. This compares favorably to reported limits of detection using the 8-17 DNAzyme for fluorescence detection of Zn^{2+} in environmental samples, which reach 0.3 ppm (4.58 μM).[23]

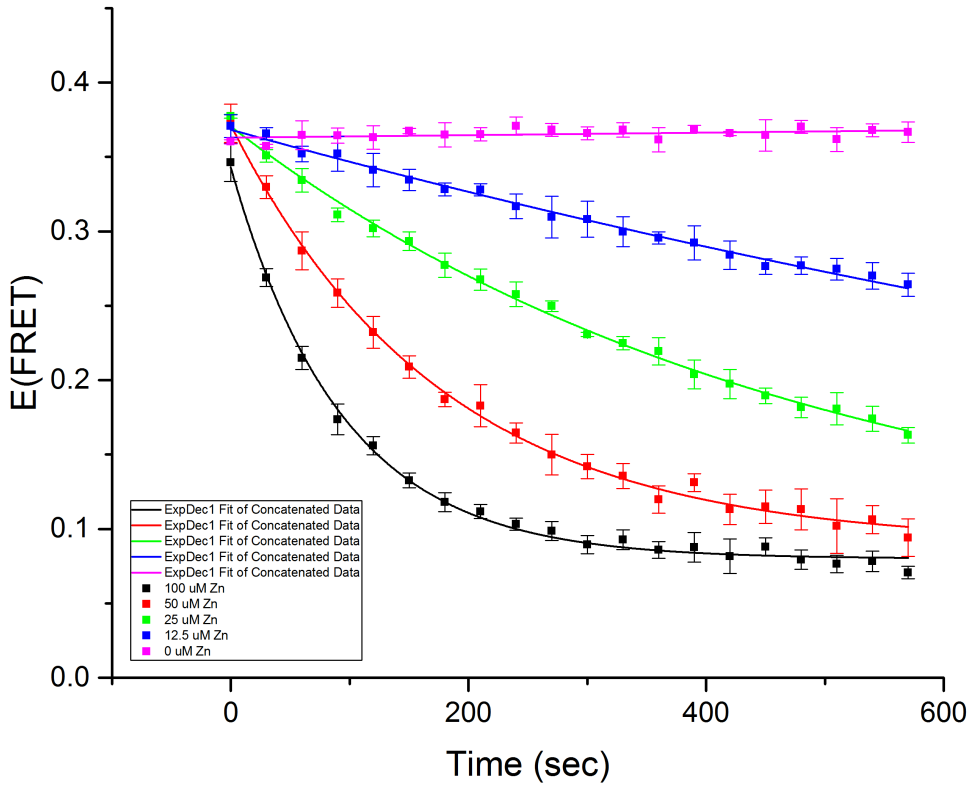

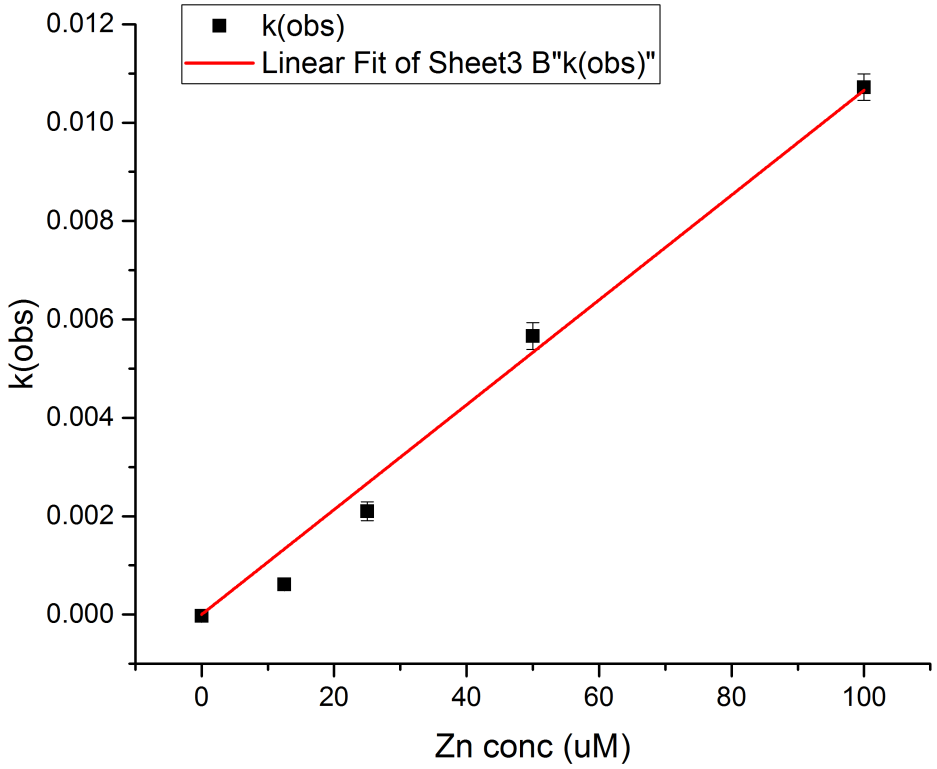

Figure 3.10. Sensor kinetics: Calculated E_{FRET} versus time, limit of detection for FAM-TAMRA design

3.3.3 Revised design of ratiometric sensor (Cy3/Cy5)

Based on the results from the earlier designs, the FRET donor/acceptor pair was changed from the xanthene dyes FAM and TAMRA to the cyanine dyes Cy3 and Cy5. The rationale for this change was twofold. First, the Förster radius (the distance at which the energy transfer efficiency is 50%) for Cy3 and Cy5 is slightly larger than that for FAM and TAMRA, with reported distances in the range of 5.3-5.4 nm.[24-26] More importantly, Cy3 and Cy5 are reported not to demonstrate collisional quenching even when directly adjacent to each other,[27] whereas xanthene dyes such as FAM and TAMRA are known to do so. As a result I investigated Design 4, which is similar to FAM/TAMRA design 1 in that Cy3 and Cy5 are directly adjacent and on opposite strands (Figure 3.11).

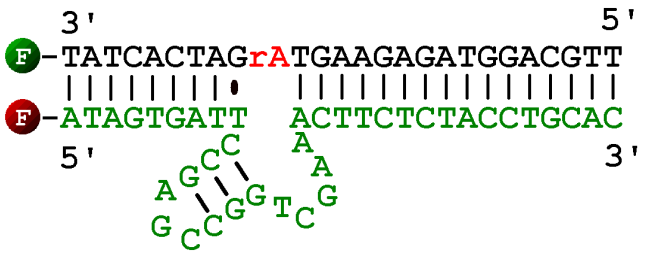

Figure 3.11. Design 4 of FRET construct. Green and red circles indicate Cy3 and Cy5 fluorophores, respectively.

3.3.4 Fluorescent properties of the Cy3/Cy5 design

The fluorescent properties of the Cy3/Cy5-functionalized DNAzyme were investigated using fluorescence spectroscopy as before. Fluorescence spectra were taken at a Cy3 excitation wavelength of 500 nm and scanned over the range of 510-800 nm. While uncleaved, the maximum intensity of both Cy3 and Cy5 were of similar magnitude, indicating significant FRET between the two dyes. After addition of 100 µM Zn, the Cy3 peak greatly increased in intensity and Cy5 peak correspondingly decreased, indicating significant loss of FRET (Figure 3.12).

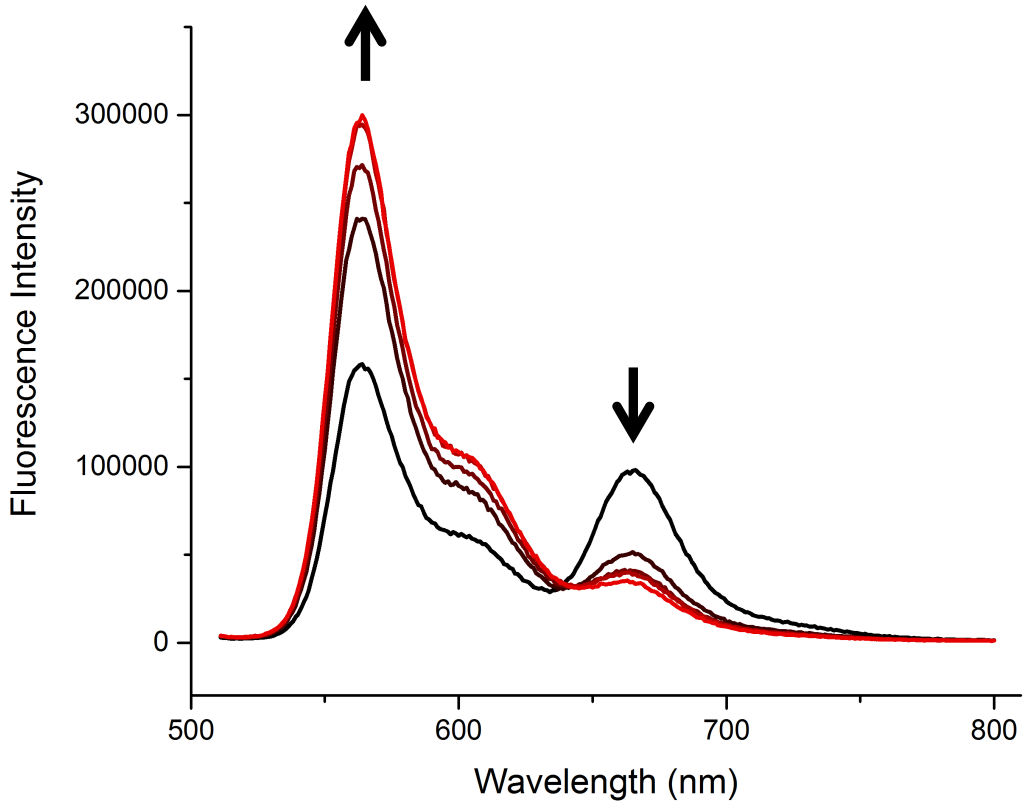

Figure 3.12. Fluorescent traces of the Cy3/Cy5 design (Design 4)

3.3.5 FRET efficiency/FRET ratio calculations

As before, FRET efficiency was calculated using the $Ratio_A$ method. Absorbance values for Cy3 and Cy5 at the wavelengths used are given in the following table:

Table 3.2 Calculated absorbance values used for E_{FRET} calculations.

	Cy3	**Cy5**
ε(500 nm)	30000 L/mol-cm	12500 L/mol-cm
ε(590 nm)	~ 0	50000 L/mol-cm

These values are calculated based on the relative absorbance at the indicated wavelengths versus maximum absorbance[28] and the following reference values for the maximal absorbance.[29,30]

ε_{max}(Cy5) = 250000 L/mol-cm

ε_{max}(Cy3) = 150000 L/mol-cm

$Ratio_A$ is calculated by subtracting a scaled donor (Cy3) emission spectrum from the combined donor + acceptor (Cy3 direct, Cy5 from FRET) fluorescence emission spectrum at donor excitation (500 nm). This value is divided by a reference value of acceptor excited directly (590 nm). E_{FRET} is then calculated using the following formula:

$$Ratio_A = [\varepsilon_D(500) * E_{FRET} - \varepsilon_A(500)]/[\varepsilon_A(590)] \quad \text{Equation 3.1}$$

However, using this formula, the calculated initial FRET efficiency for the Cy3 and Cy5 dyes in Design 4 is determined to be **1.5.** This number is nonphysiological (E_{FRET} is defined only up to a maximum of 1) and indicates the possible formation of excitonic states. This conclusion is supported by further evidence that the fluorescent properties of the Cy5 dye in the Cy3 and Cy5-labeled DNAzyme are altered. A timecourse was performed measuring at three specific pairs of excitation and emission at 30 second intervals after the addition of 100 μM Zn^{2+}.

500 nm excitation, 564 nm emission (Cy3 excitation, Cy3 emission)

500 nm excitation, 666 nm emission (Cy3 excitation, Cy5 emission – from FRET)

590 nm excitation, 666 nm emission (Cy5 excitation, Cy5 emission)

As observed previously with measurements at Cy3 excitation only (Figure 3.12), Cy3 emission increases and Cy5 FRET-based emission decreases. Unexpectedly, the fluorescence of Cy5 under direct excitation is also increased significantly at the same time. (Figure 3.13) This suggests strongly that in contrast to previous reports,[27] that there is alteration of the energy levels of Cy3 and Cy5 caused by their extreme proximity. This fact precludes calculation of E_{FRET} through the $Ratio_A$ method.[20]

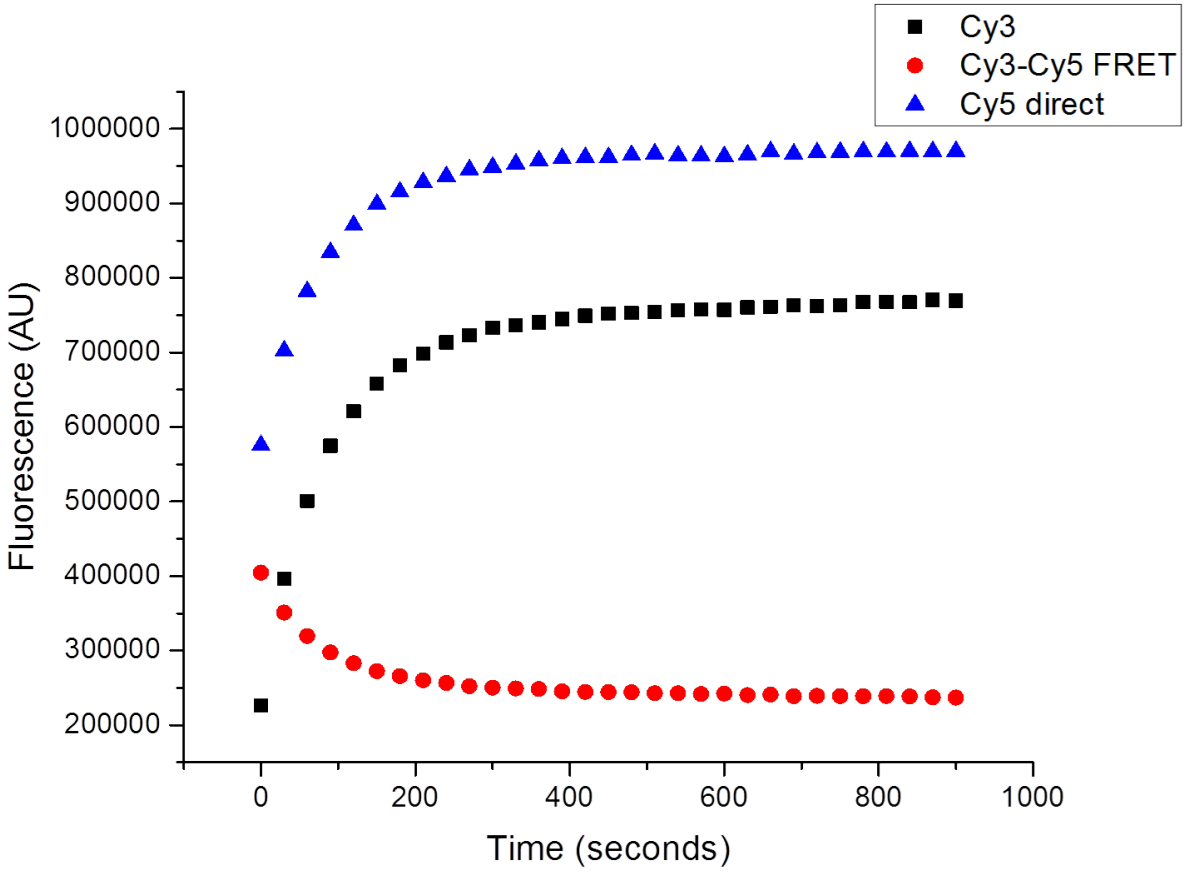

Figure 3.13. Timecourse of Cy3 and Cy5 fluorescence from direct or FRET-induced fluorescence after addition of 100 μM Zn^{2+} to 500 nM 8-17 DNAzyme (Design 4).

However, many cellular applications of FRET-based sensors often do not use E_{FRET} calculations directly, instead using either a direct ratio of integrated fluorescence[14] or utilizing one of a number of bleaching strategies to deconvolute donor and acceptor fluorescence.[31] I wished to determine whether the alteration in photophysical properties negatively affected potential quantification by use of a direct ratio of integrated fluorescence. By spectral deconvolution methods, I separated the individual contributions of Cy3 and Cy5 from the combined fluorescence spectrum. The ratio R was calculated as F(Cy5)/F(Cy3), and changes in R over time were fit to a standard exponential function. By repeating this measurement at multiple Zn^{2+} concentrations I obtained a plot of initial rate constant versus Zn^{2+} concentration (Figure 3.14). The data in this plot corresponded nicely to a linear fit, indicating that the direct fluorescence ratio may work for quantification. Based on this fit, a limit of detection of 12 μM Zn^{2+} was obtained at a 25 nM concentration of DNAzyme using the formula LOD = $3\sigma_{blank}$.

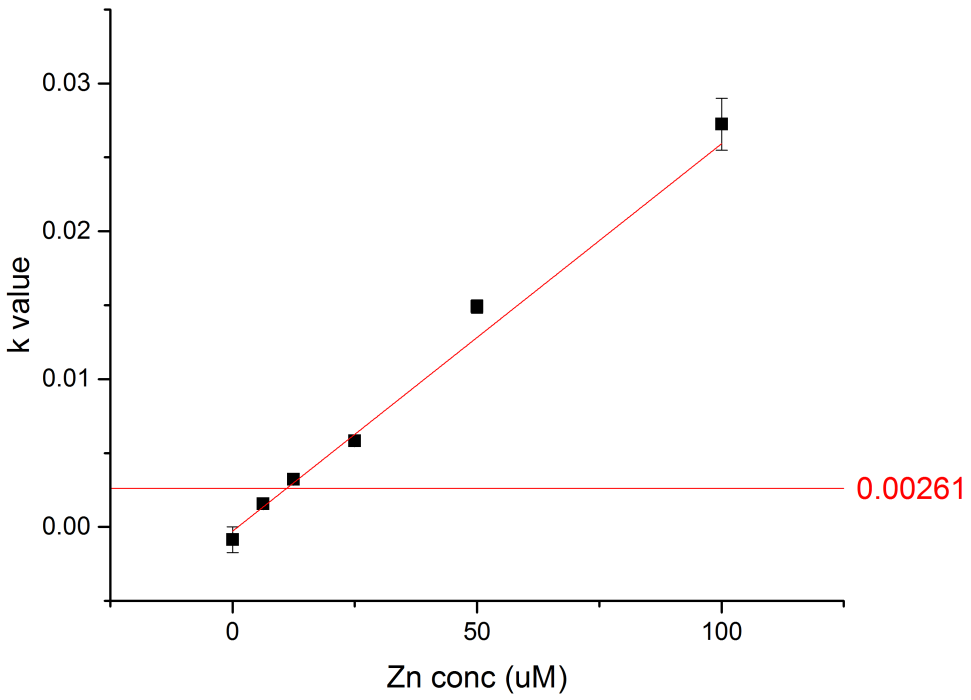

Figure 3.14. Plot of rate of change of E versus Zn concentration (Design 4 – Cy3/Cy5 DNAzyme). Red line indicates limit of detection based on definition LOD = $3\sigma_{blank}$.

3.3.6 Kinetics of 8-17 DNAzyme

Fluorescent time courses were taken using multiple concentrations of [Zn^{2+}] and [DNAzyme], with the intent of identifying the ranges of [Zn^{2+}] and [DNAzyme] over which the sensor property is linear and consistent. All experiments were carried out in triplicate, and apparent initial rate constants were calculated in Origin. As shown in figure 3.15, the sensor shows linearity in a wide range of Zn and DNAzyme concentrations. As expected, at [Zn^{2+}] below than the limit of detection, the measured value for K is no longer accurate.

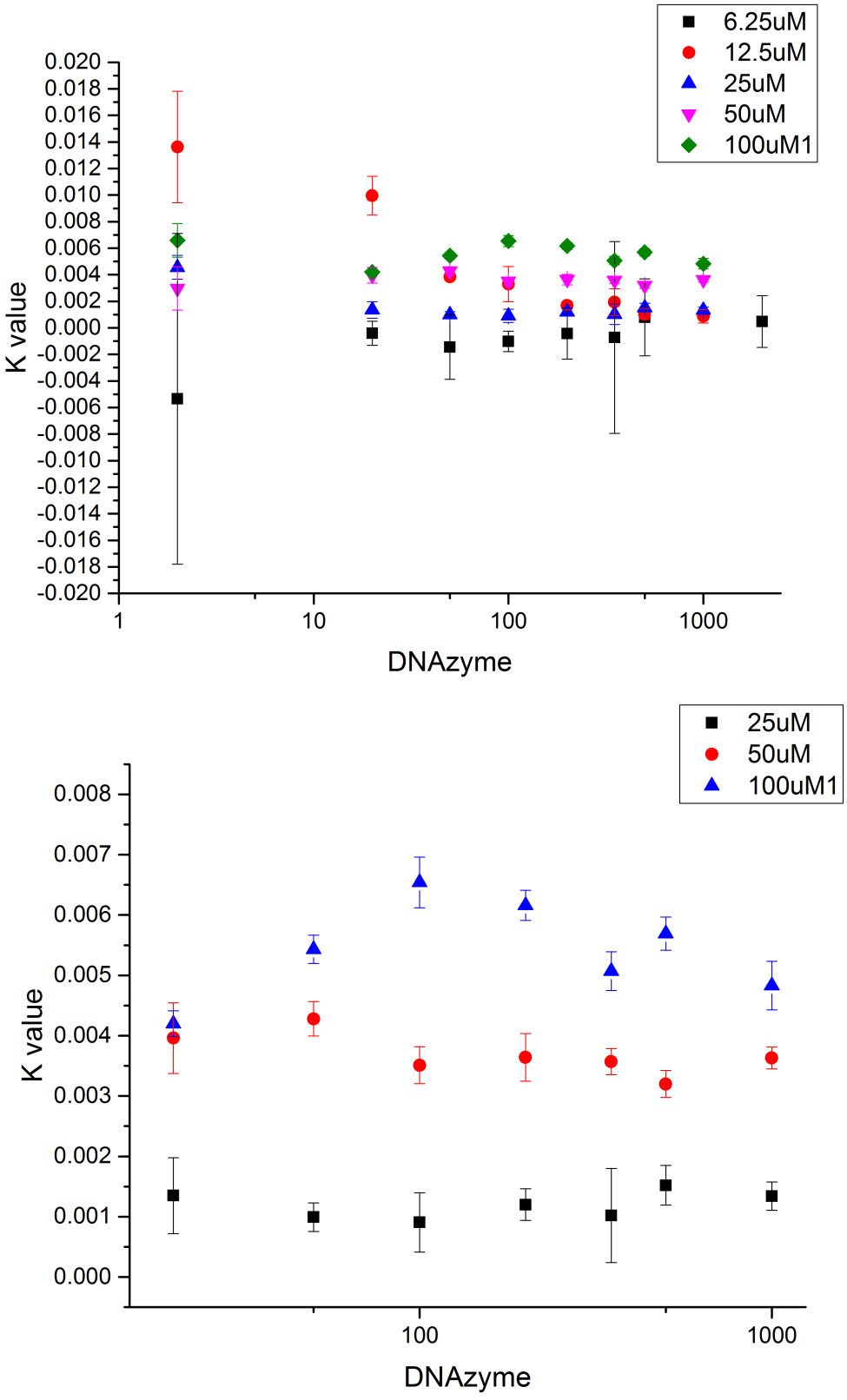

Figure 3.15. Measurement of K values for different concentrations of Zn^{2+} (a) and DNAzyme (b).

3.3.7 Improved cellular delivery using Lipofectamine

A range of conditions was investigated to optimize the process of DNAzyme delivery using Lipofectamine 2000. Prior PAGE analysis of uncaged DNAzymes indicated significant degradation after treatment following the standard recommended Lipofectamine protocol, which is attributed to the presence of metal ions such as Zn^{2+} (possibly Mg^{2+} or Ca^{2+}) within the standard Opti-MEM media formulation. However, earlier experiments indicated that cellular levels of Zn^{2+} inside HeLa cells were insufficient to cleave the 8-17 DNAzyme after UV-induced decaging, over the timescale of a normal imaging experiment.[17] This observation also suggests that the previously reported activity of the 8-17 DNAzyme towards common endogenous metal ions such as Mg^{2+} and Ca^{2+} is insufficient to show a false positive response under the cell conditions tested.[17]

The 8-17 DNAzyme motif was independently identified by several labs, in DNAzyme selections targeting different metal ions.[32] Previous reports investigating the metal ion selectivity of the 8-17 DNAzyme identified a pattern of metal ion-dependent activity in the order $Pb^{2+} >> Zn^{2+} >> Mg^{2+}$, with reported apparent K_d towards Mg^{2+} of 53 mM.[33] The relative activity of a number of 8-17 DNAzyme sequences towards Mg^{2+} and Ca^{2+} was measured by Peracchi and most sequences tested showed 10 to 20-fold higher activity towards Ca^{2+} than to Mg^{2+} (at a concentration of 3 mM of either metal ion)

Within a cellular environment, Mg^{2+} and Ca^{2+} are relatively common metal ions (labile cytoplasmic Mg^{2+} around ~1-5 mM[34], average cytoplasmic Ca^{2+} concentration in the range of 100 nM – 1 μM[35]) compared to most transition metal ions, which are present in labile form at concentrations many orders of magnitude lower than either Mg^{2+} or Ca^{2+}.[36,37] As a result, nonspecific binding to Mg^{2+} or Ca^{2+} has often been a significant hurdle for many metal ion sensors.[38] In the case of the 8-17 DNAzyme, the relatively low binding affinity of DNA for metal ions indicates low propensity for nonspecific activation in the cellular environment, albeit with a corresponding reduced sensitivity for the target transition metal ion as well.

For the 8-17 DNAzyme, it was rationalized that if a method could be identified that removed activating metal ions (Zn^{2+}, Mg^{2+}, or Ca^{2+}) from the extracellular media during the transfection step, it might allow for use of an uncaged 8-17 DNAzyme construct directly within the cellular environment. This might simplify the application of 8-17 or similar DNAzymes in the future.

A range of different buffers including Opti-MEM, PBS, DMEM, HEPES, and Tris buffers were used in place of Opti-MEM and HeLa cells treated with uncleavable FAM-labeled DNA sequences in order to assess cell uptake. Cell fluorescence was measured after 6 hours by flow cytometry (Figure 3.16, Table 3.3).

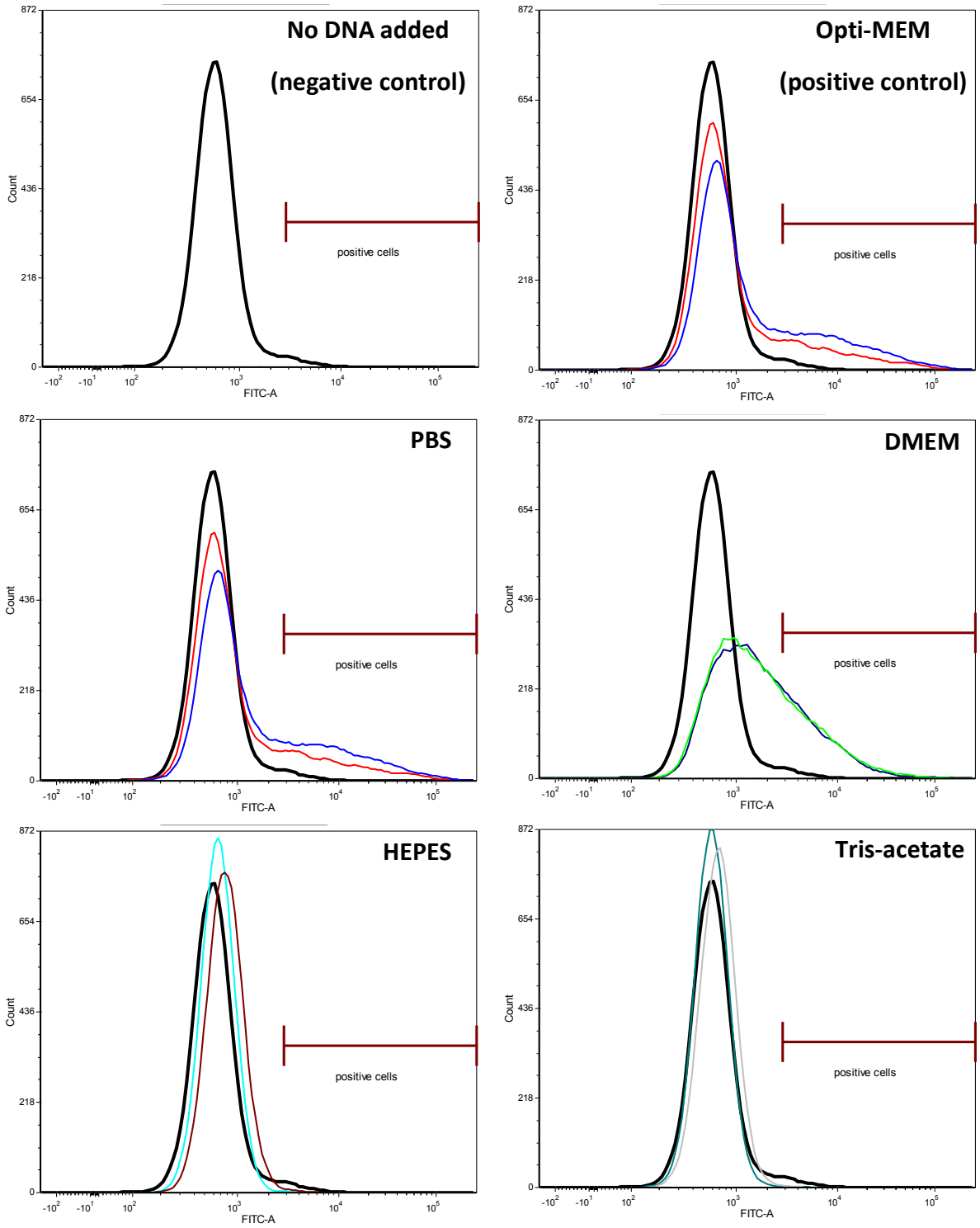

Figure 3.16. Flow cytometry results of DNAzyme uptake after Lipofectamine transfection using different buffers. Indicated region (dark red) is identical for all histograms and indicates the region of fluorescence containing less than 2% of total negative control cells. In all figures, the black trace indicates control untransfected cells. The other two overlaid traces in all histograms after the first are the results of two transfection experiments with 250 pmol DNA in the indicated buffer.

Table 3.3 Percentage of transfected cells with fluorescence greater than 98% of negative control fluorescence (defined as positive transfection). Numbers indicate results from two individual trials. Buffer conditions indicated are same as in Figure 3.16.

	No DNA	Opti-MEM	PBS	DMEM	HEPES	Tris-acetate
% positive	1.93% **(defined)**	16.18%, 25.48%	52.35%, 41.26%	28.70%, 28.48%	0.19%, 0.57%	0.28%, 0.18%

The resulting fluorescent data showed that PBS, DMEM (+ 10% FBS), and Opti-MEM were capable of efficient DNA delivery. These three conditions were further analyzed by confocal microscopy using FAM-labeled DNA strands to determine if differences in DNA localization occurred with different transfection buffer conditions (Figure 3.17).

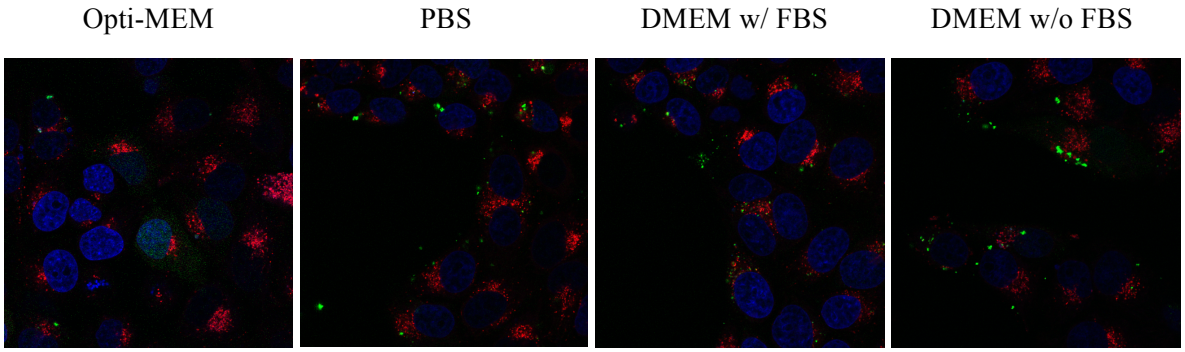

Figure 3.17. HeLa cells transfected with FAM-labeled DNA using Lipofectamine utilizing different types of incubation media. Blue channel is Hoechst 33258 for nuclear staining, green channel FAM-labeled DNA, red channel MitoTracker Red.

No significant differences in DNA localization were observed with different incubation buffers. Incubation in Opti-MEM displayed a punctate pattern of DNA fluorescence and occasional diffuse staining in the nucleus (as indicated by colocalization with Hoechst 33258 staining). This result was also generally observed with the other buffers that demonstrated successful transfection.

In order to assess whether the substitution of PBS for Opti-MEM was sufficient to deliver the 8-17 DNAzyme in an active form, an active uncaged variant of the FRET construct DNAzyme was delivered using the PBS incubation protocol (Figure 3.18). Green fluorescence (Cy3 excitation and emission) was measured at different timepoints after addition of 50 μM Zn^{2+} as the pyrithione salt on the microscope stage.

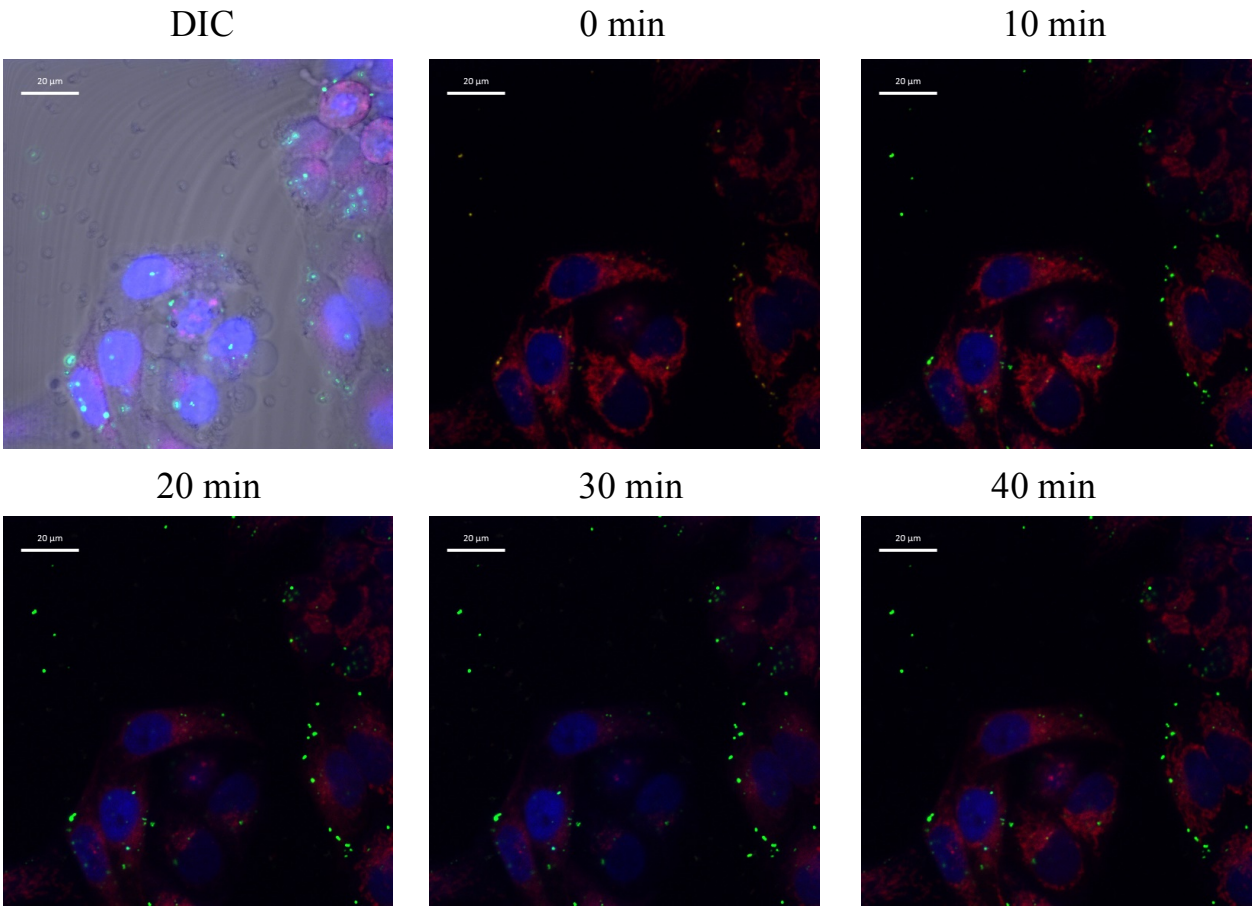

Figure 3.18. Timecourse of uncaged FRET construct fluorescence in response to Zn^{2+}. First image is overlay of DIC and fluorescent channels to show overall cell morphology. Remaining images are confocal fluorescent images taken at 10 minute intervals after addition of 50 µM Zn^{2+} as pyrithione salt. Green channel shows Cy3 fluorescence at Cy3 excitation; red channel shows Cy5 emission with direct Cy5 excitation. Blue channel is nuclear stain (Hoechst 33258), scale bar = 20 µm.

Although there was an observed diffused fluorescence within the Cy5 channel that did not seem to correspond to DNAzyme fluorescence (due to lack of colocalization with Cy3) the green fluorescence of Cy3 noticeably increased after Zn^{2+} addition, indicating that the 8-17 DNAzyme still retained activity inside cells and was thus not degraded prior to cell entry.

3.3.8 Ratiometric cellular detection of metal ions

The Cy3/Cy5-labeled 8-17 DNAzyme was delivered to HeLa cells using the PBS Lipofectamine protocol developed above with an uncaged FRET construct. Cells were stained with Hoechst 33258 and imaged via confocal microscopy. Figure 3.19 shows images of cellular fluorescence under three excitation conditions:

Cy3 (Cy3 excitation, Cy3 emission) – green channel

Cy35 (Cy3 excitation, Cy5 emission, = FRET) – red channel

Cy5 (Cy5 excitation, Cy5 emission) – red channel

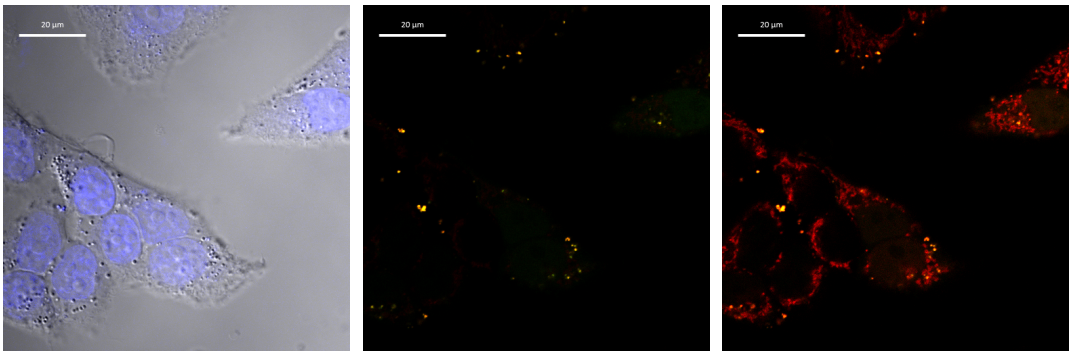

Figure 3.19. (left) DIC + DAPI overlay to show cell morphology. (center) Cy3 excitation (both Cy3 + Cy5 emission shown, false colored green and red respectively). (right) Cy5 direct excitation overlaid (Cy5 excitation/Cy5 emission). Scale bar = 20 µm.

Direct Cy5 excitation produced significant apparent nonspecific fluorescence, the pattern of which resembled mitochondrial staining. This observation further precluded use of the $Ratio_A$ method; instead the observed fluorescence ratio R was calculated as R = F(Cy5)/F(Cy3).

Fluorescence changes were then observed after the addition of 50 µM Zn^{2+} as the pyrithione salt. The punctate fluorescent spots observed under Cy3 excitation conditions are observed to shift from orange to green, indicating a shift from Cy5 emission (caused by FRET) towards Cy3 emission (Figure 3.20). This replicates the fluorescent changes observed via bulk fluorescence spectroscopy, and indicates that the ratiometric sensor design is functional even within cells.

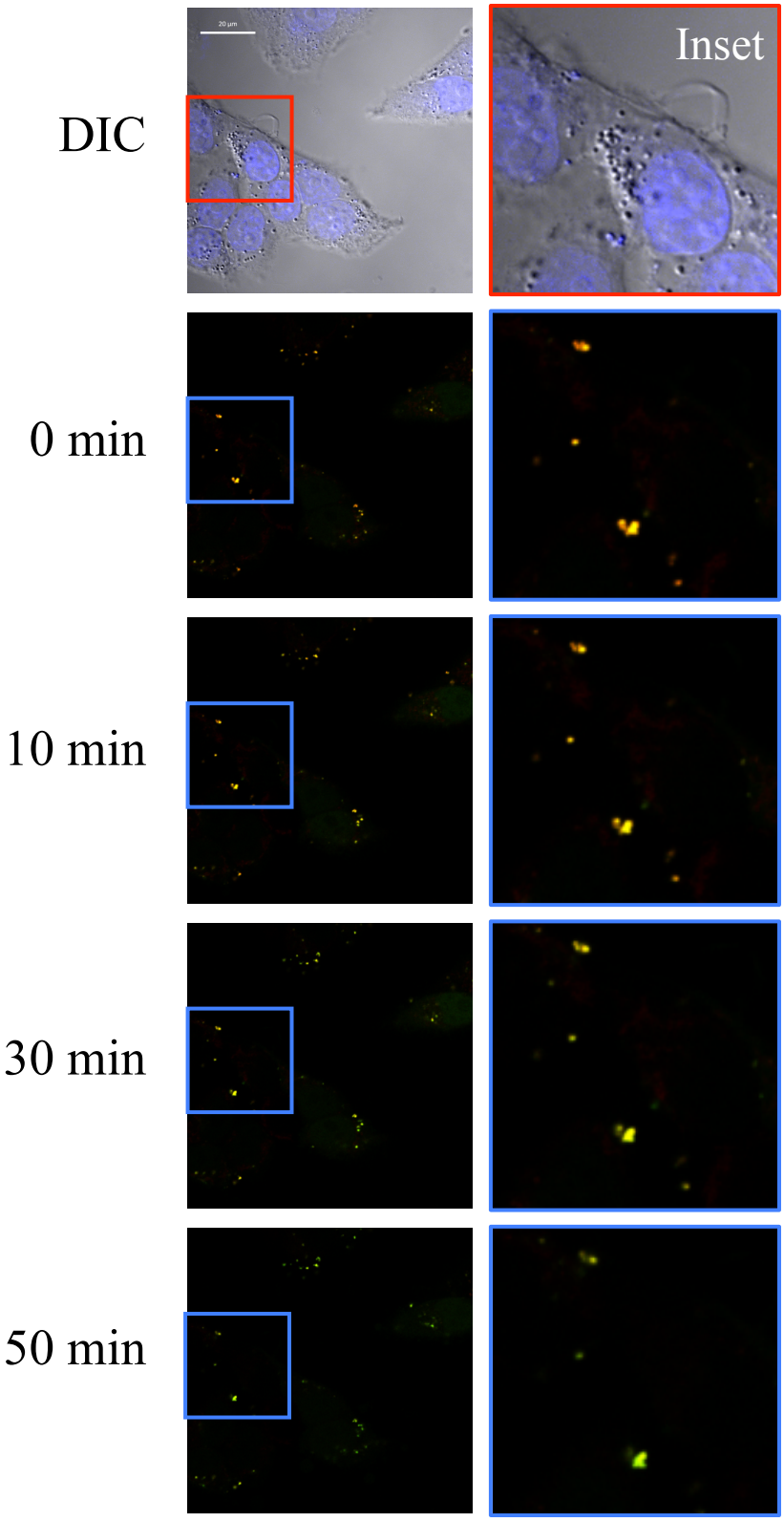

Figure 3.20. Timecourse showing Cy3 + Cy5 emission at Cy3 excitation settings, at 0 min, 10 min, 30 min, and 50 min after addition of 50 µM Zn^{2+} as the pyrithione salt on microscope stage. DIC (with Hoechst 33258 overlay) shows overall cell morphology and location of nucleus (in blue); remaining images show combined Cy3 and Cy5 fluorescence at Cy3 excitation. Scale bar = 20 µm. Indicated ROIs are expanded and shown directly to the right of full image in left column.

Using ImageJ the ratio of integrated Cy5 fluorescence to integrated Cy3 fluorescence at each timepoint above was measured. The observed FRET ratio R was observed to decrease from 3.5 initially to 1.1 over 50 minutes after addition of Zn^{2+} (Figure 3.21).

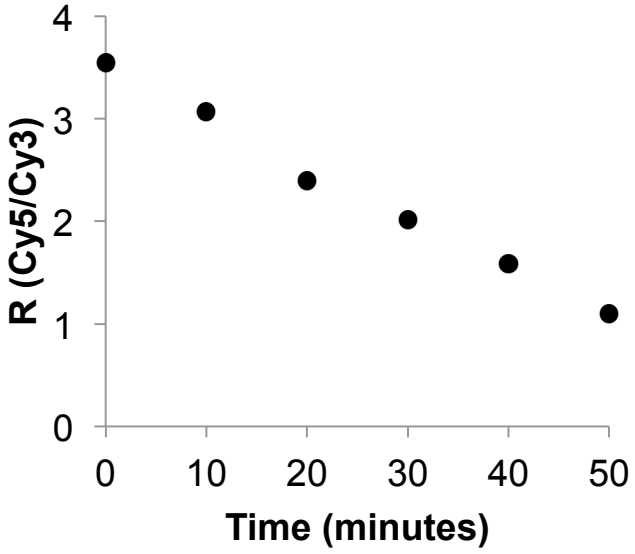

Figure 3.21. Timecourse of FRET ratio change after Zn^{2+} addition. FRET ratio R calculated as integrated fluorescence of Cy5 (from Cy3-induced FRET) divided by integrated fluorescence of Cy3 within cellular regions shown in Figure 3.20.

3.4 Summary and conclusions

In conclusion, I have demonstrated the redesign of the original catalytic beacon sensor to incorporate a FRET donor and acceptor pair. This change converts the turn-on fluorescent sensor design into one with a ratiometric readout, which allows cellular quantification because the ratiometric readout is unaffected by changes in sensor concentration. I have further investigated the concentrations of metal ion and DNAzyme over which the sensor response is linear and predictable, and have demonstrated that the ratiometric 8-17 DNAzyme functions consistently from the calculated limit of detection of 12 μM Zn^{2+} up to at least 100 μM. This sensor design should generalize towards other DNAzymes, further expanding the applications of the DNAzyme scaffold for cellular sensing. Finally, I demonstrate attempts to optimize the process of DNAzyme transfection using the commercially available transfection reagent

Lipofectamine, successfully demonstrating a method for transfecting an uncaged Zn^{2+}-responsive DNAzyme without loss of sensor to degradation. This improved process greatly simplifies the *in vitro* application of DNAzymes.

3.5 References

1. Domaille DW, Que EL, Chang CJ. Synthetic fluorescent sensors for studying the cell biology of metals. Nature Chemical Biology. 2008;4(3):168-75. Epub 2008/02/19. doi: 10.1038/nchembio.69. PubMed PMID: 18277978.
2. Lee MH, Kim JS, Sessler JL. Small molecule-based ratiometric fluorescence probes for cations, anions, and biomolecules. Chemical Society reviews. 2015;44(13):4185-91. Epub 2014/10/07. doi: 10.1039/c4cs00280f. PubMed PMID: 25286013; PubMed Central PMCID: PMC4387118.
3. Que EL, Domaille DW, Chang CJ. Metals in neurobiology: probing their chemistry and biology with molecular imaging. Chemical Reviews. 2008;108(5):1517-49. Epub 2008/04/23. doi: 10.1021/cr078203u. PubMed PMID: 18426241.
4. Pluth MD, Tomat E, Lippard SJ. Biochemistry of mobile zinc and nitric oxide revealed by fluorescent sensors. Annual review of biochemistry. 2011;80:333-55. Epub 2011/06/17. doi: 10.1146/annurev-biochem-061009-091643. PubMed PMID: 21675918; PubMed Central PMCID: PMC3117437.
5. Xing H, Hwang K, Li J, Torabi SF, Lu Y. DNA Aptamer Technology for Personalized Medicine. Current opinion in chemical engineering. 2014;4:79-87. Epub 2014/05/03. doi: 10.1016/j.coche.2014.01.007. PubMed PMID: 24791224; PubMed Central PMCID: PMC4001932.
6. Torabi SF, Lu Y. Functional DNA nanomaterials for sensing and imaging in living cells. Current opinion in biotechnology. 2014;28:88-95. Epub 2014/01/29. doi: 10.1016/j.copbio.2013.12.011. PubMed PMID: 24468446; PubMed Central PMCID: PMC4110194.
7. Xiang Y, Lu Y. DNA as sensors and imaging agents for metal ions. Inorganic chemistry. 2014;53(4):1925-42. Epub 2013/12/24. doi: 10.1021/ic4019103. PubMed PMID: 24359450; PubMed Central PMCID: PMC3955431.

8. Woodroofe CC, Lippard SJ. A novel two-fluorophore approach to ratiometric sensing of Zn(2+). Journal of the American Chemical Society. 2003;125(38):11458-9. Epub 2003/09/18. doi: 10.1021/ja0364930. PubMed PMID: 13129323.
9. Clegg RM. Fluorescence resonance energy transfer. Current opinion in biotechnology. 1995;6(1):103-10. Epub 1995/02/01. PubMed PMID: 7534502.
10. Merkx M, Golynskiy MV, Lindenburg LH, Vinkenborg JL. Rational design of FRET sensor proteins based on mutually exclusive domain interactions. Biochemical Society transactions. 2013;41(5):1201-5. Epub 2013/09/26. doi: 10.1042/BST20130128. PubMed PMID: 24059509; PubMed Central PMCID: PMC3822149.
11. Park JG, Palmer AE. Quantitative measurement of Ca2+ and Zn2+ in mammalian cells using genetically encoded fluorescent biosensors. Methods in molecular biology. 2014;1071:29-47. Epub 2013/09/21. doi: 10.1007/978-1-62703-622-1_3. PubMed PMID: 24052378; PubMed Central PMCID: PMC4051312.
12. Tsien RY. Constructing and exploiting the fluorescent protein paintbox (Nobel Lecture). Angewandte Chemie. 2009;48(31):5612-26. Epub 2009/07/01. doi: 10.1002/anie.200901916. PubMed PMID: 19565590.
13. Piston DW, Kremers GJ. Fluorescent protein FRET: the good, the bad and the ugly. Trends in biochemical sciences. 2007;32(9):407-14. Epub 2007/09/04. doi: 10.1016/j.tibs.2007.08.003. PubMed PMID: 17764955.
14. Qin Y, Dittmer PJ, Park JG, Jansen KB, Palmer AE. Measuring steady-state and dynamic endoplasmic reticulum and Golgi Zn2+ with genetically encoded sensors. Proceedings of the National Academy of Sciences of the United States of America. 2011;108(18):7351-6. Epub 2011/04/20. doi: 10.1073/pnas.1015686108. PubMed PMID: 21502528; PubMed Central PMCID: PMC3088641.
15. Rudolf R, Mongillo M, Rizzuto R, Pozzan T. Looking forward to seeing calcium. Nature reviews Molecular cell biology. 2003;4(7):579-86. Epub 2003/07/03. doi: 10.1038/nrm1153. PubMed PMID: 12838340.
16. Wu P, Hwang K, Lan T, Lu Y. A DNAzyme-gold nanoparticle probe for uranyl ion in living cells. Journal of the American Chemical Society. 2013;135(14):5254-7. Epub 2013/03/28. doi: 10.1021/ja400150v. PubMed PMID: 23531046; PubMed Central PMCID: PMC3644223.
17. Hwang K, Wu P, Kim T, Lei L, Tian S, Wang Y, Lu Y. Photocaged DNAzymes as a general method for sensing metal ions in living cells. Angewandte Chemie. 2014;53(50):13798-802. Epub

2014/10/15. doi: 10.1002/anie.201408333. PubMed PMID: 25314680; PubMed Central PMCID: PMC4297208.

18. Torabi SF, Wu P, McGhee CE, Chen L, Hwang K, Zheng N, Cheng J, Lu Y. In vitro selection of a sodium-specific DNAzyme and its application in intracellular sensing. Proceedings of the National Academy of Sciences of the United States of America. 2015;112(19):5903-8. Epub 2015/04/29. doi: 10.1073/pnas.1420361112. PubMed PMID: 25918425; PubMed Central PMCID: PMC4434688.
19. Liu J, Cao Z, Lu Y. Functional nucleic acid sensors. Chemical reviews. 2009;109(5):1948-98. Epub 2009/03/24. doi: 10.1021/cr030183i. PubMed PMID: 19301873; PubMed Central PMCID: PMC2681788.
20. Clegg RM. Fluorescence resonance energy transfer and nucleic acids. Methods in enzymology. 1992;211:353-88. Epub 1992/01/01. PubMed PMID: 1406315.
21. He Y, Lu Y. Metal-ion-dependent folding of a uranyl-specific DNAzyme: insight into function from fluorescence resonance energy transfer studies. Chemistry. 2011;17(49):13732-42. Epub 2011/11/05. doi: 10.1002/chem.201100352. PubMed PMID: 22052817; PubMed Central PMCID: PMC3311960.
22. Clegg RM, Murchie AI, Zechel A, Lilley DM. Observing the helical geometry of double-stranded DNA in solution by fluorescence resonance energy transfer. Proceedings of the National Academy of Sciences of the United States of America. 1993;90(7):2994-8. Epub 1993/04/01. PubMed PMID: 8464916; PubMed Central PMCID: PMC46223.
23. ANDalyze. Analytical Data Sheet for ANDalyze Zinc Sensor. Available from: http://andalyze.com/wp-content/uploads/ANDalyze-Zinc-Sensor-Analytical-Data-Sheet.pdf.
24. Ha T, Rasnik I, Cheng W, Babcock HP, Gauss GH, Lohman TM, Chu S. Initiation and re-initiation of DNA unwinding by the Escherichia coli Rep helicase. Nature. 2002;419(6907):638-41. Epub 2002/10/11. doi: 10.1038/nature01083. PubMed PMID: 12374984.
25. Wu P, Brand L. Resonance energy transfer: methods and applications. Analytical biochemistry. 1994;218(1):1-13. Epub 1994/04/01. PubMed PMID: 8053542.
26. Bowen ME, Weninger K, Ernst J, Chu S, Brunger AT. Single-molecule studies of synaptotagmin and complexin binding to the SNARE complex. Biophysical journal. 2005;89(1):690-702. Epub 2005/04/12. doi: 10.1529/biophysj.104.054064. PubMed PMID: 15821166; PubMed Central PMCID: PMC1366567.
27. Di Fiori N, Meller A. The Effect of dye-dye interactions on the spatial resolution of single-molecule FRET measurements in nucleic acids. Biophysical journal. 2010;98(10):2265-72.

Epub 2010/05/21. doi: 10.1016/j.bpj.2010.02.008. PubMed PMID: 20483335; PubMed Central PMCID: PMC2872366.

28. Tucker CJ. Scanners. Toxicogenomics: John Wiley & Sons, Inc.; 2005. p. 81-95.
29. Zhu Z, Chao J, Yu H, Waggoner AS. Directly labeled DNA probes using fluorescent nucleotides with different length linkers. Nucleic acids research. 1994;22(16):3418-22. Epub 1994/08/25. PubMed PMID: 8078779; PubMed Central PMCID: PMC523738.
30. Terpetschnig E, Wolfbeis OS. Luminescent Probes for NIR Sensing Applications. In: Daehne S, Resch-Genger U, Wolfbeis O, editors. Near-Infrared Dyes for High Technology Applications: Springer Netherlands; 1998. p. 161-82.
31. Berney C, Danuser G. FRET or no FRET: a quantitative comparison. Biophysical journal. 2003;84(6):3992-4010. Epub 2003/05/29. doi: 10.1016/S0006-3495(03)75126-1. PubMed PMID: 12770904; PubMed Central PMCID: PMC1302980.
32. Peracchi A. Preferential activation of the 8-17 deoxyribozyme by Ca(2+) ions. Evidence for the identity of 8-17 with the catalytic domain of the Mg5 deoxyribozyme. The Journal of biological chemistry. 2000;275(16):11693-7. Epub 2000/04/15. PubMed PMID: 10766789.
33. Kim HK, Liu J, Li J, Nagraj N, Li M, Pavot CM, Lu Y. Metal-dependent global folding and activity of the 8-17 DNAzyme studied by fluorescence resonance energy transfer. Journal of the American Chemical Society. 2007;129(21):6896-902. Epub 2007/05/10. doi: 10.1021/ja0712625. PubMed PMID: 17488081.
34. Romani AM. Cellular magnesium homeostasis. Archives of biochemistry and biophysics. 2011;512(1):1-23. Epub 2011/06/07. doi: 10.1016/j.abb.2011.05.010. PubMed PMID: 21640700; PubMed Central PMCID: PMC3133480.
35. Bootman MD. Calcium signaling. Cold Spring Harbor perspectives in biology. 2012;4(7):a011171. Epub 2012/07/04. doi: 10.1101/cshperspect.a011171. PubMed PMID: 22751152; PubMed Central PMCID: PMC3385957.
36. Finney LA, O'Halloran TV. Transition metal speciation in the cell: insights from the chemistry of metal ion receptors. Science. 2003;300(5621):931-6. Epub 2003/05/10. doi: 10.1126/science.1085049. PubMed PMID: 12738850.
37. Eide DJ. Zinc transporters and the cellular trafficking of zinc. Biochimica et biophysica acta. 2006;1763(7):711-22. Epub 2006/05/06. doi: 10.1016/j.bbamcr.2006.03.005. PubMed PMID: 16675045.
38. Somlyo AV, McClellan G, Gonzalez-Serratos H, Somlyo AP. Electron probe X-ray microanalysis of post-tetanic Ca2+ and Mg2+ movements across the sarcoplasmic reticulum in situ. The

Journal of biological chemistry. 1985;260(11):6801-7. Epub 1985/06/10. PubMed PMID: 3158652.

Chapter 4:

Synthesis of upconverting nanoparticle-caged DNAzyme conjugates for long-wavelength activation of DNAzymes

4.1 Introduction

The photocaging method originally described in Chapter 2 is a widely generalizable strategy for the conversion of DNAzyme sensors obtained through *in vitro* selection into cellular sensors usable within cells.[1] This approach has seen recent application in our group in the production and cellular application of a Na^+-specific DNAzyme sensor (Figure 4.1).[2] The incorporation of the photolabile nitrobenzyl moiety in the substrate strand of this DNAzyme enables the delivery and use of a sodium-responsive DNAzyme even though the conditions necessary for delivery contain sodium. The orthogonality between the photocaging system and delivery method suggests that any DNA delivery method applicable to unmodified DNA or an unmodified DNAzyme should be equally applicable to the caged DNAzyme, which was used to great effect in the use of a cationic helical peptide-based delivery method to deliver caged DNAzymes to the cytoplasm.

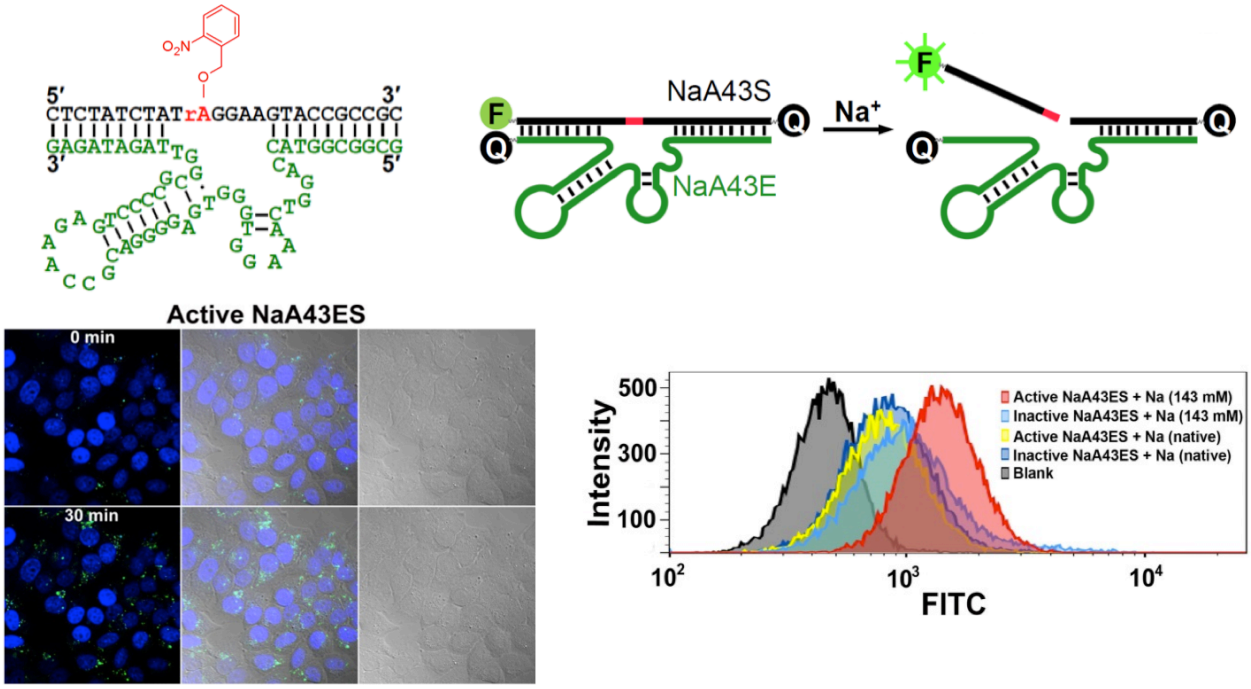

Figure 4.1. Cellular detection of Na^+ using a Na^+-specific DNAzyme. Cellular application of this recently-selected DNAzyme was made possible by the previously described photocaging strategy to inhibit premature activity caused by sodium common in the intra- or extracellular environment.

However, despite the demonstrated strengths of the photocaging strategy, there are a number of limitations introduced by its implementation. One major limitation is the requirement for UV irradiation (≤ 365 nm) to remove the o-nitrobenzyl photolabile protecting group.[3,4] UV light is readily absorbed by biological media and by cells; extensive use of UV light can cause cell damage. Due to the lower cytotoxicity of longer-wavelength (lower energy) light, a strategy that has been investigated is the use of visible or near-infrared (NIR) light irradiation in place of UV.[5-7] Both visible and NIR light are less toxic to cells than UV; furthermore, biological solutions typically have very low absorbance in the NIR region, allowing NIR light much greater tissue penetration.[5,8] As a result the development of NIR-responsive compounds has been a subject of significant research interest.[8] However, to date there are still very few reported photolabile groups that can be removed with NIR light.[4,9] The best-characterized NIR-accessible photoremovable protecting group is the 3-nitro-2-ethyldibenzylfuran (NDBF) moiety (Figure 4.2), which can be efficiently removed by two-photon excitation using doubled-wavelength light of approximately 700 nm.[10] However, while this moiety has been demonstrated to have excellent decaging properties, the NDBF group is synthetically challenging to prepare,[11,12] and to date no variant of the NDBF compound is commercially available. As a result, I am interested in investigating alternative methods allowing UV-free photoactivation of DNAzymes.

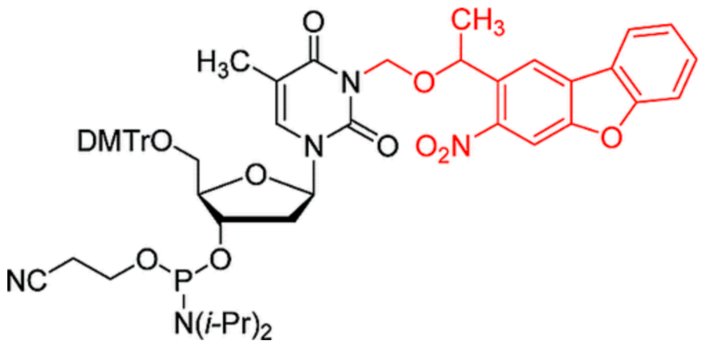

Figure 4.2. Near-infrared-absorbing photolabile group 3-nitro-2-ethyldibenzylfuran (NDBF). From Ref. 11.[11]

A novel nanomaterial of increasing general interest is a class of lanthanide-doped metal nanoparticles known as "upconversion" nanoparticles (UCNPs).[13,14] Due to a particular combination of energy states within the particle from embedded lanthanide ions, UCNPs are capable of effectively absorbing light in the NIR region. Furthermore, the particles have luminescent properties that can be tuned by modulating the particle composition, allowing for emission of higher-energy light from the particle.[13,14] This overall process of absorption of lower-energy light, emission of higher-energy light is the opposite of the normal Stokes shift common to fluorophores, and is thus a property of significant interest as a potential method for minimizing UV usage in biological systems.[13,14]

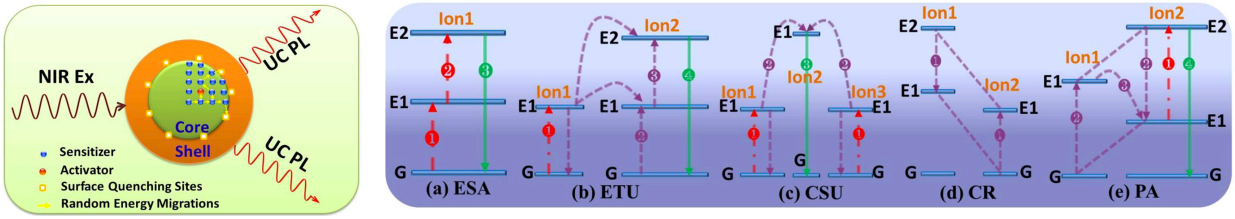

Figure 4.3. Upconversion nanoparticle scheme and principal mechanisms leading to upconversion. Originally from Ref 13.[13]

UCNPs have been utilized for UV-responsive photoremovable protecting groups previously.[15-18] The concept of local UV production by UCNP excitation has been further demonstrated to reduce the effects of phototoxicity within cells,[19] but has not yet been applied in conjunction with caged DNAzymes. In this chapter I present the design and initial demonstration of an upconversion nanoparticle-DNAzyme complex for long-wavelength activation of a nitrobenzyl photolabile group. This allows long-wavelength photoactivation of a caged DNAzyme and may be useful in subsequent use of caged DNAzymes *in vitro* or *in vivo*.

4.2 Materials and methods

4.2.1 Oligonucleotide synthesis

DNA sequences (see Table 4.1 for sequences) were obtained from Integrated DNA Technologies (Coralville, IA).

Table 4.1 DNA sequences used

Name	**Sequence (5' to 3')**
Caged substrate	/56-FAM/ACT CAC TAT /iNiBenz-rA/GG AAG AGA TGG ACG TG/3-BHQ1/
FAM-only strand	/56-FAM/ACT CAC TAT rAGG AAG AGA TGG ACG TG
17E-12T-SH	CAC GTC CAT CTC TTC TCC GAG CCG GTC GAA ATA GTG AGT TTT TTT TTT TTT /3ThioMC3/
39E-12A-amine	C*A*C GTC CAT CTC TGC AGT CGG GTA GTT AAA CCG ACC TTC AGA CAT AGT GAG TAA AAA A*A*A/3AmMO/
Alkyne-12A-17E-Dabcyl	/5Hexynyl/ AAA AAA AAA AAA CAC GTC CAT CTC TTC TCC GAG CCG GTC GAA ATA GTG AGT /3Dab/

All sequences were obtained from IDT (Coralville, IA) and use the following notation:

/3AmMO/ = 3'- amine linker

/3ThioMC3/ = 3'- thiol linker

/5Hexynyl/ = 5'-alkyne linker

/3Dab/ = 3'- Dabcyl (quencher)

* = phosphorothioate linker

4.2.2 UCNP synthesis

UCNPs were synthesized following standard protocol for the synthesis of β-NaYF4:Yb,Er nanoparticles using rare earth chlorides and oleic acid as a stabilizing ligand.[20-22] UCNPs were purified by centrifugation after addition of ethanol, washed extensively, and redispersed in cyclohexane until further use. TEM was carried out at the UIUC Materials Research Laboratory (MRL). Transmission electron

microscopy (TEM) images were taken on a JEOL 2100 Cryo transmission electron microscope with accelerating voltage of 200 kV.

4.2.3 Silica and DNA functionalization

Silica coating was carried out by addition of tetraethyl orthosilicate (TEOS) to UCNPs in water. Functionalization of DNA to the silica surface was carried out using two different methods:

i. Sulfo-SMCC functionalization

UCNPs were amine-functionalized with (3-aminopropyl)triethoxysilane (APTES), then modified with Sulfo-SMCC (Thermo-Fisher) following manufacturer protocols. Thiol-functionalized DNAzyme sequences were deprotected right before use with TCEP, purified by 10k MWCO centrifugal filter (Amicon), and reacted with Sulfo-SMCC-functionalized UCNPs.

ii. Azide-Alkyne coupling

Azide functionalization of the silica coating was carried out following a previously published protocol.[23] Briefly, the silica-coated UCNPs were mixed with 3-azidopropyl trimethoxysilane (AzPTMS) in ethanol, and refluxed overnight for 10 h at 80 °C. Particles were purified by centrifugation and washed 3x with methanol, then resuspended in PBS for DNA coupling.

Amine-modified DNA was mixed with 20 equivalents ADIBO-NHS in 0.5 mL dioxane and allowed to react overnight at room temperature. The crude reaction product was extracted 5x with an equal volume (0.5 mL) of dichloromethane to remove excess ADIBO and dioxane. Nitrogen gas was bubbled through the remaining aqueous phase to remove residual dichloromethane. For characterization of purified DBCO-DNAzyme, a 10k MWCO centrifugal filter (Amicon) was used to change the buffer to ammonium acetate, and the DNA was analyzed via MALDI-MS.

Strain-catalyzed click chemistry was carried out by mixing azide-functionalized UCNPs with freshly prepared ADIBO-modified DNAzymes in PBS. The reaction was carried out for 72 hours at room temperature.

The OliGreen DNA quantification assay was tested following manufacturer's protocols on both DNA-functionalized UCNPs and on azide-functionalized UCNPs as a control.

DNA loading was also assessed by hybridization of a fluorescent complementary DNA sequence. A FAM-labeled complementary sequence was annealed to the DNA-functionalized UCNPs at 80 °C for 5

minutes and cooled to room temperature over 30 minutes, then purified by centrifugation 3 times. FAM fluorescence was measured on a HORIBA Jobin Yvon FluoroMAX-P using 490 nm excitation and 518 nm emission, and quantified versus solutions of known FAM-DNA concentrations.

4.2.4 Luminescence measurements

Spectra were taken on a HORIBA Jobin Yvon FluoroMAX-P equipped with a commercial CW IR laser (980 nm) (Thorlabs, Inc). Luminescence was scanned over the range 200-900 nm.

4.2.5 Activity measurements

Activity of the caged 8-17 DNAzyme was carried out by hybridization of the caged substrate strand to UCNP-DNAzyme. 50 μM Zn^{2+} was added to the solution and irradiation was carried out using either a 980 nm 1 W laser (BOB Laser Company, China) or Spectroline hand lamp set to long wavelength mode (365 nm). Activity was assessed by fluorescence of the supernatant at a given time point.

4.3 Results and discussion

4.3.1 Synthesis of UCNPs, optimization of UCNP size

Yb and Tm-doped $NaYF_4$ nanoparticles were synthesized following previously published protocols. Improved size control was obtained by carefully controlling the rate of temperature increase during nucleation and synthesis. The luminescence properties of the synthesized UCNPs were measured at 980 nm excitation. (Figure 4.4). The spectrum shows several peaks, which are in close agreement with previous reports of UCNPs with the same composition. Notably, there is a small emission peak within the range 361-365 nm, which was envisioned to enable decaging of the nitrobenzyl-caged DNAzyme (which is effectively decaged at wavelengths ≤ 365 nm).

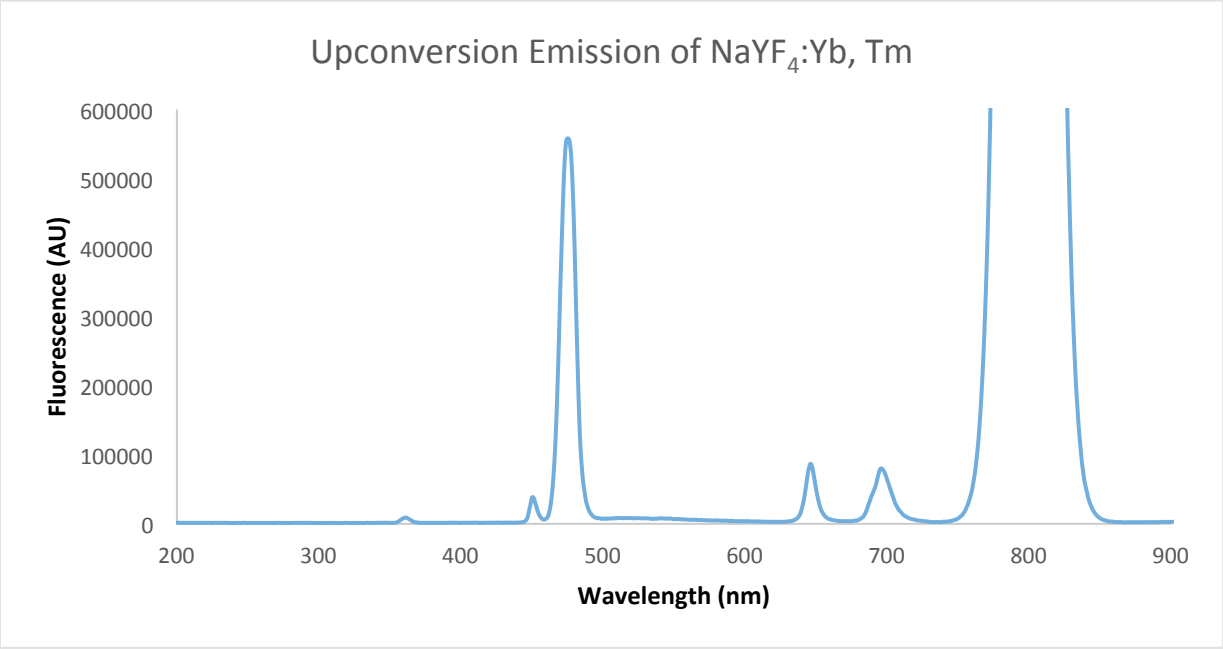

Figure 4.4. Luminescence spectrum of uncoated UCNPs.

4.3.2 Silica functionalization and characterization

The UCNPs were coated with silica by reaction with TEOS after removal of oleic acid, again following standard protocols. TEM images of the silica-coated particles (Figure 4.5) indicated successful and consistent silica coating of radius ~ 25 nm, covering ~ 25 nm diameter UCNPs.

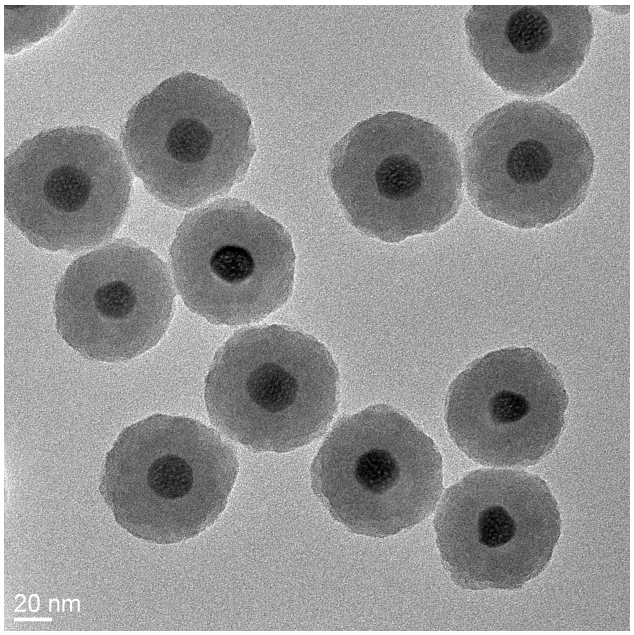

Figure 4.5. TEM image of silica-coated UCNPs.

The luminescence spectrum of the silica-coated UCNPs was measured at 980 nm excitation (Figure 4.6). Aside from a moderate quenching of overall luminescence, no other apparent changes to the emission spectra were observed.

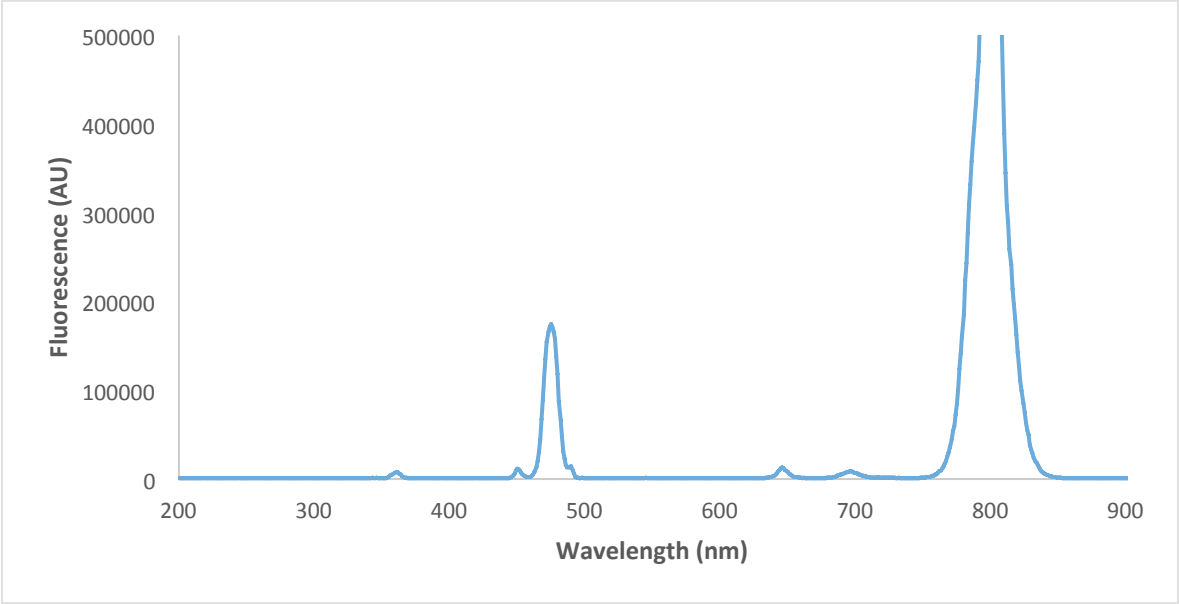

Figure 4.6. Luminescence spectra of silica-coated UCNPs excited at 980 nm.

Azide-functionalization of silica-UCNP was carried out following an established protocol for synthesis and use of of 3-azidopropyl trimethylsilane. Azide-functionalized UCNPs were directly used for DNA conjugation.

4.3.3 Strain-catalyzed alkyne-azide cycloaddition

The ADIBO-functionalized DNAzyme was synthesized by reaction of ADIBO-NHS (Figure 4.6) with amine-functionalized DNA. After removal of excess ADIBO-NHS and dioxane, the efficiency of ADIBO-functionalization of the DNAzyme was assessed by MALDI-MS. As seen in Figure 4.8, although the DNA peak is broad, a significant shift of the peak maximum from 18827 MW to 19310 MW is observed after reaction of amine-DNAzyme with ADIBO-NHS.

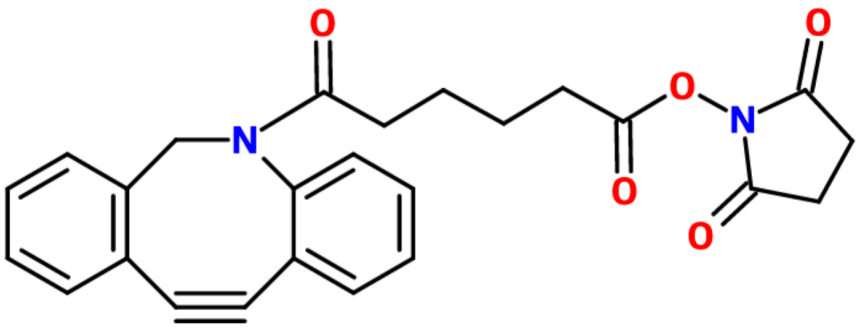

Figure 4.7. Structure of ADIBO-NHS

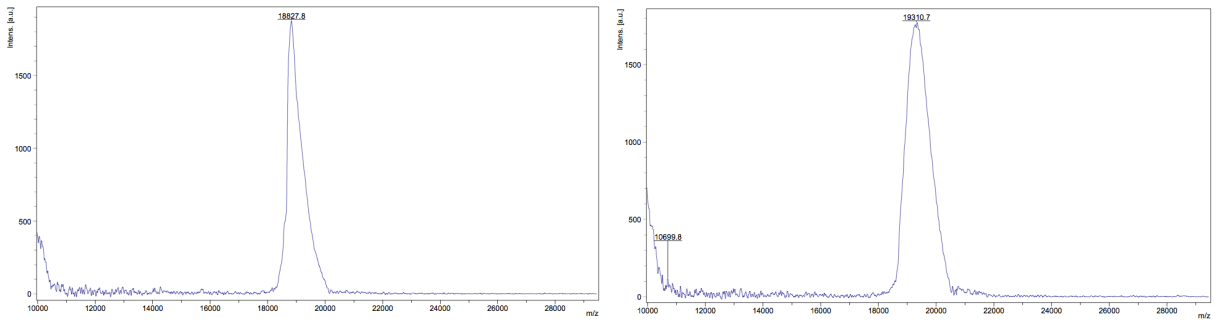

Figure 4.8. MALDI-MS of NH2-DNAzyme (expected mass 18744.4) and ADIBO-DNAzyme (expected mass 19062.8)

4.3.4 DNAzyme functionalization of UCNP and DNA quantification

The strain-catalyzed click reaction between ADIBO-DNAzyme and azide-functionalized UCNPs was carried out at room temperature for 72 hours in pH 7.4 PBS. The resulting UCNPs were purified by centrifugation and DNA quantified using either the OliGreen DNA quantification assay or binding of a complementary FAM-labeled DNA strand.

The OliGreen DNA quantification assay was initially used to determine the loading of DNA on functionalized UCNPs. However, it was observed that OliGreen shows nonspecific fluorescence turn-on not only with DNA, but also in the presence of azide-functionalized UCNPs alone (Figure 4.9).

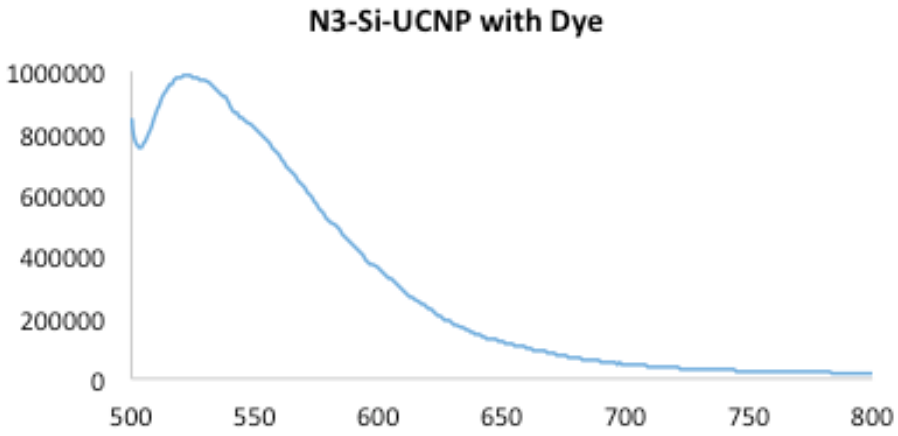

Figure 4.9. Nonspecific fluorescence increase of OliGreen dye (emission maximum 520 nm) in the presence of azide-functionalized UCNPs

A complementary DNA approach was used to more accurately measure the total DNA loading. A fluorescently modified complementary DNA sequence was hybridized to the DNAzyme-UCNP conjugate and fluorescence compared to a calibration curve derived from known concentrations of FAM-DNA fluorescence. Based on this method, the observed total concentration of DNA was calculated to be approximately 0.06 nM.

4.3.5 Long-wavelength decaging of a caged DNAzyme

The activity of the caged 8-17 DNAzyme functionalized to the UCNP surface was investigated. A caged 8-17 DNAzyme substrate was hybridized to the UCNP-conjugated DNAzyme and Zn^{2+} (100 μM) was added to the solution. Irradiation was performed using 365 nm or 980 nm irradiation, and supernatant fluorescence measured to determine the extent of DNAzyme decaging. Little fluorescence was observed before decaging, confirming that the caged DNAzyme remained inactive even in the presence of Zn^{2+}.

Irradiation with either UV or NIR light (Figure 4.10) produced an increase in supernatant fluorescence caused by cleavage of the decaged DNAzyme, indicating that the DNAzyme was both still active and could be decaged with NIR light.

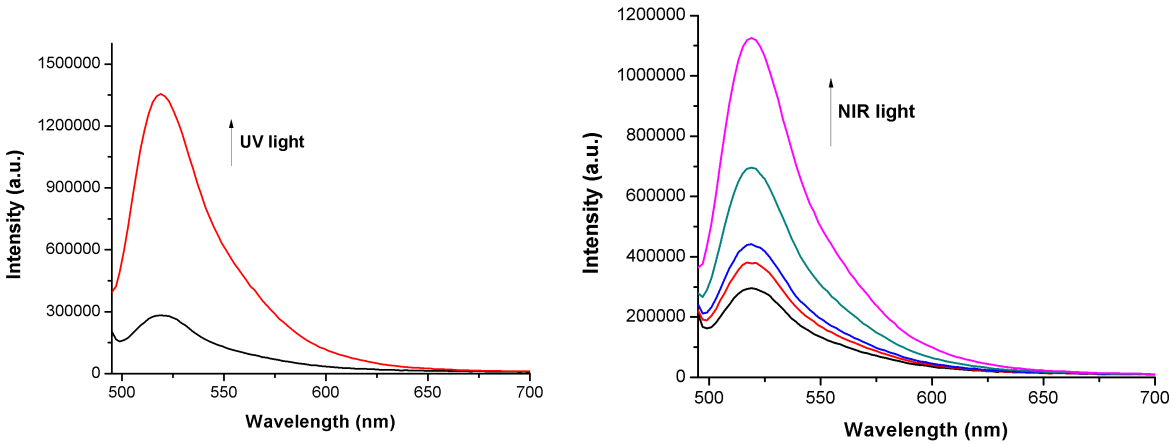

Figure 4.10. Decaging of UCNP-caged DNAzymes with (a) 365 nm light or (b) 980 nm light. Fluorescent signal at 518 nm corresponds to cleavage of (decaged) 8-17 DNAzyme.

The degree of decaging is observed to directly correlate with total irradiation time (Figure 4.11), further providing that the upconversion of the nanoparticle is the cause of the observed DNAzyme activation.

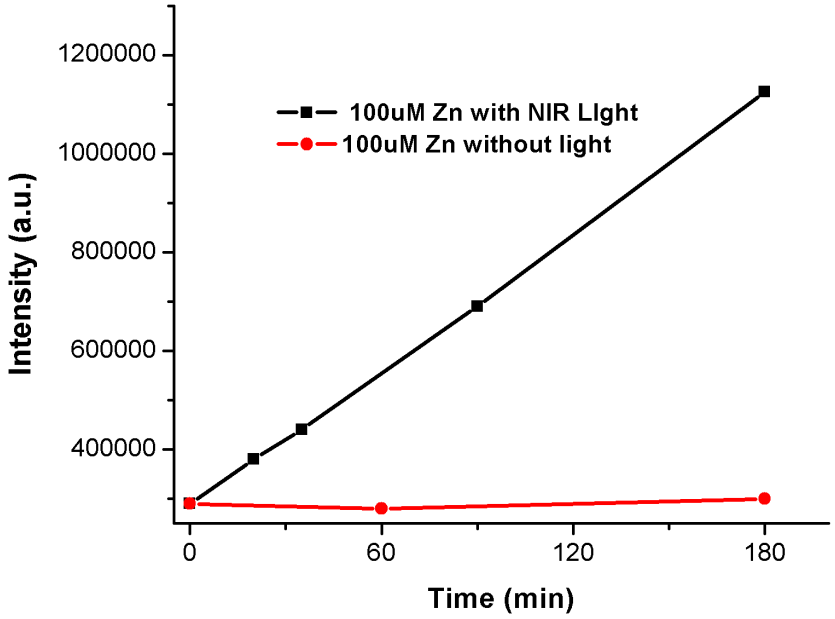

Figure 4.11. Kinetics of decaging using 980 nm light (laser power 1 W)

4.4 Summary and conclusions

In this chapter I demonstrated the initial design and demonstration of a strategy for avoiding the negative effects of UV irradiation on cells originally necessary for activating photocaged DNAzymes. The use of upconverting lanthanide-doped nanoparticles allows the use of near-IR excitation, which is more biologically compatible than UV wavelengths and may allow for future applications *in vivo* as well as *in vitro*. Future work will focus on demonstrating the continued usability of this design within the cellular environment, as well as optimization of conjugation methods to maximize decaging efficiency and generalizability towards other DNAzymes or nanoparticle types.

4.5 References

1. Hwang K, Wu P, Kim T, Lei L, Tian S, Wang Y, Lu Y. Photocaged DNAzymes as a general method for sensing metal ions in living cells. Angewandte Chemie. 2014;53(50):13798-802. Epub 2014/10/15. doi: 10.1002/anie.201408333. PubMed PMID: 25314680; PubMed Central PMCID: PMC4297208.

2. Torabi SF, Wu P, McGhee CE, Chen L, Hwang K, Zheng N, Cheng J, Lu Y. In vitro selection of a sodium-specific DNAzyme and its application in intracellular sensing. Proceedings of the National Academy of Sciences of the United States of America. 2015;112(19):5903-8. Epub 2015/04/29. doi: 10.1073/pnas.1420361112. PubMed PMID: 25918425; PubMed Central PMCID: PMC4434688.

3. Chaulk SG, MacMillan AM. Synthesis of oligo-RNAs with photocaged adenosine 2'-hydroxyls. Nature protocols. 2007;2(5):1052-8. Epub 2007/06/05. doi: 10.1038/nprot.2007.154. PubMed PMID: 17546010.

4. Klan P, Solomek T, Bochet CG, Blanc A, Givens R, Rubina M, Popik V, Kostikov A, Wirz J. Photoremovable protecting groups in chemistry and biology: reaction mechanisms and efficacy. Chemical reviews. 2013;113(1):119-91. Epub 2012/12/22. doi: 10.1021/cr300177k. PubMed PMID: 23256727; PubMed Central PMCID: PMC3557858.

5. Smith AM, Mancini MC, Nie S. Bioimaging: second window for in vivo imaging. Nature nanotechnology. 2009;4(11):710-1. Epub 2009/11/10. doi: 10.1038/nnano.2009.326. PubMed PMID: 19898521; PubMed Central PMCID: PMC2862008.

6. Trigo FF, Corrie JE, Ogden D. Laser photolysis of caged compounds at 405 nm: photochemical advantages, localisation, phototoxicity and methods for calibration. Journal of neuroscience methods. 2009;180(1):9-21. Epub 2009/05/12. doi: 10.1016/j.jneumeth.2009.01.032. PubMed PMID: 19427524.

7. Furuta T, Wang SS, Dantzker JL, Dore TM, Bybee WJ, Callaway EM, Denk W, Tsien RY. Brominated 7-hydroxycoumarin-4-ylmethyls: photolabile protecting groups with biologically useful cross-sections for two photon photolysis. Proceedings of the National Academy of Sciences of the United States of America. 1999;96(4):1193-200. Epub 1999/02/17. PubMed PMID: 9990000; PubMed Central PMCID: PMC15439.

8. Guo Z, Park S, Yoon J, Shin I. Recent progress in the development of near-infrared fluorescent probes for bioimaging applications. Chemical Society reviews. 2014;43(1):16-29. Epub 2013/09/21. doi: 10.1039/c3cs60271k. PubMed PMID: 24052190.

9. Wirz J. Photoremovable protecting groups: development and applications. Photochemical & photobiological sciences : Official journal of the European Photochemistry Association and the European Society for Photobiology. 2012;11(3):445. Epub 2012/02/22. doi: 10.1039/c2pp90005j. PubMed PMID: 22344622.

10. Momotake A, Lindegger N, Niggli E, Barsotti RJ, Ellis-Davies GC. The nitrodibenzofuran chromophore: a new caging group for ultra-efficient photolysis in living cells. Nature methods. 2006;3(1):35-40. Epub 2005/12/22. doi: 10.1038/nmeth821. PubMed PMID: 16369551.

11. Lusic H, Uprety R, Deiters A. Improved synthesis of the two-photon caging group 3-nitro-2-ethyldibenzofuran and its application to a caged thymidine phosphoramidite. Organic letters. 2010;12(5):916-9. Epub 2010/02/02. doi: 10.1021/ol902807q. PubMed PMID: 20112966; PubMed Central PMCID: PMC2830370.

12. Chen X, Tang S, Zheng JS, Zhao R, Wang ZP, Shao W, Chang HN, Cheng JY, Zhao H, Liu L, Qi H. Chemical synthesis of a two-photon-activatable chemokine and photon-guided lymphocyte migration in vivo. Nature communications. 2015;6:7220. Epub 2015/05/27. doi: 10.1038/ncomms8220. PubMed PMID: 26008852; PubMed Central PMCID: PMC4455097.

13. Chen G, Qiu H, Prasad PN, Chen X. Upconversion nanoparticles: design, nanochemistry, and applications in theranostics. Chemical reviews. 2014;114(10):5161-214. Epub 2014/03/13. doi: 10.1021/cr400425h. PubMed PMID: 24605868; PubMed Central PMCID: PMC4039352.

14. DaCosta MV, Doughan S, Han Y, Krull UJ. Lanthanide upconversion nanoparticles and applications in bioassays and bioimaging: a review. Analytica chimica acta. 2014;832:1-33. Epub 2014/06/04. doi: 10.1016/j.aca.2014.04.030. PubMed PMID: 24890691.

15. Yang Y, Shao Q, Deng R, Wang C, Teng X, Cheng K, Cheng Z, Huang L, Liu Z, Liu X, Xing B. In vitro and in vivo uncaging and bioluminescence imaging by using photocaged upconversion nanoparticles. Angewandte Chemie. 2012;51(13):3125-9. Epub 2012/01/14. doi: 10.1002/anie.201107919. PubMed PMID: 22241651.

16. Dai Y, Xiao H, Liu J, Yuan Q, Ma P, Yang D, Li C, Cheng Z, Hou Z, Yang P, Lin J. In vivo multimodality imaging and cancer therapy by near-infrared light-triggered trans-platinum

pro-drug-conjugated upconverison nanoparticles. Journal of the American Chemical Society. 2013;135(50):18920-9. Epub 2013/11/28. doi: 10.1021/ja410028q. PubMed PMID: 24279316.

17. Yang Y, Velmurugan B, Liu X, Xing B. NIR photoresponsive crosslinked upconverting nanocarriers toward selective intracellular drug release. Small. 2013;9(17):2937-44. Epub 2013/04/05. doi: 10.1002/smll.201201765. PubMed PMID: 23554151.

18. Shen J, Chen G, Ohulchanskyy TY, Kesseli SJ, Buchholz S, Li Z, Prasad PN, Han G. Tunable near infrared to ultraviolet upconversion luminescence enhancement in (alpha-NaYF4 :Yb,Tm)/CaF2 core/shell nanoparticles for in situ real-time recorded biocompatible photoactivation. Small. 2013;9(19):3213-7. Epub 2013/05/23. doi: 10.1002/smll.201300234. PubMed PMID: 23696330.

19. Jayakumar MK, Idris NM, Zhang Y. Remote activation of biomolecules in deep tissues using near-infrared-to-UV upconversion nanotransducers. Proceedings of the National Academy of Sciences of the United States of America. 2012;109(22):8483-8. Epub 2012/05/15. doi: 10.1073/pnas.1114551109. PubMed PMID: 22582171; PubMed Central PMCID: PMC3365215.

20. Wang F, Deng R, Liu X. Preparation of core-shell NaGdF4 nanoparticles doped with luminescent lanthanide ions to be used as upconversion-based probes. Nature protocols. 2014;9(7):1634-44. Epub 2014/06/13. doi: 10.1038/nprot.2014.111. PubMed PMID: 24922272.

21. Li LL, Zhang R, Yin L, Zheng K, Qin W, Selvin PR, Lu Y. Biomimetic surface engineering of lanthanide-doped upconversion nanoparticles as versatile bioprobes. Angewandte Chemie. 2012;51(25):6121-5. Epub 2012/05/09. doi: 10.1002/anie.201109156. PubMed PMID: 22566291; PubMed Central PMCID: PMC3516999.

22. Li LL, Wu P, Hwang K, Lu Y. An exceptionally simple strategy for DNA-functionalized up-conversion nanoparticles as biocompatible agents for nanoassembly, DNA delivery, and imaging. Journal of the American Chemical Society. 2013;135(7):2411-4. Epub 2013/01/30. doi: 10.1021/ja310432u. PubMed PMID: 23356394; PubMed Central PMCID: PMC3608408.

23. Abadeer NS, Brennan MR, Wilson WL, Murphy CJ. Distance and plasmon wavelength dependent fluorescence of molecules bound to silica-coated gold nanorods. ACS nano. 2014;8(8):8392-406. Epub 2014/07/26. doi: 10.1021/nn502887j. PubMed PMID: 25062430.